Optimization of a propulsion plant for a submarine based on first principles

Mission profile based design and comparison of various system configurations

By

L.P.W. Rietveld

Performed at

Nevesbu

In partial fulfilment of the requirements for the degree of

Master of Science
in Mechanical Engineering

Specialization Mechanical Systems and Integration

This thesis SDPO.17.001.m. is classified as confidential in accordance with the general conditions for projects performed by the TU Delft.

16-03-2017

Company supervisor

Responsible supervisor:	ir. R.M. Boogaart
E-mail:	R.M.Boogaart@nevesbu.com

Thesis exam committee

Chair/Responsible Professor:	Rear-Admiral (ret.) ir. K. Visser	TU Delft
Staff Member:	ir. P. de Vos	TU Delft
Staff Member:	Dr. ir. M. Pini	TU Delft
Company Member:	ir. R.M. Boogaart	Nevesbu
Company Member:	ing. C.J.C.M Posthumus	DMO

Author Details

Study number:	4192257
Author contact e-mail:	Leon.Rietveld@gmail.com

Abstract

The function of a propulsion plant of a submarine is to generate, store and supply the required power for propulsion and auxiliary systems. The electric power generation and distribution system is considered part of the propulsion plant. The propulsion plant is one of the most important factors contributing to the total size and weight of a submarine. New and existing technologies can reduce the required weight and volume for the propulsion plant, resulting in decreased submarine size or more room for crew, sensor and weapon systems in case of an equally sized submarine. The objective of this study is to evaluate and optimise a number of concept propulsion plant configurations for the replacement of the submarines of the Royal Netherlands Navy in terms of size, weight, efficiency and life cycle costs.

The concept propulsion plant configurations must meet the design requirements which are captured in an assumed mission profile. The assumed mission profile is a representation of a mission in time domain that includes surfaced, snorting and deeply submerged operation and speed variation ranging from dead-slow to burst speed.

Two concept propulsion plant configurations have been modelled. Quasi-static modelling has been used to simulate an optimal propulsion plant based on a time variant mission profile. The components in the propulsion plant are modelled based on first principles. First principle modelling is used to increase fidelity. The results of the simulation are weight, volume and efficiency of the plant's components. Together, they make up the concept systems weight, volume and efficiency.

Both concepts are diesel electric configurations. In the first concept diesel generator power is supplied to lead-acid batteries. Stored energy in the batteries is distributed to mission-related auxiliary systems and to a direct current compound motor that drives the propeller resulting in propulsive power. The lead-acid batteries are replaced by lithium-ion technology in the second concept configuration.

The weight and volume of the propulsion motor depends on the maximum required power output and motor parameters. Besides the constants, the efficiency is influenced by the momentaneous power requirements and available battery voltage. Battery voltage depends on the number of battery cells in series and on the battery cell parameters. The optimum number of battery cells with respect to weight and volume is found using an optimization algorithm. The simulations showed that lead-acid batteries need to be 6.1 times heavier and 3.3 times more volume compared to lithium-ion batteries in order to meet the same requirements set in the assumed mission profile.

The mission profile requirements define the amount of generator power that is required to charge the batteries during snorting operation. The propulsion plant efficiency with lithium-ion batteries is 6% higher compared to lead-acid, resulting in lower charge powers and therefor smaller diesel generator set. Resulting in possible lower indiscretion ratios for lithium-ion batteries. The optimum number of batteries and mass per battery cell do not affect the required generator power. The number of cell does however affect the maximum charge power. The maximum charge power of lead-acid battery cells is limited. High charge powers can damage the cells when the maximum cell voltage is exceeded.

Several mission variations have been executed to investigate the effect of the burst, auxiliary load and the amplitude of the burst in the mission profile. It is recommended to use the models and define multiple realistic mission profiles and analyse the properties of the optimized propulsion plants.

The concept propulsion configurations are limited to conventional diesel electric propulsion plants. Increasing the library of components by adding atmospheric air independent power generation systems increases the number of possible propulsion plant configurations and other optimum propulsion plant

configurations with respect to the defined criteria. An atmospheric air independent propulsion plant could be the optimum propulsion plant configuration. The same holds for the type of propulsion engine.

It can be concluded that the diesel electric propulsion plant with lithium-ion battery technology requires less weight, less volume and a higher efficiency compared to the lead-acid variant for the assumed mission profile. Therefore, the submarine design can potentially benefit from the implementation of lithium cells. It is recommended to investigate in the required volume and weight of the auxiliary systems associated with the lithium-ion batteries.

Preface

This thesis is the final assignment of the Master of Science program of Mechanical Engineering at the Technical University Delft. The track is Transportation Engineering with the specialization Mechanical Systems and Integration (MSI). The main focus of the specialization is the integration of systems on board of ships, especially complex vessels. The research topic is the perfect combination of the integration of mechanical systems and a complex vessel.

The thesis was done at Nevesbu (Nederlandse Verenigde Scheepsbouw Bureaus) at the department of mechanical and marine engineering. I would like to thank Nevesbu for the opportunity to work on my thesis and being available for discussions and questions. A special word of thanks to Rolf Boogaart for his involvement and guidance.

I want to thank Mr. Visser for being the chair of my exam committee and the good cooperation during my time as board member of Vulcanus – the student association of Marine Engineering and MSI. His network made it possible for me to arrange a visit to ThyssenKrupp Marine Systems in Kiel, formerly known as the Howaldtswerke-Deutsche Werft GmbH (HDW). In addition, he gave me the unique opportunity to sail on aboard the submarine *Zr. Ms. Walrus*, an unforgettable experience.

Furthermore, I like to thank my supervisor from TU-Delft, Peter de Vos. Peter introduced me to Nevesbu, and was always available for questions and feedback and a good conversation, thank you Peter.

Furthermore I would thank friends and family for supporting me during my studies. A special thanks to Jim Otjens for the support during courses and Rosanne Rietveld for her feedback on the thesis. Last but not least my girlfriend Dominique Eggink, for supporting and encouraging me.

L.P.W. Rietveld
Alblasserdam, March 2017

Index

1 Introduction

1.1 Back ground

The submarine fleet of the *Royal Netherlands Navy* – RNLN - consists of four *Walrus-class* submarines. These are attack submarines, specifically designed for attacking submarines and surface ships, deploying Special Forces and gathering intelligence. Figure 1 is an artistic impression of a *Walrus-class* submarine. The overall length of the illustrated submarine is 68 [m], the breadth is 8.5 [m] and diving depth over 300 [m]. The crew consists of 55 persons. [1]

The first of four submarines, christened as *Zr. Ms. Zeeleeuw*, was commissioned in April 1990. In December 2015 *Zr. Ms. Zeeleeuw* was relaunched after a refit. The refit program *Instandhoudings-programma Walrusklasse* (IPW) is intend to extend the technological lifetime of the fleet. The fleet will be in operational service for 35 years by 2025 and have reached their technological lifetime. The successor of the *Walrus-class* is planned to go into service in 2025. The Ministry of Defence is investigating the required capabilities of the new submarines given the tasks.

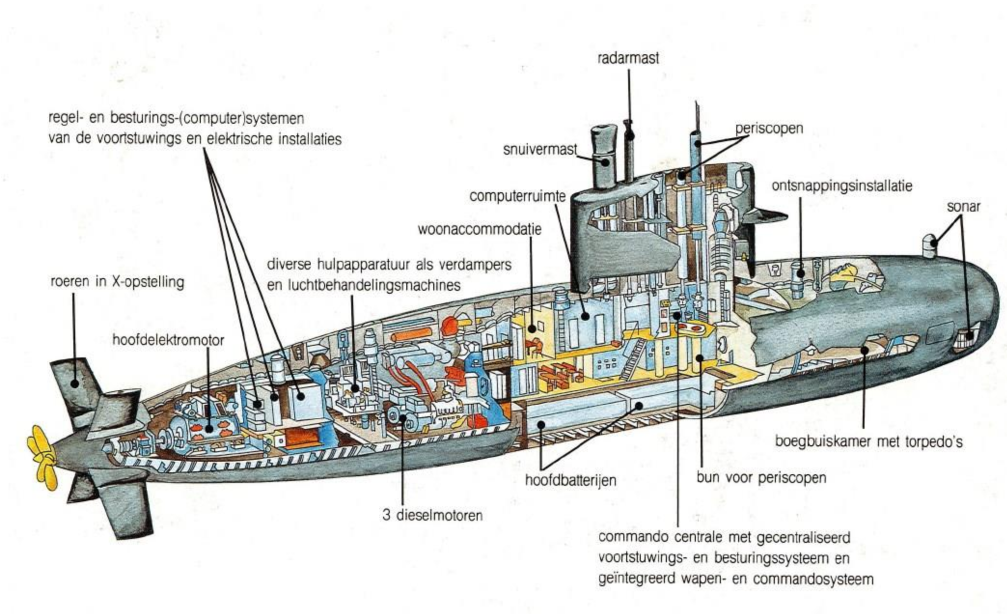

Figure 1 artistic impression of a submarine [2]

The conceptual design of the new submarine class is made by in the so called golden triangle. The corners of the triangle are the government, industry and research institutions. The government is represented by the Ministry of Defence and *Defensie Materieel Organisatie* (DMO) and is involved as customer and user of the system. Research institutes as *TU Delft*, *TNO* and *Marin* execute specialized profound research to improve the performance. The industry is represented by companies as *Nevesbu* and *Damen Schelde Naval Shipbuilding. Nevesbu* is a marine engineering and naval architecture company involved in the design of ships, offshore, naval and specialist vessels. The company offers supports in all project phases, including feasibility studies. The company can offer a wide range of services, ranging from specific study assignments to complete detail design and engineering projects. The research is conducted at *Nevesbu*, in cooperation with *DMO* and *TU Delft.*

1.2 Problem

The function of the propulsion plant of a submarine is to generate, store and supply required power for propulsion and auxiliary systems. The propulsion plant is one of the most important factors determining the submarine size. The system makes up around 35% of a submarine's weight and takes up to 50% of the total volume available in a submarine [3].

The dimensions of the propulsion plant are dependent on the performance requirements. The primary factors that govern the power and energy storage are the maximum speed and the submerged endurance. The maximum speed requirement determines the size of the propulsion motor, while the energy storage capacity is determined by the submerged time, speed and auxiliary load. The maximum speed is one of the most difficult aspects of the design. For military operations having a high speed is desirable. This way, the submarine can outrun attackers or intercept the target more rapidly. Since submarine warfare tactics are largely involved with stealth it can be argued that the use of high speed in evasion or attack is not the only tactic. The propulsive power requirements vary with the cube of speed, resulting in a large increase of the propulsion plant components dimensions. [3]

A comparison between various concept system configurations, with different propulsion plant technologies is desired to find the optimum propulsion plant. New and existing propulsion plant technologies could reduce the required weight and volume of the propulsion plant, resulting in a decreased submarine size. The concept propulsion plants need to meet set design requirements, which are combined in an assumed mission profile that varies in the time domain. Besides finding the optimum propulsion plant for the assumed mission profile is it interesting to investigate the effect of varying performance requirements on the propulsion plant's efficiency, weight, volume and life cycle cost.

1.3 Objective

From the problem description above the objective of this thesis is to evaluate a number of concept propulsion plant configurations that meet the design requirements. This results in the concept propulsion plants that are most favourable with respect to; efficiency, weight, volume and life cycle cost (LCC).

The design requirements for the propulsion plant are expressed in a mission profile. The mission profile defines a propulsive and auxiliary load for a period of time. The uses mission profile is an example and has all elements of a realistic submarine mission, such as snorting, slow submerged speed, high submerged speed and speeds in between. The simulation shall be set up to accommodate various mission profiles as input for the simulation. Technical and financial feasibility are the two criteria which determine whether the system is a conceivable option for the new submarines of the RNLN. The objective is reflected in the main research question:

What are the optimum propulsion plant configurations for the replacement of the Walrus-class submarine given an assumed mission profile?

The related research questions:

- *Which propulsion plant has the highest efficiency for the assumed mission profile?*
- *Which propulsion plant has the lowest weight for the assumed mission profile?*
- *Which propulsion plant has the smallest volume for the assumed mission profile?*
- *Which propulsion plant has the lowest LCC for the assumed mission profile?*

1.4 Report overview

This subchapter gives a brief overview of report structure.

The mission profile is the input to the propulsion plant. Chapter 0 elaborates on the assumed mission profile used to find the optimum propulsion plant configuration. Chapter 0 elaborates on the components of the propulsion plant layout. The first chapter is a general introduction into propulsion plants in submarines. The followed by the concept propulsion plant configurations that are taken into account for the optimization.

Chapter 4 describes the methodology that is used to determine the efficiency, weight and volume of the concept propulsion plant configurations as function of the assumed mission profile.

Chapter 0 explains the propulsion motor performance and propulsion motor dimensions as function of the assumed mission profile. The relation between the performance and dimensioning model is described. The performance model and the dimensioning model are verified with available measurements. Chapter 6 elaborates on the battery performance model and the relation between battery dimensions and battery capacity. The battery performance model is verified with available measurements of the manufacturer of the batteries. Chapter 0 describes the diesel generator set performance model and the dimensioning of the diesel generator set as function of the generator output power.

In chapter 0 are the propulsion motor, battery cell a diesel generator performance models combined to propulsion plant configuration A. The lead-acid batteries are optimized for optimum mass and volume as function of the assumed mission profile. The optimization is done with a battery optimization algorithm. The diesel generator set is dimensioned for the assumed mission profile. The propulsion plant efficiency is expressed in the fuel consumption required to fulfil the mission.

In chapter 9 are the performance models combined to propulsion plant configuration B. The propulsion plant is optimized in the same way as propulsion plant configuration A. The difference between the concept configurations is the energy storage. The energy storage for concept B is lithium-ion battery technology.

A rough estimate of the life cycle cost is made in chapter 10. The comparison of the propulsion plant configurations and the answer to the research question is given in chapter 11. The conclusions are summarized the recommendations are stated.

2 Mission profile

2.1 Introduction

The goal of the research is to find the optimum propulsion plant configuration given an assumed mission profile. The mission profile is a representation of a realistic mission. It represents a possible mission containing the various aspects that are relevant from design perspective. The mission profile is the input to the propulsion plant. This chapter elaborates on the assumed mission profile used to find the optimum propulsion plant configuration.

2.2 Mission profile

The assumed mission starts at a port, from which the submarine sails to a surveillance area. In the surveillance area an action is executed followed by the return to port. The various parts of the mission have various power loads. There are two power loads, the propulsive power and the auxiliary power load. The propulsive power load is the result of the set submarine speed and the resistance of the submarine. For this study submarine speed and resistance are defined and incorporated in the required power in the mission profile.

The main auxiliary loads are the cooling systems, SEWACO systems; (SEnsoren, WApen-, Commando systemen), HVAC; (heating, ventilation and air-conditioning), freshwater systems and manoeuvring systems. The auxiliary load changes during the mission.

2.2.1 Assumed mission profile

The assumed mission profile is illustrated in Figure 2. The mission profile is illustrated in two graphs. The upper graph illustrates the set submarine speed in knots. The lower graph illustrates the auxiliary load. The submarine speed is varying in time. At time *t0* the set speed is 10 knots up to time *t1*. The dashed line indicates the submarine is sailing in surfaced operation and can make use of atmospheric air. This phase is called the Overt Transit 1 (OT1) and is defined as a period of 260 hours.

Overt Transit 1 passes into Covert Transit 1 (CT1). CT1 starts at *t1* and ends at *t2*, the assumed mission profile prescribes a period of 470 hours. During the covert transit the submarine sails alternated deeply submerged and snorting. The submerged part is indicated as CT1 SM. The snorting part is indicated as CT1 SR. The ratio between the submerged parts and surfaced parts is defined by an indiscretion ratio (IR). The indiscretion ratio is the snorting time, divided by the total time. The total time is the submerged time plus the snorting time. The IR is stated in equation 2-1, the IR for CT1 is 0.10.

$$IR = \frac{T_{snort}}{T_{snort} + T_{subm}} = \frac{CT1\ SR}{CT1\ SR + CT1\ SM} = 0.10 \qquad \text{2-1}$$

Figure 2 illustrates three snorting and submerged blocks during CT1, this is illustrative in reality is this a plurality of the blocks, depending on stored energy capacity and boundary conditions. The boundary conditions will be explained in chapter 4 Methodology description.

During the snorting period the set auxiliary load is increased to 260 kW. The increase is due to several extra activities compared to submerged operation; the air in the submarine is scavenged and more power is required for the HVAC system, the compressors can be switched on to pressurize the compressed air storage tanks and the battery cooling system is switched on.

The surveillance and attack (SA) phase can be seen as one phase. The submarine sails submerged and will not reach the surface to snort. The heat of the exhaust gases and the snorting pipes may reveal the presence of the submarine, assuming a diesel electric submarine. An assumed mission could be the surveillance of an area and detecting an enemy vessel followed by the manoeuvring to an ideal position for the attack followed by a getaway. The indicated times in Figure 2; SA1 up to SA4 are defined and are elaborated in chapter 4 Methodology description.

After the surveillance and attack the submarine heads home in a convert transit. Covert transit 2 (CT2) differs from CT1 in speed and defined indiscretion ratio. The indiscretion ratio for CT2 is 0.28. The IR indicates the submarine snorts longer compared to CT1. The duration of covert transit is 135 hours.

After CT2 the submarine sails to port in overt transit 2 (OT2) with the same load specifications as OT1. The duration of CT2 is 230 hours.

The assumed mission profile is based on a typical submarine mission. The duration of those missions is limited by the diesel storage capacity and provisions this is around the 1105 hours or 46 days. New submarine design could be based on this data.

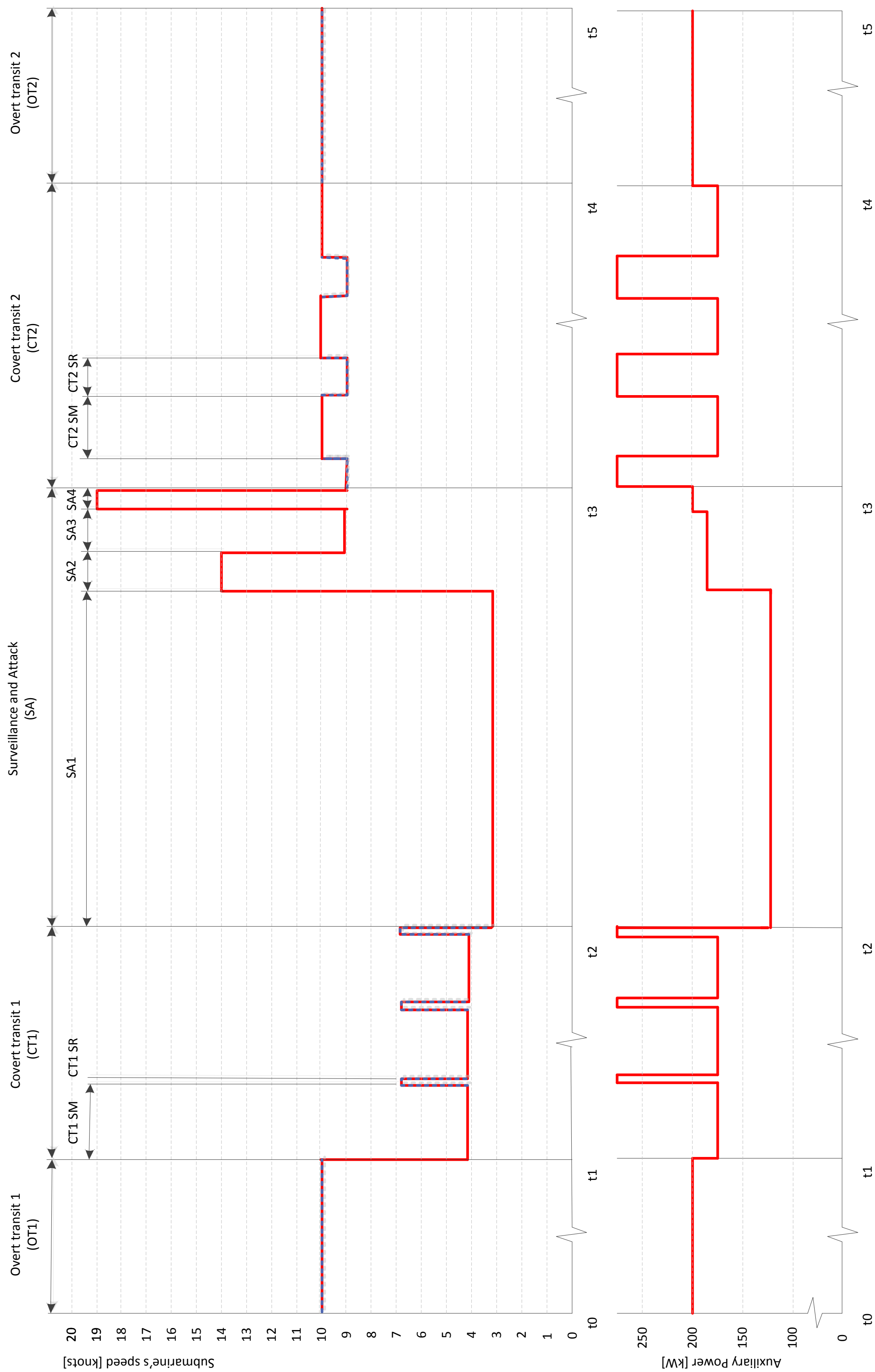

Figure 2 Assumed mission profile

2.3 Propeller load characteristic

The mission profile defines the submarines speed and auxiliary power load. The propulsive power required to meet the defined speed results in the required propulsion motor brake power. This subchapter elaborates on the required engine brake power as function of the mission profile.

The boundary conditions and constants used to determine the brake power as function of the set speed are obtained from measurement data of *Zr. Ms. Zwaardvis. Zr. Ms. Zwaardvis* is a predecessor of *Zr. Ms. Walrus.* A new submarine design would have a different power revolutions curve. The relation between power and rate of rotation or the propeller of *Zr. Ms. Zwaardvis* is a good representation. The relation between brake power and the revolutions of the propulsion motor is relevant for the dimensioning of the propulsion motor.

2.3.1 Load characteristics

It is acceptable to assume the submarine resistance is roughly proportional to the square of the ship speed for relative low speeds as stated in equation 2-2. The power required to tow a vessel through the water at ship speed, v_s, with resistance, R, is the effective towing powerP_E. [4].

$$R = c_1 \cdot v_s^2 \tag{2-2}$$

$$P_E = R \cdot v_s = c_1 \cdot v_s^3 \tag{2-3}$$

The power delivered to the propulsor, P_D, is defined as the effective towing power, P_E, divided by the propulsive efficiency, η_D, as stated in equation 2-4.

$$P_D = \frac{P_E}{\eta_D} = \frac{(c_1 \cdot v_s^3)}{\eta_D} = c_2 \cdot v_s^3 \tag{2-4}$$

$$n_p = c_3 \cdot v_s \tag{2-5}$$

The relation between the power delivered to the propulsor, P_D, and shaft speed is known as the propeller law. From experience it is known that shaft speed is almost linearly proportional to the ships speed. With equations 2-4 and 2-5 it can be shown that the delivered power, P_D, is not only proportional to the cube of the ship speed but also to the cube of the shaft speed. This is also known as the propeller law and defined in equation 2-6

$$P_D = c_4 \cdot n_p^3 \tag{2-6}$$

The relation between the propulsion's engine brake power, P_B, and the delivered power to the propeller, P_D, can is defined in 2-7 [4]. The transmission efficiency, η_{TRM}, is the delivered power to the propeller divided by the delivered power by the propulsion motor. The shaft efficiency is equal to the transmission efficiency. The shaft loss is typically 0.5 to 1.0 percent at nominal power [4].

$$P_B = \frac{P_D}{\eta_{TRM}} = \frac{c_4}{\eta_{TRM}} \cdot n_p^3 \tag{2-7}$$

2.3.1 Load characteristics *Zwaardvis*

Relation between power and revolutions is measured by *HOLEC* [5] on board of the *Zr. Ms. Zwaardvis*. *HOLEC* is the manufacturer of direct current propulsion motors. The power revolutions curve is varying due to draught e.g. there is a difference between; surfaced, snorting and submerged and deep submerged. This is not included, only the submerged relation is used. The measurement data is illustrated in Figure 3.

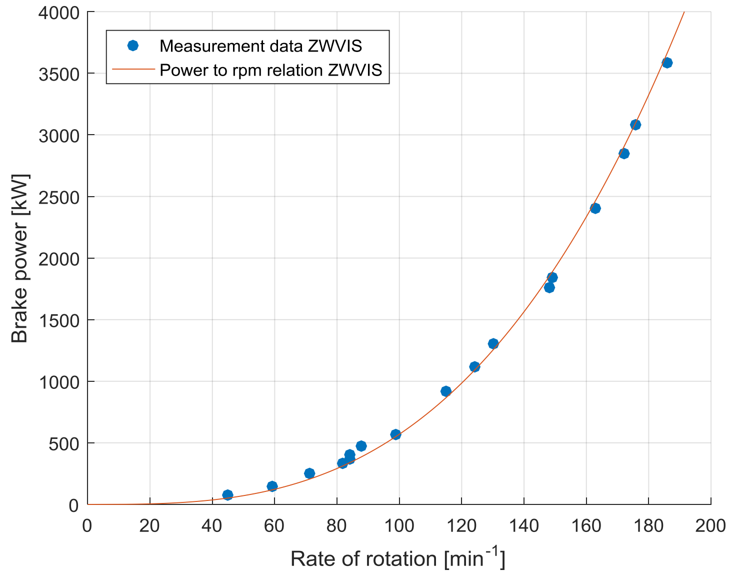

Figure 3 Power revolutions curve Zwaardvis

The relation stated in equation 2-7 defines the rate of rotation of the propeller as function of the propulsive power. The measurement data of *Zr. Ms. Zwaardvis* are used defining the relation between power and speed.

$$P_B = \frac{c_4}{\eta_{TRM}} \cdot n_p^3 = 123.12 \cdot n_p^3 \qquad \text{ref. 2-7}$$

The required brake power can be expressed as function of the prescribed submarine speed.

$$P_B = \frac{c_4}{\eta_{TRM}} \cdot n_p^3 = \frac{c_4}{\eta_{TRM}} \cdot (c_3 \cdot v_s)^3 \qquad \text{ref. 2-7 and 2-5}$$

$$P_B = (123.12) \cdot (c_3 \cdot v_s)^3 \qquad \text{ref. 2-5}$$

The value of c_3 can be obtained from the mission profile.

$$v_{s\,max} = 19\ [kn] = 9.77\ \left[\frac{m}{s}\right]$$

$$c_3 = \frac{n_p}{v_s} = \frac{3.10}{9.77\ [m/s]} = 0.315 \qquad \text{ref. 2-5}$$

$$P_B = (123.12) \cdot (0.315 \cdot v_s)^3 \qquad \text{ref. 2-7}$$

Resulting in an expression for the required propulsive power as function of the set speed.

$$P_B = (3.85) \cdot (v_s)^3 \qquad \text{2-8}$$

2.4 Conclusion

The mission profile prescribes the submarine speed and the auxiliary power demands for a period of time. The set submarine speed results brake power and rate of rotation using the properties of *Zr. Ms. Zwaardvis* as boundary conditions.

3 Propulsion plant concept configuration

3.1 Introduction

The propulsion plant requirements have been specified in the mission profile. The propulsion plant concept configuration has to meet the propulsion plant requirements. This chapter elaborates on the components of the propulsion plant. The first chapter is a general introduction into propulsion plants in submarines. The following chapters describe the concept propulsion plant configurations that are taken into account for the optimization.

3.2 Introduction into propulsion plants

The components in the propulsion plant are the diesel engine, the generator, the batteries, the propulsion motor and the propulsor. Stored chemical energy is converted into mechanical power by the main engine. The mechanical power is converted into electric power by the main generator, and the stored in the energy storage component. The energy storage component feeds the auxiliary users and the propulsion motor.

The function of the main diesel engine is to deliver mechanical power. This can be coupled mechanically to the propulsor or electric. In the case of diesel electric submarines, is the diesel generator set and is connected electrically connected to the propulsor by means of a propulsion motor. The propulsion motor is sometimes referred to main electric motor (MEM). The diesel engine needs oxygen for the combustion process. The oxygen is obtained from atmospheric air. Atmospheric air is not available during submerged operation; the submarine is an enclosed space. Consequently diesel engine power is not available. Stored energy in batteries is used to power the propulsion and auxiliary systems during submerged and surfaced operation. Figure 4 is a simplified representation of the propulsion plant installed on-board of *Zr. Ms. Walrus.*

Recharging of the batteries is done in snorting operation. During snorting operation the fresh air is supplied to the engine through a snorting system. The diesel engines creates an under pressure in the submarine. This under pressure causes airflow from the outside of the submarine to the engine room through the air intake system. Waves at the surface can cause the intake air snorkel valve to close, preventing water flowing into the engine intake.

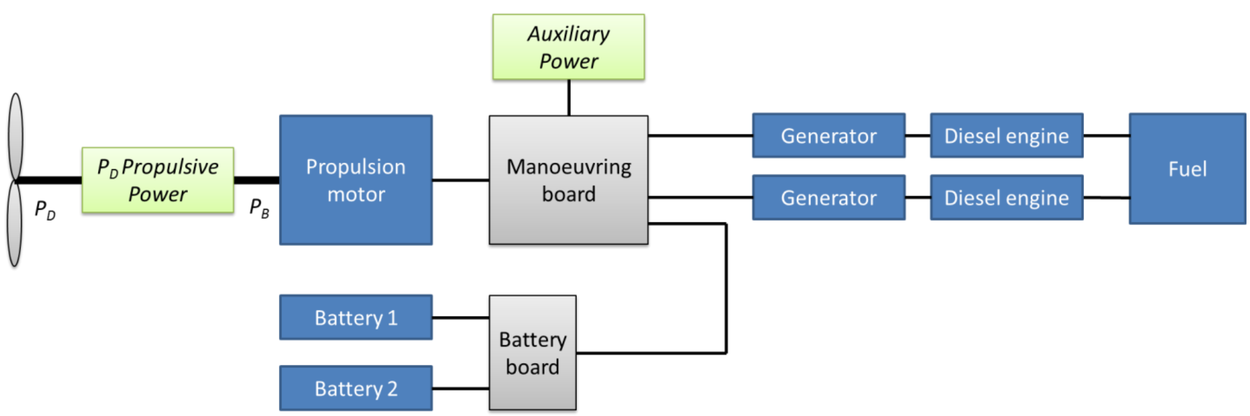

Figure 4 Propulsion plant

The function of the propulsion motor is to deliver rotating mechanical energy to the propulsor. It converts electric energy from an energy source to mechanical energy. The electric motor is designed to deliver the shaft power at top speed of the submarine. The speed of rotation of the rotor is equal to the speed of rotation of the shaft. The propulsion motor is usually arranged with the rotor directly coupled to the propeller shaft. Therefor the torque output of the motor needs to be similar to the requested torque of the propeller at full power. A gearbox is excluded because of acoustic aspects. The propulsor converts the rotating mechanical power into thrust to propel the ship.

The mission profile defines the submarine speed. The speed results in a required power to deliver to the propeller, P_D. Taking the shaft losses into account results in the required brake power, P_B. This is the required brake power to be delivered by the propulsion engine. The corresponding rate of rotation is obtained from equation 2-7.

The components that are taken into account for the determination of the optimum propulsion plant configuration are coloured in blue in Figure 4. Weight, volume, efficiency and the life cycle cost of the manoeuvring and battery board are not taken into account.

3.3 Concept propulsion plant configuration A

Conceptual system A is a conventional diesel electric-concept with lead-acid batteries. This concept is installed on board of the *Walrus-class* submarine. Figure 5 shows the energy flow diagram (EFD) of concept system A. An energy flow diagram is the chain of energy transfer and conversion from the energy source to the energy consumers. This configuration is installed on board of the *Walrus-class (Dutch design), Kilo-class (Russian design), 209-class (German design) and Moray-class* submarine.

Diesel oil is stored in diesel tanks. At or near the surface (snorting), diesel generator sets provide electric energy for the primary net. In the *Walrus-class*, this is a DC net from which energy is stored in lead-acid batteries. The electric conversion before the main *switchboard* (DC bus) consists of rectifiers which convert the AC-power generated by the generators to DC power. The propulsion motor is a dc-compound motor. The propulsion motor used in the current submarine class is a direct current compound machine. The direct current is obtained from the batteries. The electrical consumers are assumed to be the auxiliary load.

Other machine types as the brushless DC machines (BLDC) and the permanent magnet synchronous machines (PMSM) can be used in other concept configurations, but is not included in this research.

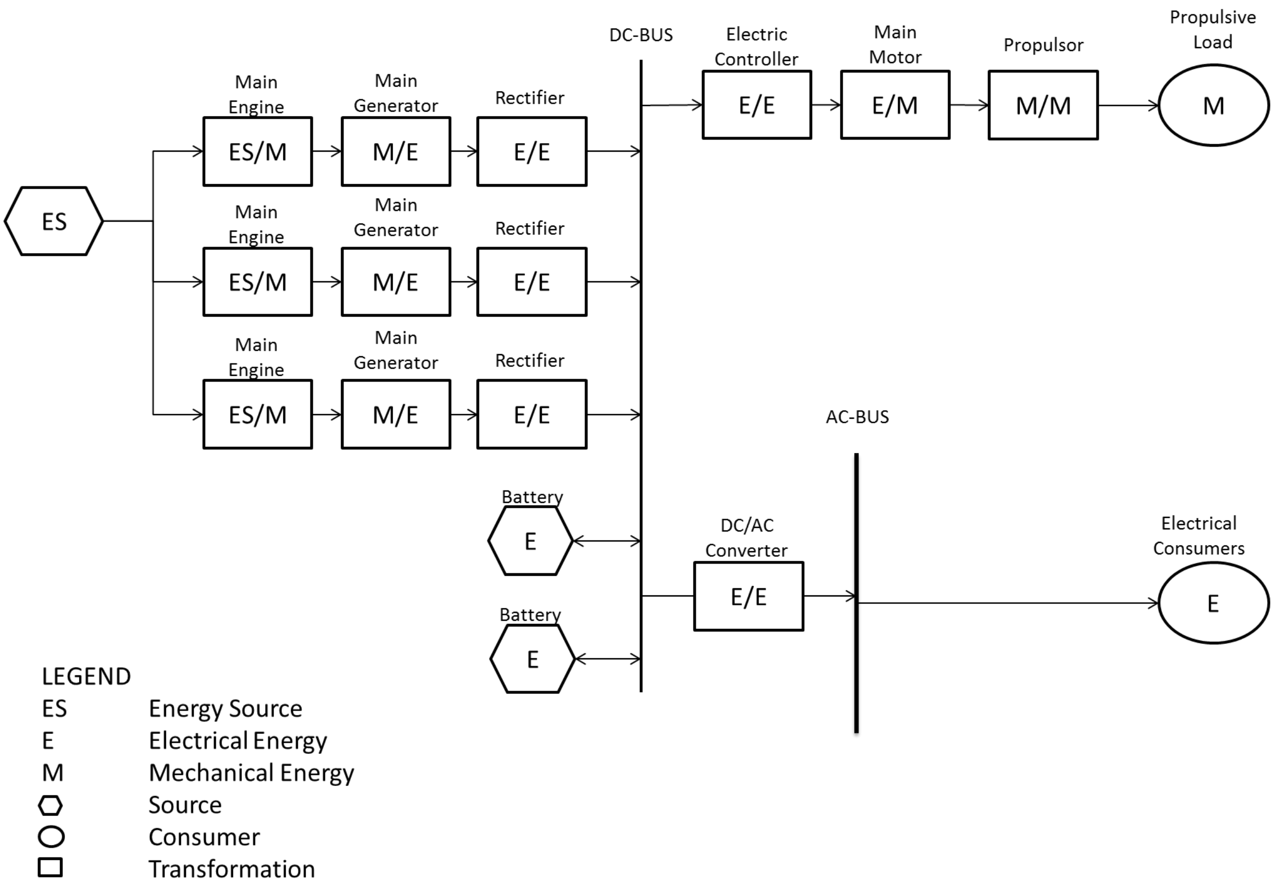

Figure 5 EFD concept system A [4]

Lead-acid batteries have been used as energy storage components in conventional submarines for more than 100 years. The technology has continuously improved and evolved to mature energy storage technology. The lead-acid battery uses lead dioxide as the active material of the positive electrode and metallic lead as the negative active material. The electrolyte is a sulfuric acid solution. As the cell discharges, both electrodes are converted to lead sulphate, the process reverses on charge.

The lead-acid submarine battery is specially designed for the submarine application. The cell design is optimized for high capacity and energy density. This is achieved by high specific gravity, electrolyte circulation, double cell decks arrangement, large areas with high porosity and a battery cooling system.

The battery capacity at low discharge currents is mainly determined by the amount and specific gravity of the electrolyte. At higher discharge rates, the electrolyte in the pore structure of the plates becomes depleted and the electrolyte cannot diffuse rapid enough to maintain the cell voltage. Intermittent discharge, which allows time for the electrolyte to circulate, or forced circulation in case of the submarine cells, improves high rate performance. [6]

Shock resistance and high safety standards are submarine specific design criteria. A shock absorber is included per cell, to reduce the impact on the battery cell components. The hydrogen produced during the recharging process is mechanically ventilated to the engine room and burned in the diesel engines.

Two batteries are used in concept configuration A. Two batteries are used for redundancy reasons. When one battery fails, the other battery is capable of delivering enough power for propulsion. Another reason for applying two batteries is voltage regulation. The voltage supplied to the propulsion motor can be regulated by switching the batteries in series and parallel. The switching enables to operate at maximum propulsion motor efficiency over the total power output.

The batteries consist of multiple cells. The cells are switched in series. Switching cells in series results in higher voltages while the battery capacity maintains constant. The high cell voltages are required to deliver enough voltage to the propulsion motor. Figure 6 illustrates submarine battery cells. The dimensions of the cells can be over a meter in height, and a single cell can weight more than 600 kg. Figure 7 is a picture of the battery cells in the *Tonijn.*

Figure 6 Examples of submarine battery cells [7]

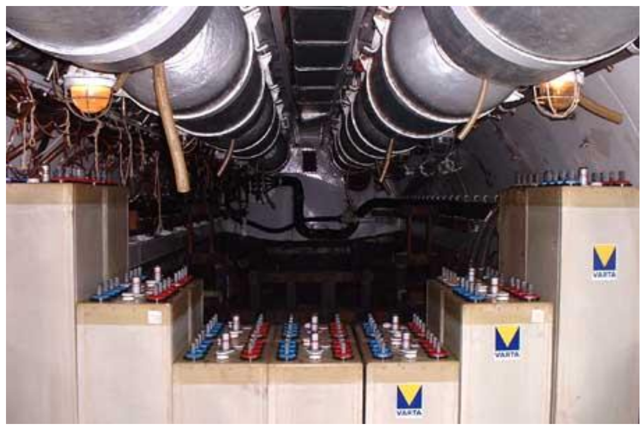

Figure 7 Multiple submarine cells forming a battery in the *Tonijn* [8]

Figure 8 is a cross sectional view of a submarine. The batteries are located under the lower deck, in the battery room. Figure 9 is a longitudinal cross-section of the battery room.

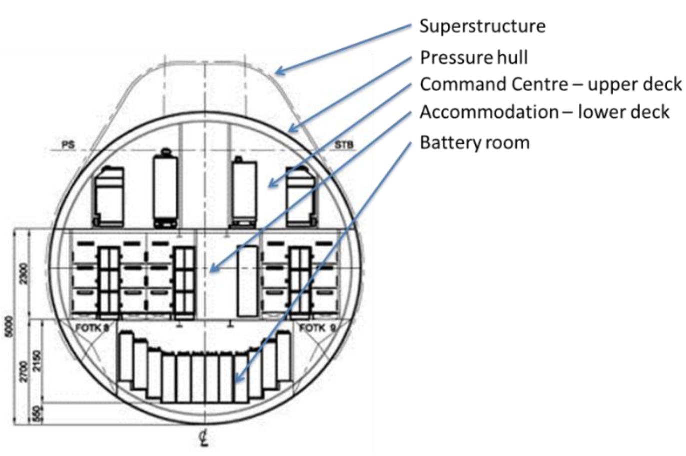

Figure 8 crossection of a submarine

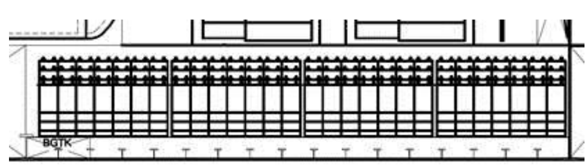

Figure 9 longitudunal section of the battery room

3.4 Concept propulsion plant configuration B

The energy storage component in propulsion plant configuration B is a Lithium-ion battery. Lithium-ion batteries dominate the market for cell phones, tablets, power tools and electric cars. This is due to the high energy densities and specific densities i.e. mass and volumetric properties of stored energy. A possible new application could be the source of energy in a submarine during submerged operation. Several submarine design institutes have claimed to use Lithium-ion technology in their designs [9] [10]. Literature of cell types and supporting technology is however not available. This chapter elaborates on the possibility to apply Lithium-ion storage technology to submarines.

Concept configuration system B is the Lithium-ion configuration. This configuration is applied in the Japanese *Soryu* class. The Japanese designers have chosen for the Lithium-ion technology instead of the lead-acid technology in combination with an AIP-system. [11] [12]

The term lithium-ion battery refers to a battery design where the anode and cathode materials serve as a host for lithium-ion. Lithium-ions intercalate into the anode during charging and into the cathode during discharging. The batteries consist of four primary functional components; the negative electrode, the positive electrode, the separator and electrolyte. The positive and negative electrodes are sandwiched between the negative and positive current collectors, separated by the separator. The liquid electrolyte is imbibed into the separator.

3.4.1 Energy density

The energy density can be expressed in volume and mass for all types of batteries, as illustrated in Figure 10. On the horizontal axis is the stored energy per litre, on the vertical axis is the stored energy per kilogram. High values indicate high energy storage capabilities per volume and mass.

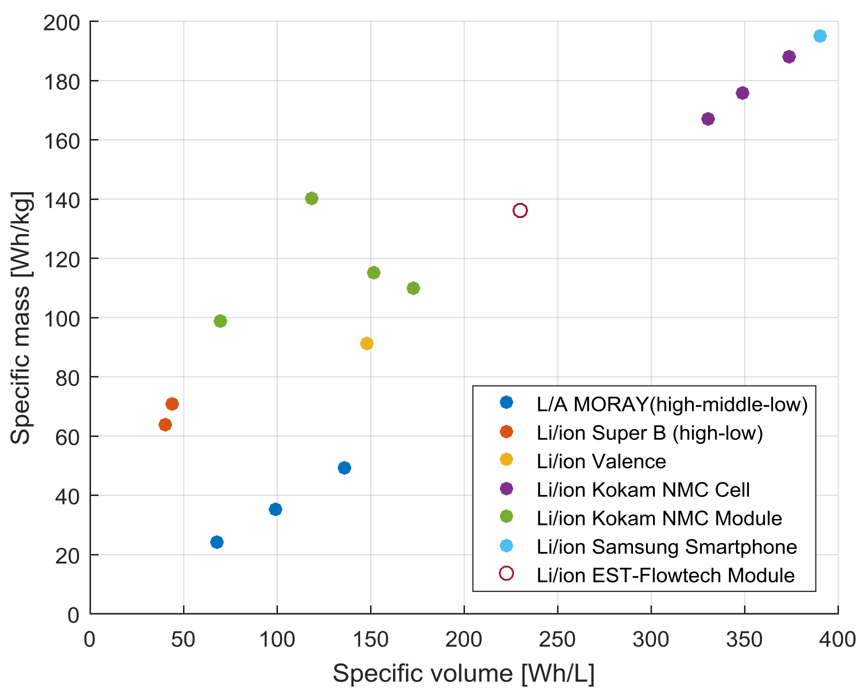

Figure 10 Energy density and specific density

The blue dots indicate the MORAY battery. The MORAY battery is a lead-acid type of battery, optimized for submarine application. The MORAY cell is produced by VARTA. The three dots represent one battery. The upper right dot is the capacity of the battery at low discharge current. Low discharge current mean a discharge time of the battery of 100 hours. The dot in the middle is the capacity at medium discharge time, 5 hours. The blue dot near the origin represents the capacity at 1.25 hours discharge time. The degradation of the capacity as function of the current is caused by the electrochemical process in the battery.

The red dots indicate the super B battery at high and low discharge times. The term high and low are not further specified by the manufacturer. The super B cell is a lithium-ion cell with a Lithium iron phosphate oxide ($LiFePO_4$) cathode. This cathode material is safer in terms of a thermal runaway, but results in a less energy dens battery design. Thermal runaway is an energetic failure of the battery. Cell thermal runaway refers to rapid self-heating of a cell derived from the exothermic chemical reaction of the oxidizing positive electrode and the reducing negative electrode. The more energy stored in a cell, the more energetic a thermal runaway reaction will be. One of the reasons a lithium-ion cell thermal runaway reaction can be very energetic is because the cells have a very high energy density compared to other cell types for example lead-acid. The electrolyte of a lithium-ion cell behaves fundamentally different than the water-based electrolyte in the lead-acid cell. The electrolyte is flammable at high temperatures. So the cell has electric energy stored and chemical energy in the form of combustible materials. The deviation in specific density and energy density at high and low discharge times is not as large as for the lead-acid battery. The cell stores more energy per kilo then the lead-acid cell, but it requires more volume. This can be explained by the addition of a battery management system (BMS) and a hard casing. The battery management system monitors the state of charge of the cell and the state of health, to prevent thermal runaway. Figure 11 is a representation of the Super B module. The Super B cell is not further investigated. It can be concluded on advance that the volume of the battery is larger with respect to the lead-acid battery whatever the mission profile is.

The yellow dot is a Valence battery. The battery is also equipped with a BMS, but has a less rigid and thus lighter protective casing compared to the super B battery. The battery is illustrated in Figure 12.

Figure 11 Super B module [13]

Figure 12 Valence module [14]

The purple dots represent a lithium polymer cell, for high-middle-low discharge capacity. The material in the cell used in NMC. (NMC = NiMnCo) cell which means, no protective casing, no cooling and no battery management system. The green dots are modules that contain multiple polymer cells. The module has a BMS, cooling applications, and a casing. These additions result in significantly less performance properties, compared to the single cell.

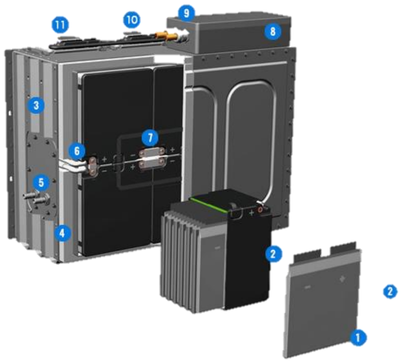

Figure 13 Lithium-ion Rack of multiple modules [15]

1. Cell
2. Module
3. High-strength battery tray
4. Thermal insulation
5. Coolant connection
6. Coolant connector
7. Electric connectors
8. Main contactor box
9. High voltage connection
10. BMS
11. Safety control unit

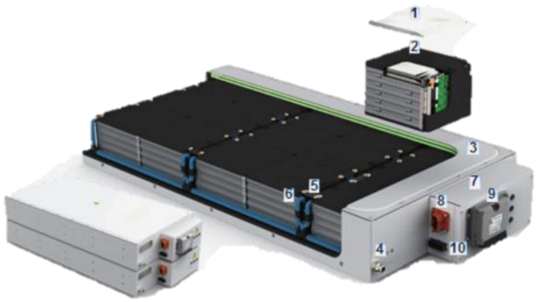

Figure 14 Lithium-ion battery module [15]

1. Cell
2. Module
3. High-strength battery tray
4. Thermal insulation
5. Coolant connection
6. Coolant connector
7. Electric connectors
8. Main contactor box
9. High voltage connection
10. BMS

The light blue dot in the top right corner of Figure 10 is a single Samsung cell smart phone battery cell. The smartphone cell is optimized for low discharge currents of mille Amperes (10^{-3} [A]). The currents that are required for submarine application are in the range of several kilo Ampere's (10^{3} [A]). Therefore, smartphones cells cannot be used in a submarine as they do not meet the requirements.

The batteries of interest are the optimized lead-acid batteries and the single lithium-ion cell. The VARTA cell is a battery optimized for submarine application and a mature technology. The lead-acid technology has been further improved from 1992 up to now, resulting in a higher energy density and specific energy. The VARTA cell is used in concept system configuration A. This data is the most recent available non-classified data.

The single lithium cell performs superior compared to Lithium-ion modules and lead-acid batteries. The packing of a single cell into a module decreases in particular the volumetric properties. The open red dot is the energy density that possible can be achieved for submarine specific design. This lithium cell is used on concept system configuration B. This value is obtained during conversations with the supplier of the modules; EST-Flowtech.

The high energy capacity of the lithium cell provides opportunities, but the high energy is also a potential danger. Several incidents have occurred with Lithium-ion batteries [16] [17] [18]. The galaxy Note 7 is the latest known accident [19]. The batteries become overheated, resulting in thermal runaway.

3.5 Summary concept configuration

The two concepts are illustrated in Table 1 Concept configuration systems

Table 1 Concept propulsion plant configurations

Concept system configuration	Power generation	Energy storage Technology	Propulsion motor
Concept configuration A	Diesel generator power	Lead-acid	DC machine
Concept configuration B	Diesel generator power	Lithium-ion NMC	DC machine

4 Methodology description

4.1 Introduction

The research question is stated as: What is the optimum propulsion plant configuration for the replacement of the Walrus-class submarine given an assumed mission profile? This chapter describes the methodology that is used to determine the efficiency, weight and volume of the concept propulsion plant configurations as function of the assumed mission profile.

The approach is illustrated in Figure 15. The mission profile is the input, the efficiency, weight, volume and LLC are the output. The different propulsion plant concept configurations are parallel in the middle in the figure. The concepts are modelled and optimized, resulting in the properties of the components. The properties of the components are the weight, volume and efficiency. The total weights and volumes of the components result in the propulsion plant configuration weights and volumes. The efficiency is obtained with the simulations of the total propulsion plant.

The different propulsion plant configurations are modelled. The modelling of the propulsion plant is done by modelling the different components and connects the components to form the propulsion plant model. The different components have their own technical parameters. The technical parameters are used in the models. The performance of the components and the interaction with the connected components can be simulated with the models and parameters.

The propulsive and auxiliary power demand affects the performance of the components. The technical parameters of the components can be changed to improve the performance. The changing of the parameters and results in different component properties; efficiency, weight and volume. The properties of the components result in the total propulsion plant efficiency, weight, volume and life cycle cost.

The optimum propulsion plant is the plant that meets the mission profile with the minimum required weight and volume, highest efficiency and lowest life cycle cost. This chapter describes the methodology that is used to come to the four outputs given a mission profile.

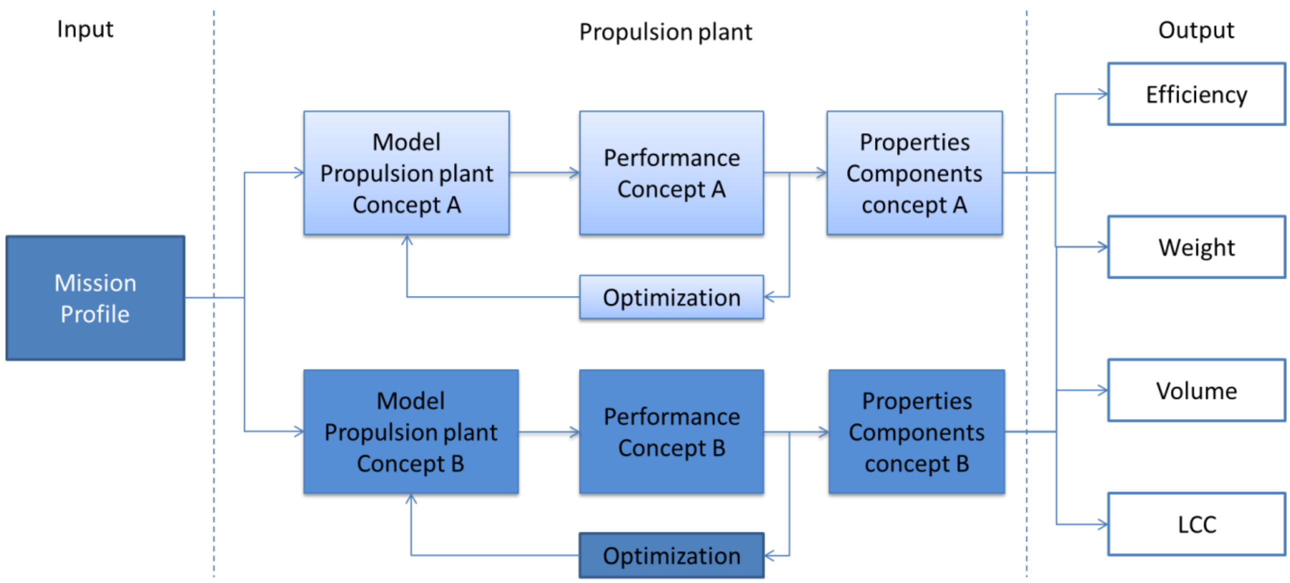

Figure 15 System approach

4.2 Methodology

The mission profile contains the required information to dimension the propulsion plant. The components; propulsion motor, battery and diesel generator set have the mission profile as input. Besides the mission profile the first principles, technical parameters and boundary conditions are required to define the efficiency and components volume and weight. The first principles modelling is said to be a modelling starting from the established laws of physics. The technical parameters are used to supplement the first principle models and optimize the volume, weight and efficiency.

The propulsion motor is dimensioned for the required maximum brake power. The maximum brake power is required during the surveillance and attack phase. More specific, in the case of the mission profile defined in chapter 0, during period SA4 in Figure 2.

The battery efficiency and dimensions are depending on the longest set period without recharging the batteries. This period is the surveillance and attack phase indicated in Figure 2. The propulsive and auxiliary load act on the batteries. The optimization is done using a battery optimization algorithm. The objective of the battery mass optimization algorithm is to find the optimum battery mass. The optimum battery mass is defined as the lowest battery cell mass that meets the set requirements. The battery mass is the battery mass per cell times the required number of cells. It is assumed that the battery volume is linear dependent on the battery mass. Finding the optimum battery mass results in finding the optimum battery volume.

The volume, weight and efficiency of the diesel generator set are dependent on the required generator output power. The generator output power is dependent on (3) inputs. (1) The first principles, technical parameters and boundary conditions associated to the diesel generator set. (2) The optimized battery layout and battery performance model, as the charge current is a function of the battery voltage. (3) The propulsion motor performance model with the associated parameters. The propulsion motor delivers power during the covert transit. The charging power of the batteries is the generator power minus the propulsive power. The required diesel generator set power output is obtained with performance simulations of the propulsion plant.

The required diesel fuel to complete the mission is the result of all the mentioned components and the mission profile. Figure 16 illustrates the relations between the mission profile and the components. The following subchapters elaborate on the methodology that is applied per component.

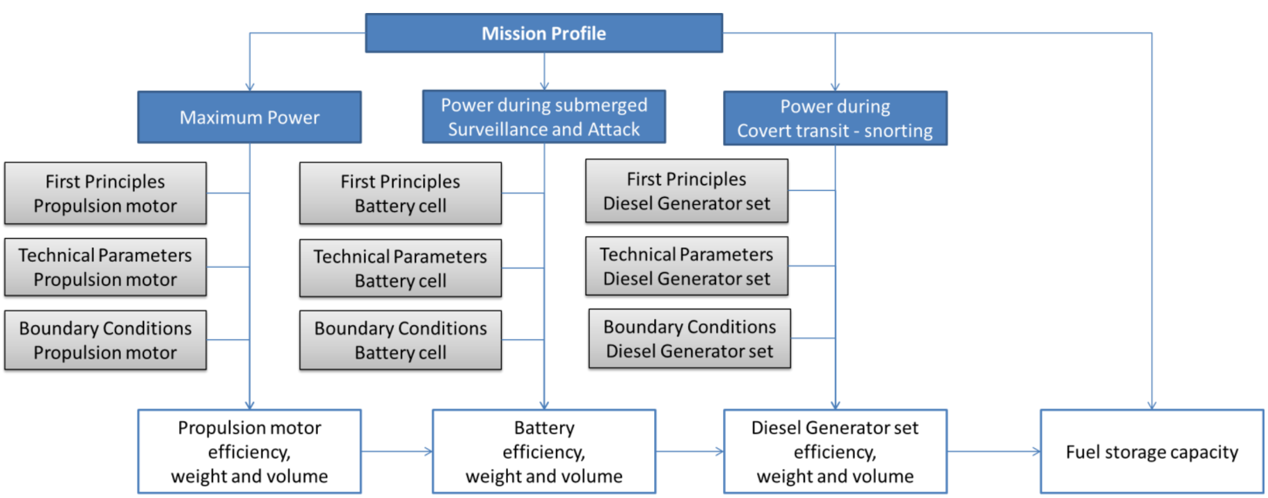

Figure 16 Calculation flow

4.2.1 Propulsion motor performance model and dimensions

There are two models required to determine efficiency and the dimensions of the propulsion motor. The dimensions, expressed in weight and volume are determined with a first principle dimension prediction model. The efficiency is simulated with a propulsion motor performance model.

The propulsion motor performance model is used to simulate the performance of the propulsion motor for varying loads and available battery voltages. The propulsion motor model is developed by D.M. Meuldijk [20] at the NLDA. This quasi-static performance model is based on first principles. The input of the propulsion model is modified to meet the properties of the output of the mission profile, the requested propulsive power at the related rate of rotation. With the boundary conditions related to *Zr. Mr. Zwaardvis.*

The propulsion motor dimensions are determined with a dimension prediction model. The idea behind first principle dimension prediction is that the dimensioning of the propulsion motor, and other electric machines, can be estimated by sizing the core of the machine to the required power output using first principles [21]. The core consists out of primary and secondary elements. The primary element of the propulsion motor is the rotor. In the rotor electric energy is converted into mechanical energy. The secondary element is the stator. The machine dimensions can be obtained by multiplying the core dimensions, times a correction factor. The correction factor is obtained using regression analysis.

The relation between the dimensioning model and the performance model are the rotor dimensions. The rotor dimensions are a part of the technical parameters. Other technical parameters are for example the number of windings and the air gap between rotor and stator. Figure 17 is a schematically representation of the propulsion motor dimensioning and efficiency as function of the mission profile.

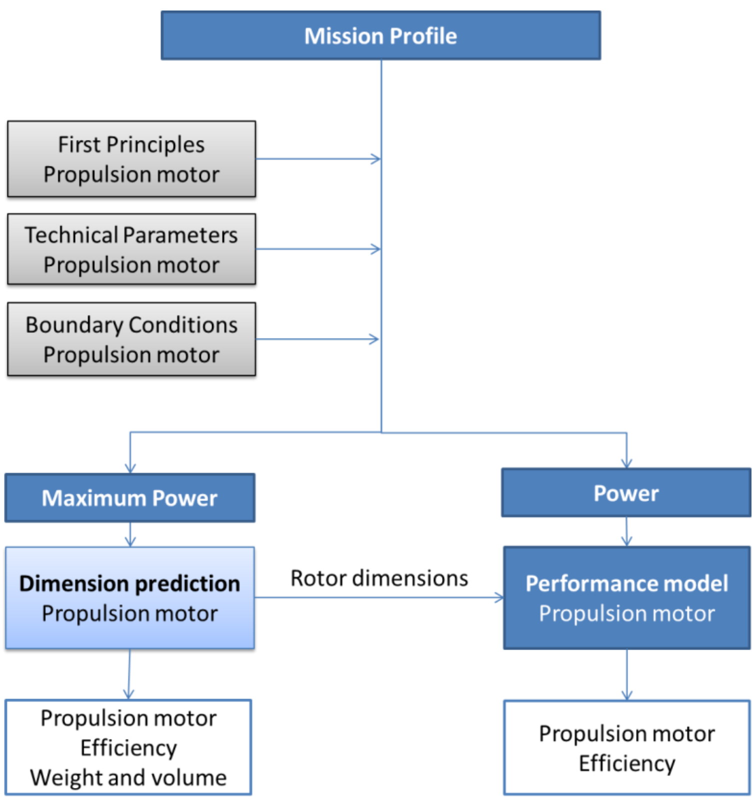

Figure 17 schematically representation of the propulsion motor weight, volume and efficiency as function of the mission profile

Available measurement data of a similar propulsion motor has been made available. The measurement data is used and compared to the simulation results of the performance model. Numerical simulation and experimental results show relative good agreement and justifies the use of the performance model for the simulation of the discharge current and efficiency. Chapter 0 elaborates on the propulsion motor performance, verification and dimension prediction model.

4.2.2 Battery performance model and dimensions

The required stored energy capacity of the batteries is determined by the current demand of the propulsion motor and the auxiliary consumers, during the surveillance and attack phase of the mission. This is the longest period without recharging to reduce the risk of exposure. The energy flow diagram of the concept configuration propulsion plants during the surveillance and attack part of the mission is illustrated in Figure 18.

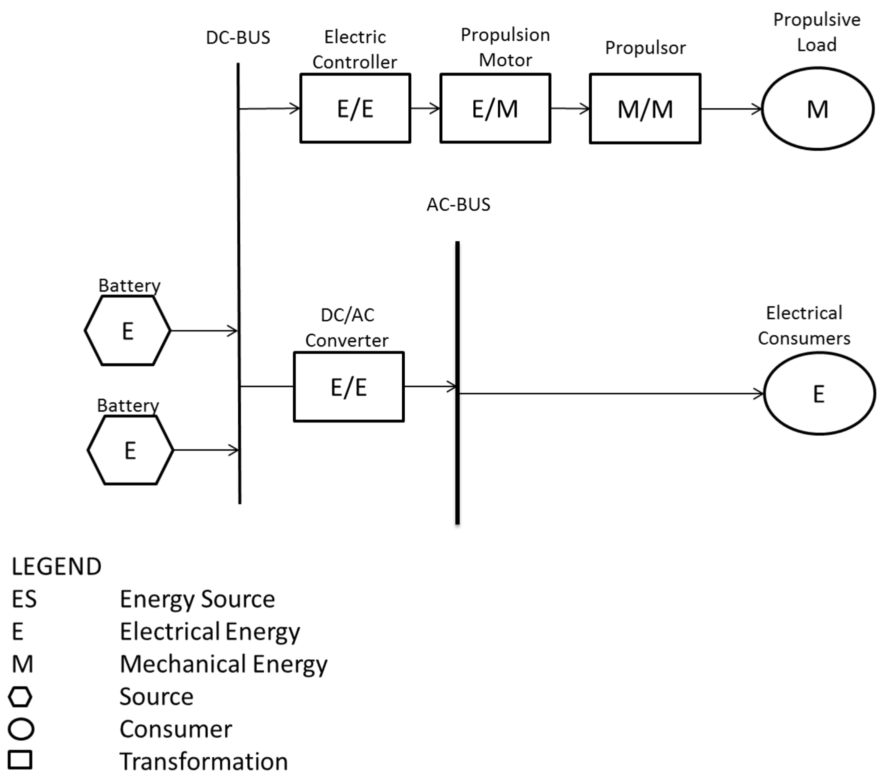

Figure 18 EFD Surveillance and attack phase

The battery cell performance model is developed by D. Stapersma [22]. The model can be considered as voltage source with an energy capacity. The models input are the charge or discharge current, the output of the model is the cell voltage. Data of the manufacturer of the battery cells is available and is used to supplement the battery cell constants resulting in an accurate performance model.

For the dimensioning of the battery size are the verified propulsion motor performance model and the verified battery cell performance model used. A schematic overview of the relation between the models is illustrated in Figure 19. The propulsive power, rate of rotation and the available battery voltage are the input for the propulsion motor performance model. The output of the performance model is the discharge current and propulsion motor efficiency.

The propulsion motor is not directly coupled to the batteries. According to Figure 4 are the battery board and manoeuvring board in between the propulsion motor and the batteries. In the simulation are the manoeuvring-, and battery board modelled as the switchboard. The switchboard connects the two components. The switchboard model has two functions. The first function is the switching of the batteries and armatures of the propulsion motor in series and parallel. The second function is the calculation of the dis-, charge current at battery cell level. The moments of switching are optimized for propulsion motor efficiency. The cells are connected in series to form a battery. The battery voltage is dependent on the number of battery cells in series. It is assumed that the cells in the battery have the same behaviour, independent of their position in the battery. The battery voltage has influence on the propulsion motor performance, and is connected to simulate their performance.

The optimization of the battery mass is done using a battery optimization algorithm. The objective of the battery mass optimization algorithm is to find the optimum battery mass. The optimum battery mass is defined as the lowest battery cell mass that meets the set requirements. The battery mass is function of two variables. (1) The number of cells and (2) the mass per cell. The numbers of cells in series define the battery voltage and the mass per cell defines the available capacity per cell. Larger batteries have more stored capacity compared to smaller batteries. These two variables cannot be seen separately.

As the number of cells increases, the voltage of the battery increases. This affects the discharge current from the propulsion motor and the discharge current of the auxiliary load. The discharge current and efficiency of the propulsion motor are modelled in the propulsion motor performance model. Lower discharge currents result in lower battery cell capacity. The battery cell performance and capacity as function of the discharge current cell is modelled in the battery cell performance model. The battery performance is a function of three functional dependencies. (1) The battery capacity as function of the discharge current. (2) The open cell voltage as function of the pseudo discharge state and (3) the pseudo resistance as function of the pseudo discharge state [22]. The required cell capacity results in the battery mass. Varying the number of battery cells result in the optimum battery mass.

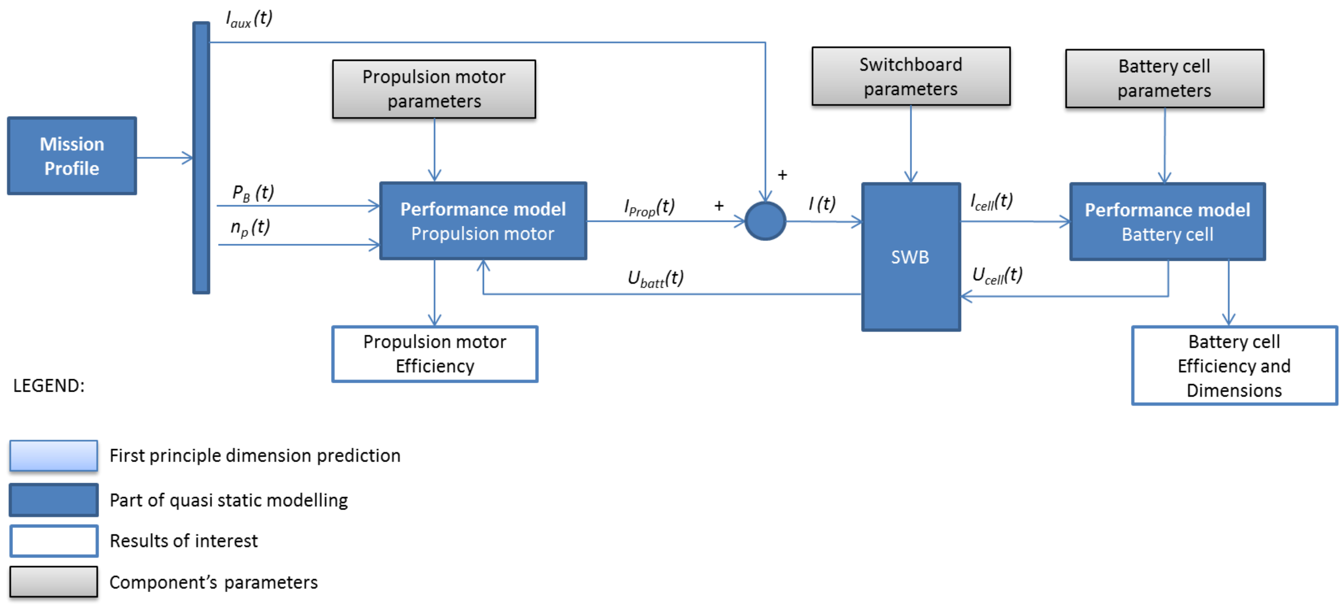

Figure 19 Propulsion plant model during submerged operation

4.2.3 Main Generator and Diesel engine dimensions and efficiency

The methodology that is used to determine the generator power is illustrated in Figure 20. The input is the mission profile. From the mission profile the performance requirements are obtained. These are the propulsive power and auxiliary power during the snorting and deep submerged operation and the given indiscretion ratio. These requirements are the input for the performance model of the propulsion plant. The power is limited by the maximum cell voltage during charging. The cell voltage may not exceed 2.45 [V] [23]. The cell voltage is a function of the charge current. The used battery model simulates the cell voltage during the charging.

The calculated generator power is the input for the dimensioning of the generator and the propulsion plant performance simulations. The propulsion plant performance is expressed in the fuel efficiency.

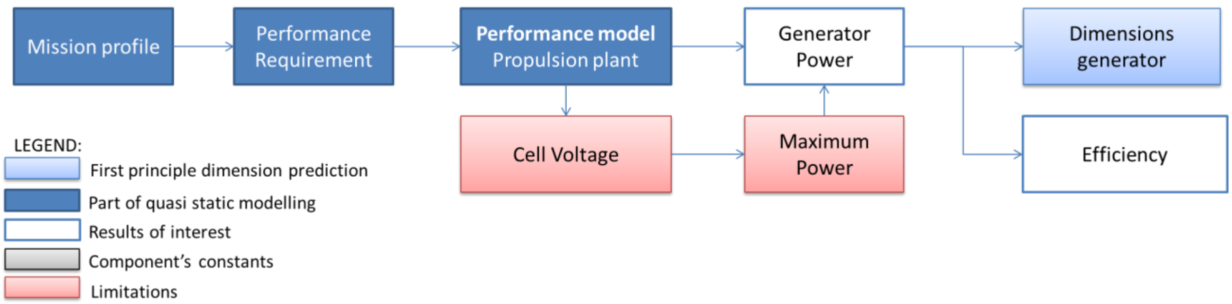

Figure 20 calculation methodology generator power output

The propulsion plant performance model is illustrated in Figure 21. This is the same model as illustrated in Figure 21 with in addition the diesel generator model. The generator output power is divided by the available battery voltage. The result is the generator current, I_{gen}. The discharge current and the generator current result in the battery current. Depending on the sign is the current charging or discharging.

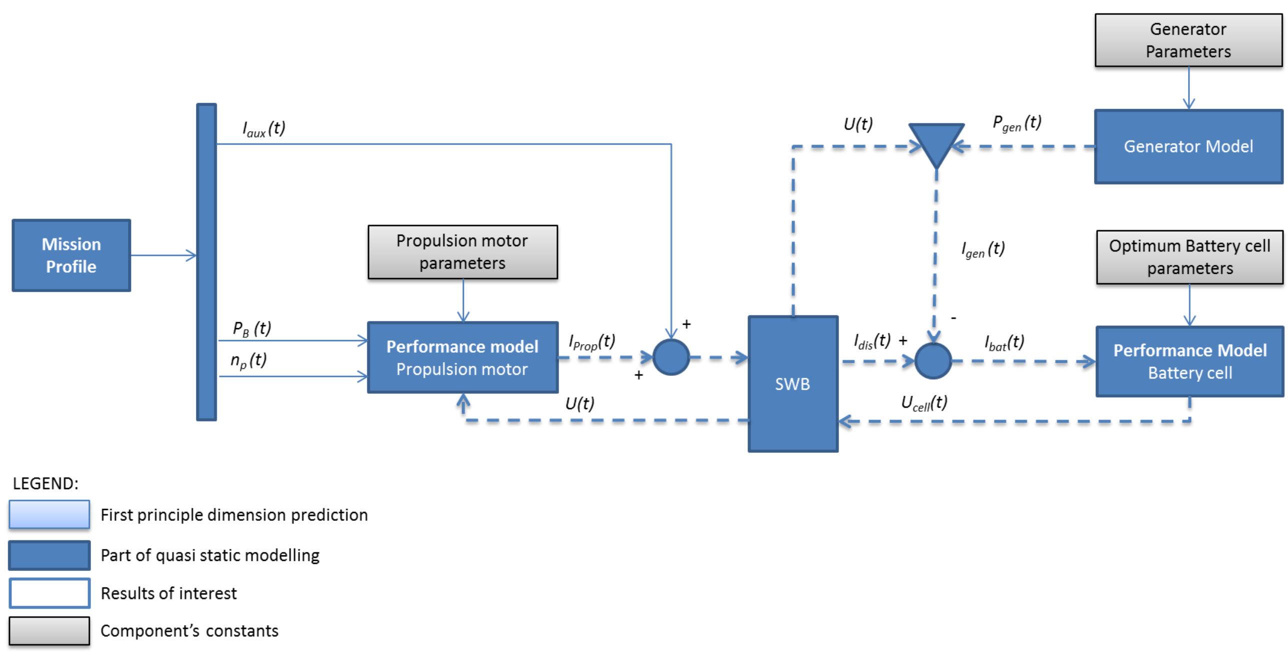

Figure 21 Propulsion plant performance model

The result of the generator power is the input for the dimension prediction of the main generator(s). The required power output of the main engine is dependent on the required mechanical power input of the generator. The dimension prediction of the diesel engine and generator are done using first principle dimension prediction. The optimum diesel generator weight, volume and efficiency are obtained by comparing the results of dimension prediction for various diesel generator set configurations.

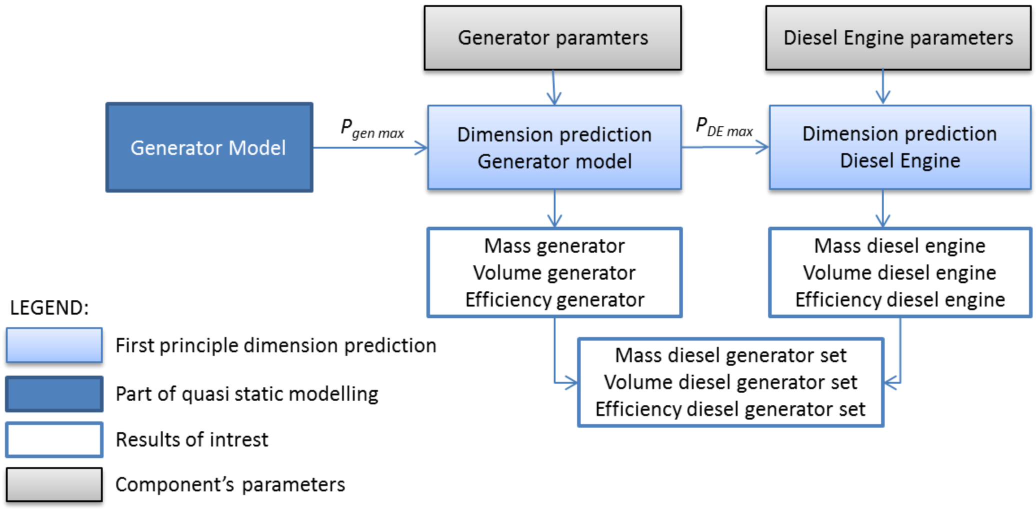

Figure 22 Optimization of the dimension of the diesel generator set

4.2.4 Diesel fuel tank capacity

The required diesel oil storage capacity is obtained with a simulation of the total assumed mission profile. The snorting time and the specific fuel consumption results in the required full tank capacity.

5 Propulsion motor performance model and dimensions

5.1 Introduction

The research question defines the optimum as the optimum propulsion plant configuration in weight, volume efficiency and LCC. The weight of the propulsion plant configuration is defined as the weight of the components. This chapter elaborates on the weight, volume and efficiency of the propulsion motor.

There are two types of models required to answer the research questions. (1) A propulsion motor performance model. The results of interest of the model are the efficiency and the discharge current. Efficiency is explicitly defined in the research question. The discharge current is a result of interest because the current need to be supplied by the battery. (2) A dimensioning prediction model. The purpose of the propulsion motor dimension prediction model is to predict the dimensions, expressed in weight and volume, as function of the maximum set output power at a given revolutions rate.

The relation between the dimensioning model and the performance model are the rotor dimensions. The rotor dimensions are a part of the motor parameters used in the performance model. This chapter elaborates on those two models, the relation between the two models and the results of the simulations.

5.2 Propulsion motor performance model

The DC propulsion motor is attractive on warships and submarines for the low vibration level, which is beneficial for the low underwater signature. [4] There are three possible types of DC motors which can be used for the propulsion of a submarine; series motor, shunt-motor and a compound motor.

- In a dc-series motor, the field windings are connected in series with the armature windings;
- In a dc-shunt motor, the field winding is connected in parallel with the armature circuit;
- In a dc-compound motor both shunt- and series-field windings are applied. The resulting field is a combination of the contribution of the two windings. See Figure 29 for the schematic overview.

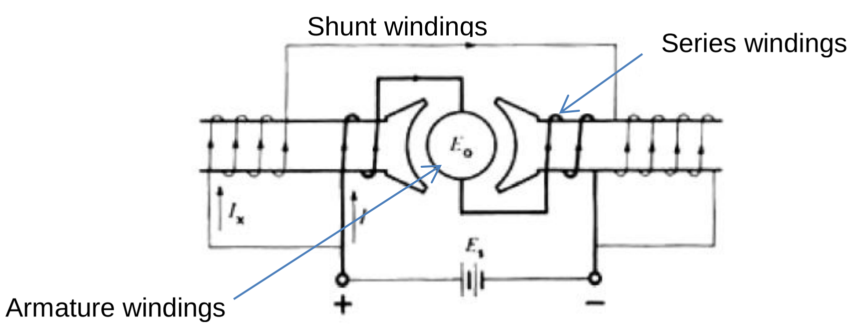

Figure 23 Series and field windings of a DC-compound motor (cumulative)

The propulsion motor of the concept systems configurations is a dc-compound motor. The selection of the propulsion motor is based on the benefits of the two types of windings that are applied. The series motor torque-speed characteristic can be obtained by reducing the current in the shunt windings, resulting in a maximum torque at no load. The advantage of the shunt motor is the no-load speed, the motor can rotate at no-load and go smooth into generator mode. The propulsion motor of the concept systems configuration motor cannot fully behave as a shunt motor as the current in the series windings cannot be reduced without reducing the armature current. [24].

The field windings of a dc-machine are placed in the stator and the armature windings are mounted on the rotor. A dc current is passed through the field windings, see Figure 24. The current produce an air gap flux in the d-axis, shown in Figure 26.

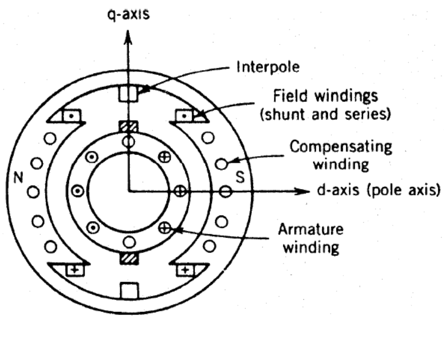

Figure 24 Cross section of a dc-machine [25]

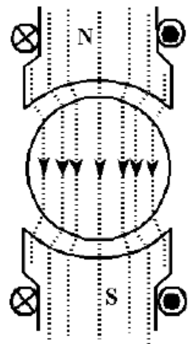

Figure 25 Flux created by the shunt and series windings d-axis [20]

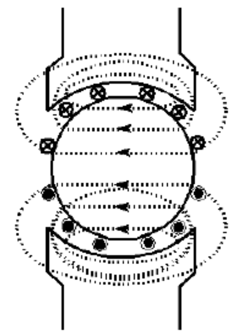

Figure 26 Flux created by the armature windings q-axis [20]

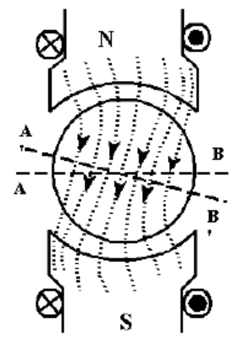

Figure 27 Resulting flux of the field and armature windings [20]

The equivalent circuit of a dc-compound machine is shown in Figure 28. An equivalent circuit is a simplified representation of the system, while the electric characteristics are retained. There are two separated circuits; the shunt field windings and the armature with the series windings. The voltage equations can be obtained from the equivalent circuit. The constant terms illustrated in the equivalent circuit are specified in Table 2 List of Symbols.

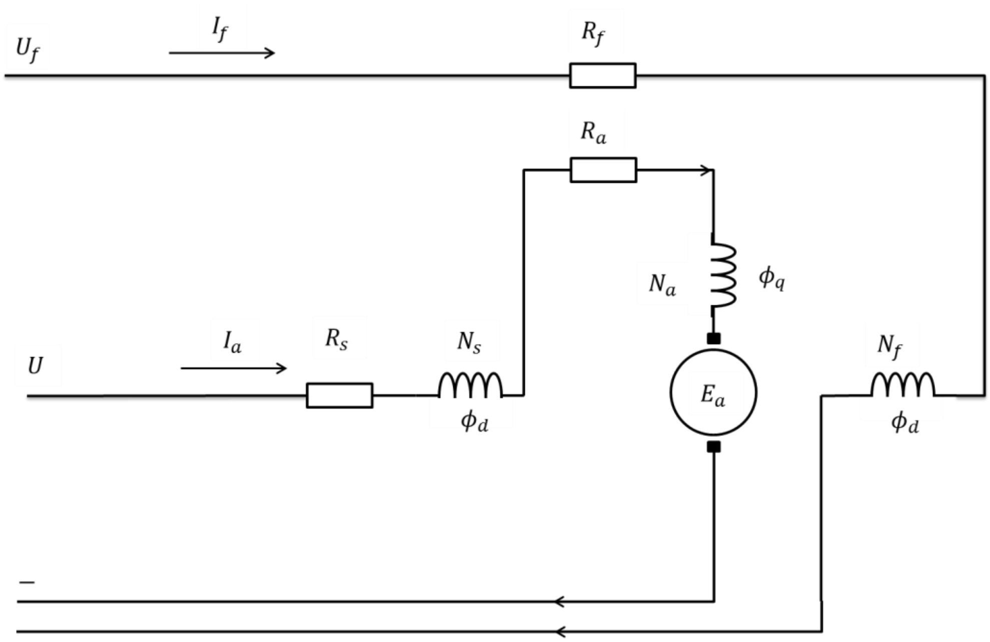

Figure 28 Equivalent circuit DC compound propulsion motor [20]

Table 2 List of Symbols

Symbol	Description
U	Armature voltage
U_f	Shunt field voltage
I_a	Armature current
I_f	Shunt field current
N_f	Number of shunt windings
N_s	Number of series windings
N_a	Number of armature windings
R_f	Shunt windings resistance
R_s	Series windings resistance
R_a	Armature windings resistance

The shunt and series windings have a contribution to the d-axis, while the compensating and armature winding have a contribution to the q-axis. This equation is set up by D.M Meuldijk. [20]

$$\begin{cases} U_f = R_f \cdot I_f + N_f \dfrac{d\phi_d}{dt} \\ U = (R_a + R_s) \cdot I_a + N_s \dfrac{d\phi_d}{dt} + N_a \dfrac{d\phi_q}{dt} + E_a \end{cases} \tag{5-1}$$

The equivalent circuits re-written in differential equations: [20]

$$\begin{cases} \dfrac{d\phi_d}{dt} = \dfrac{1}{N_f} \cdot \left(U_f - R_f \cdot I_f\right) \\ \dfrac{d\phi_q}{dt} = \dfrac{1}{N_a} \cdot \left(U - (R_a + R_s) \cdot I_a - \dfrac{N_s}{N_f} \cdot \left(U_f - R_f \cdot I_f\right) - E_a\right) \end{cases} \tag{5-2}$$

The differential equations are used to construct a block model in MATLAB/Simulink. For this model are the Maxwell second law, also known as Faraday's law. The contour integral of the electric field intensity is equal to the derivative of the surface of the magnetic flux density.

$$\oint_C \bar{E}\, \overline{dl} = -\frac{d}{dt} \iint_S \bar{B} \cdot \overline{dA} \tag{5-3}$$

The left half of the equation is the contour integral of the electric field intensity. This is equal to the integral of the current density times the electric resistance minus the voltage.

$$\oint_C \bar{E}\, \overline{dl} = \int \rho_{Cu} \cdot \bar{J} \cdot \overline{dl} - u = \int_{lCu} \rho_{Cu} \cdot \frac{i}{A_{Cu}} \cdot dl - u = R \cdot i - u \tag{5-4}$$

The derivative of the surface of the magnetic flux density can be written as:

$$-\frac{d}{dt} \iint_S \bar{B}\, \overline{dA} = -\frac{d\lambda}{dt} = -N \frac{d\phi}{dt} = E_a \tag{5-5}$$

The power and torque for a DC motor is expressed by equation 5-6, [4] [25] Where Z_a is the number of armatures, and ω_m is the mechanical frequency in rad/second.

$$\begin{pmatrix} 0 \\ 0 \\ T_{MEM} \end{pmatrix} = \begin{pmatrix} K_a \cdot \phi_d \\ K_a \cdot \phi_q \\ 0 \end{pmatrix} \times \begin{pmatrix} I_{ad} \\ I_{aq} \\ 0 \end{pmatrix} \tag{5-6}$$

$$T_{MEM} = (K_a \cdot \phi_d \cdot I_{ad} + K_a \cdot \phi_q \cdot I_{aq})$$

$$T_{MEM} = (K_a \cdot \phi_d \cdot I_{aq})\, Z_a = (K_a \cdot \phi_d \cdot I_a)$$

As illustrated in Figure 26 is there only a contribution in the q-axis induced by the armature current. Resulting in equation 5-7.

$$P_{MEM} = T_{MEM} \cdot \omega_m \cdot Z_a \tag{5-7}$$

5.2.1 Propulsion motor efficiency

This chapter explains the effect of a fluctuating armature voltage on the efficiency. The losses of the MEM are divided in three components. (1) The losses in the rotor due to the magnetization and demagnetization. (2) The losses in the series circuit due to the series and armature resistance and (3) the losses in the shunt circuit due to the shunt resistance.

5.2.1.1 Rotor losses

The rotor losses due to the magnetization are defined and modelled by D.M. Meuldijk [20], also known as Eddy current losses. Where ω_e is the electric frequency, which is defined as $\omega_e = p \cdot \omega_m$ and ω_m is the mechanical frequency? V Is the volume of the iron in the rotor. ρ Is the specific electric resistivity, B is the amplitude of the flux density. At constant power and constant frequency, it can be stated that:

$$P_{losses\ rotor} = \frac{V}{24 \cdot \rho} \cdot \left(\omega_e \cdot \Delta \cdot \hat{B}\right)^2 \tag{5-8}$$

$$P_{losses\ rotor} = K_v \cdot \omega^2 \cdot \hat{B}^2 = f(B) \tag{5-9}$$

5.2.1.2 Resistance losses

The power losses due to the resistance can be written as equation 5-10 and 5-11. Where I_a is the armature current and I_f is the shunt current, and so is R_a the armature resistance, R_s the series resistance and R_f the shunt resistance.

$$P_{losses\ series} = I_a^2 \cdot (R_a + R_s) \tag{5-10}$$

$$P_{losses\ shunt} = I_f^2 \cdot (R_f) \tag{5-11}$$

5.2.1.3 The overall efficiency

The overall efficiency is the sum of the losses and a function of the power and battery voltage.

$$\eta_{MEM} = \frac{P_{MEM}}{P_E} = \frac{P_{MEM}}{P_{MEM} + P_{Losses}} \tag{5-12}$$

5.3 Performance model motor controller

The propulsion motor is for redundancy reasons composed of two identical the same halves. Both armature halves are separated from each other by means of a partition, which acts as a fire shield. To realize variable speed in the system, the selection of the two main batteries and the two armatures of the MEM are done by switching them in parallel and series and controlling the current by the shunt field chopper. Speed control is achieved by field weakening with the with the shunt field choppers in the slow, cruise and high mode. Field weakening is the reduction of the magnetic flux. For dead slow speed (2-5 kn) a third chopper across the armatures is available, this chopper can be considered as variable voltage source. The armature chopper in combination with the shunt field chopper ensures a high efficiency in the dead slow mode. [26] The chopper is not used in the armature circuit because of noise. The switching of the armature circuit would involve high currents and therefor high noise [4]. For redundancy there are two shunt field choppers, one in operation, one stand-by.

5.3.1 Modes of operation

There are 4 modes of operation. The lowest speed is dead slow speed. The MEM armatures are switch in series with parallel switched shunt fields in dead slow settings and controlled by one of the two shunt field choppers. The armature chopper is a second controller to control the armature voltage. [27] The layout is illustrated in Figure 29. In the slow speed condition both MEM armatures are in series, and the batteries are switched in parallel. The speed is controlled by one of the shunt field choppers, as illustrated in Figure 30. [27]

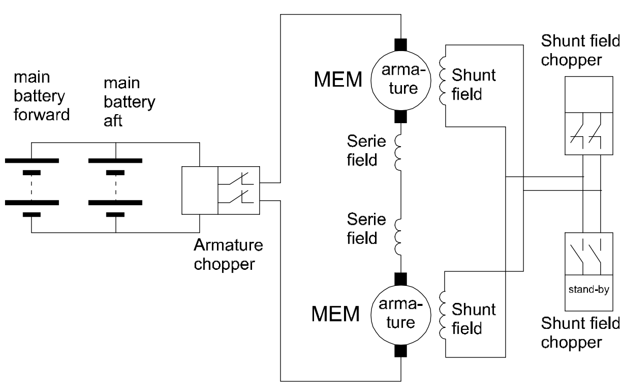

Figure 29 Dead slow speed switch settings – (Zeer langzame Sluipvaart)

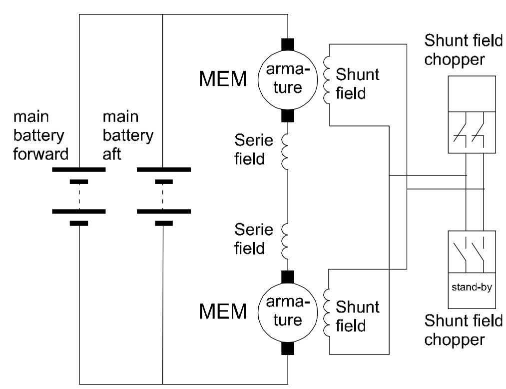

Figure 30 Slow speed switch settings (Stapvaart)

In the cruise speed settings the MEM armatures as switched in parallel as well as the batteries, see Figure 31. The speed is controlled by one of the shunt field choppers. [27] In high speed switching settings, the MEM's and the batteries are switched in series. This is illustrated in Figure 32. The speed is controlled by one of the shunt field choppers. [27]

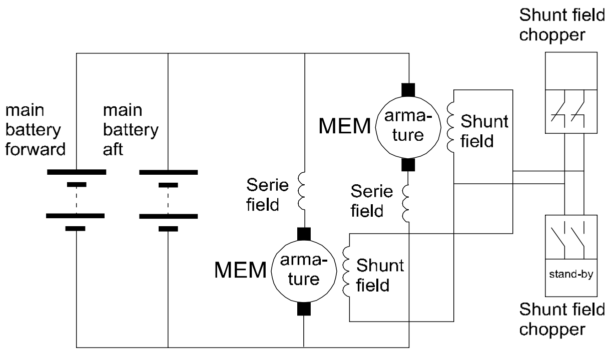

Figure 31 Cruise speed switch settings (Kruisvaart)

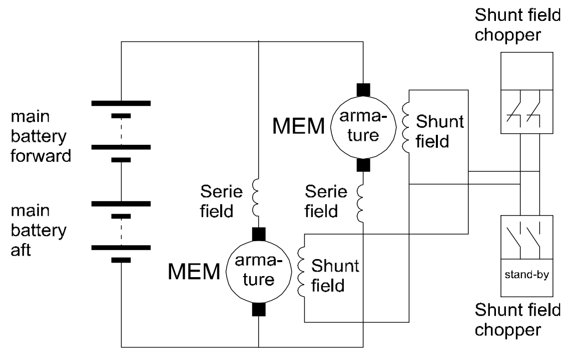

Figure 32 High speed switch settings (Hogevaart)

The armature voltage controller is the controller that controls the battery voltage between the batteries and the MEM. This power supply can control the voltage. In the used model is this controller not implemented. The three modes of operation are the slow speed; cruise speed and high speed switch settings to find the optimum battery mass.

The battery voltage is not constant during submerged operation. The battery voltage drops during discharge. This needs to be compensated to maintain power at constant rotating frequency. This is controlled by the motor controller.

5.3.2 Motor controller

The control loop feedback mechanism calculates the error between the set power and simulated power and minimizes this error over time by controlling a variable until the set power is equal to the delivered power by the propulsion motor. The variable unit is U_f. U_f Is the voltage in the shunt field circuit. The shunt voltage results in a shunt field current. The shunt field current is limited to an output of 80 [A].

$$P_{B\ set}\ (t) = P_{B\ MEM}\ (t) \tag{5-13}$$

$$\{P_B, t \in \mathbb{R} \mid P, t \geq 0\}$$

The controller is a proportional-integral-derivative controller (PID-controller). The PID-controller is a mathematical representation of the chopper in the shunt field circuit. See Figure 33 Propulsion motor and controller . The chopper is in a static switch, which can be operated with a controllable pulse-width and/or pulse-frequency. The incoming voltage from the batteries will be switch on and off very quick and fed to the MEM. By varying the pulse-pause ratio it is possible to control, in theory, the mean voltage between zero and actual battery voltage. The used switching element is a thyristor [26]. The PID controller is limited to non-negative reel numbers; $\mathbb{R}^+$. A negative shunt voltage is no solution.

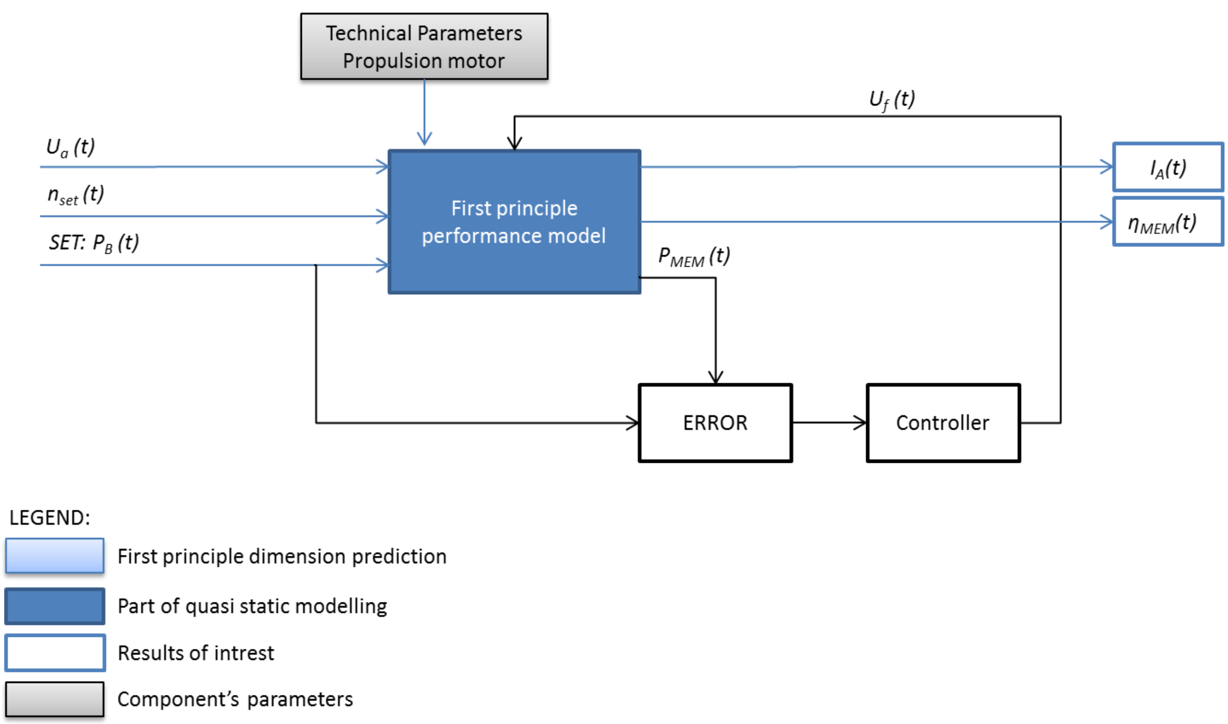

Figure 33 Propulsion motor and controller performance model

5.4 Verification performance model propulsion motor

The verification of the propulsion model is done with available measurement data. The measurement data is from the same machine type, but another maximum power output. The maximum power output of the propulsion motor is 4000 [kW]. The technical parameters are assumed to be the same for both propulsion motors. The variables that are assumed to be different are rotor dimension related. The rotor dimensions of the propulsion motor are changed and the simulation results are changed until there is a good fit between the numerical simulations and the experimental measurement data.

5.4.1 Technical Parameters

The propulsion motor model has parameters classified into physical constants and machine parameters. The physical constants describe material these constants are known. Machine parameters describe the specific machine properties.

5.4.1.1 Physical constants

The physical constants are defined in Table 3.

Table 3 Physical Constants

Symbol	Description	Value	Unit
ϕ_{sat}	Saturation flux	2.3	Vs
B_{sat}	Saturation flux density	2	T
μ_0	Permeability of a vacuum	4 pi e-7	H/m
μ_r	Permeability of iron	2000	-

5.4.1.2 Machine parameters

The machine parameters are defined in Table 4.

Table 4 Machine parameters

Symbol	Description	Value	Unit
N_f	Number of shunt windings	89	-
N_s	Number of series windings	2	-
N_a	Number of armature windings	13	-
N_c	Number of compensating windings	10	-
R_f	Shunt windings resistance	1	Ohm
R_s	Series windings resistance	5 e-3	Ohm
R_a	Armature windings resistance	10 e-3	Ohm

5.4.2 Rotor dimensions approach

Available performance data of a similar type of machine was made available [5]. This performance data is over the full range of the propulsion motor’s power output; from dead slow to high speed. The performance data have been measured at constant power output for various battery voltages and constant voltages and various power output. This data is used to complement the unknown rotor parameters is such a way that the simulated performance would correspond to the performance data.

The technical parameters and load is input for the performance model of the propulsion motor. The output of the simulations is the efficiency and armature current. Output of the simulation is compared to the available measurement data. The size of the rotor is changed and is changed in the technical parameters.

This process is repeated until the error between the simulated results and the experimental data has come to a minimum. This process is schematically illustrated in Figure 34.

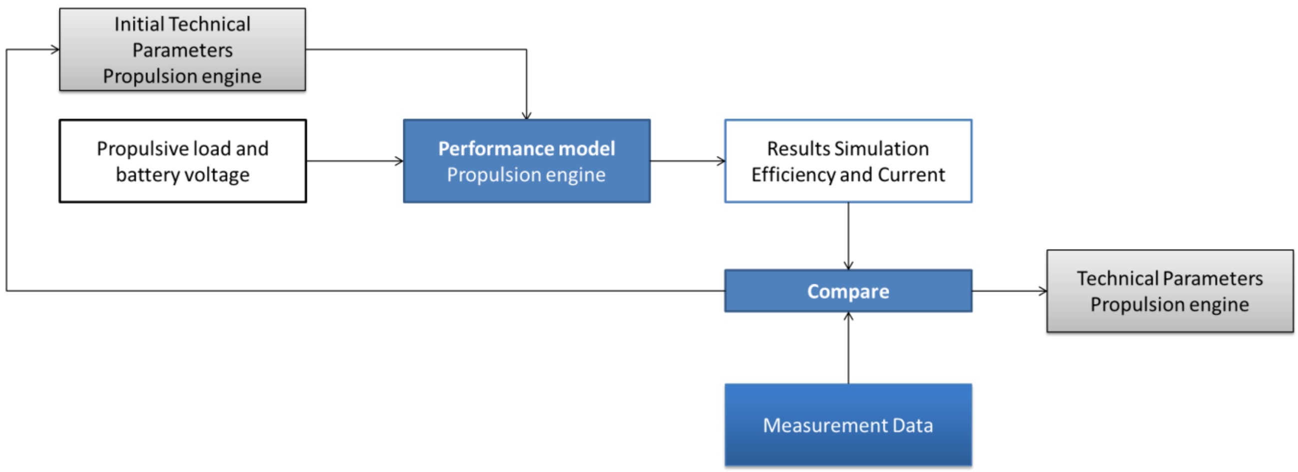

Figure 34 Rotor dimensioning

The changing of the rotor dimensions changes the effective cross sectional area of the rotor, as illustrated in Figure 35. As the area changes, the flux changes. In order to meet the maximum power output the armature current has to increase as calculated in equation 5-14.

$$\phi_d = \iint_S \bar{B}\,\overline{dA} \qquad \text{5-15}$$

$$P_{MEM} = T_{MEM} \cdot \omega_m \cdot Z_a \qquad \text{ref. 5-6}$$

$$T_{MEM} = (K_a \cdot \phi_d \cdot I_a)\,Z_a \qquad \text{ref. 5-7}$$

The rotor dimensions are defined as the area cross section, rotor length and rotor diameter. It is assumed that the diameter of the rotor is 2.0 [m] and that only the length of the machine varies. This assumption allows using a constant airgap length. Figure 35 illustrates the rotor dimensioning.

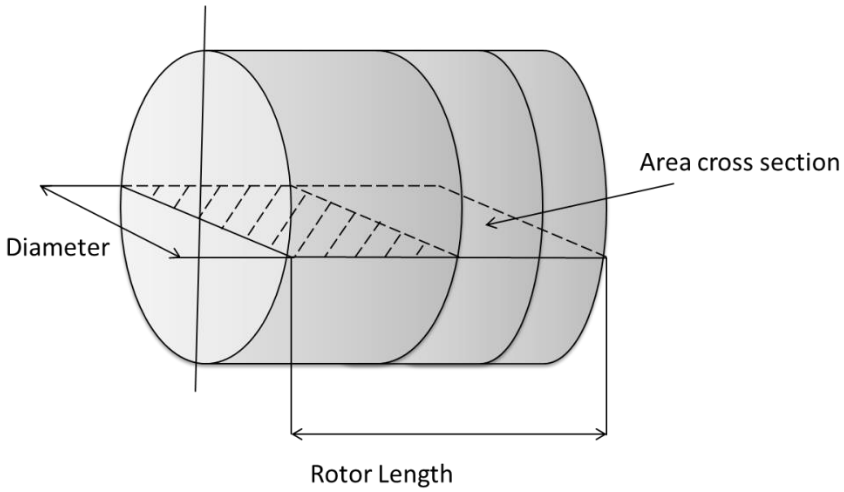

Figure 35 Rotor dimensioning

5.4.3 Rotor dimensions

The measured armature current and the simulated armature current are plotted in Figure 37. The measurements data with the subscript surfaced indicates a constant voltage over the range of the measurements. During the surfaced operation are the diesel generators running allowing constant voltage operation. The subscript submerged indicates a decreasing voltage during the measurements as the batteries drain. The simulated and efficiency and the efficiency obtained from the measurement data is plotted in Figure 37. The shape and value of the lines have a good fit. The simulation results fit well for a rotor length of 1.44 [m] and 2 [m] in diameter. The resulting cross sectional area is 2.88 [m].

$$A_d = D_{rotor} \cdot L_{rotor} = 2.88\ [m^2] \qquad 5\text{-}16$$

Table 5 Rotor dimension results

Symbol	Value	Unit	Description	Source
A_d	2.88	m^2	Area cross section d-axis	Fit
A_q	2.88	m^2	Area cross section q-axis	Fit
l_d	5.0	m	Magnetic length in d-direction	Fit
l_{yq}	2	m	Effective length q-axis	Function of Ad
l_{yrd}	2	m	Effective length d axis	Function of Ad
dd	0.0105	m	Airgap length on the d-axis	Schulten/Stapersma/Meuldijk [28]
dq	0.0148	m	Airgap length on the q-axis	Schulten/Stapersma/Meuldijk [28]
Ls	3.5	m	Iron length stator	

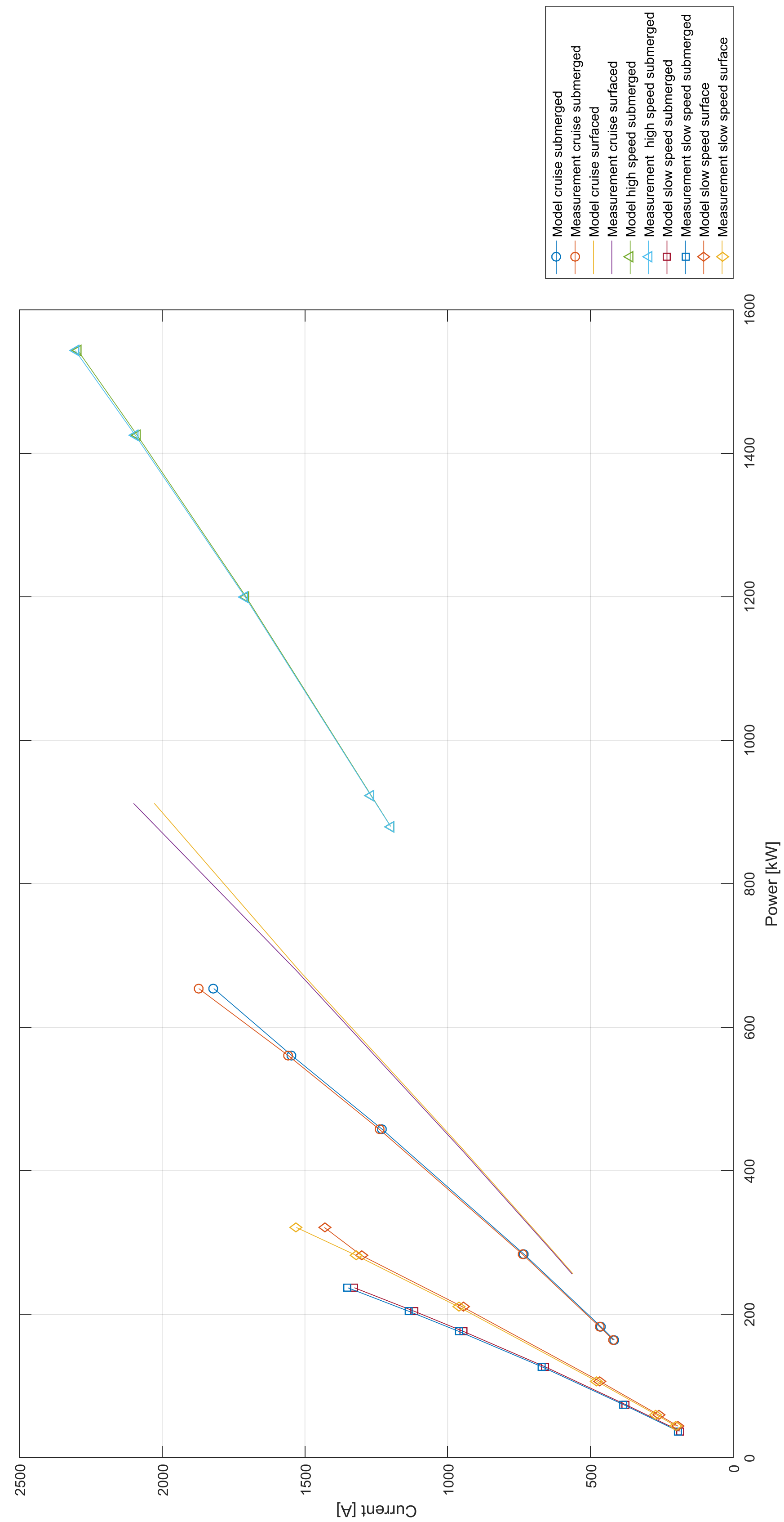

Figure 36 Modelled and measured current

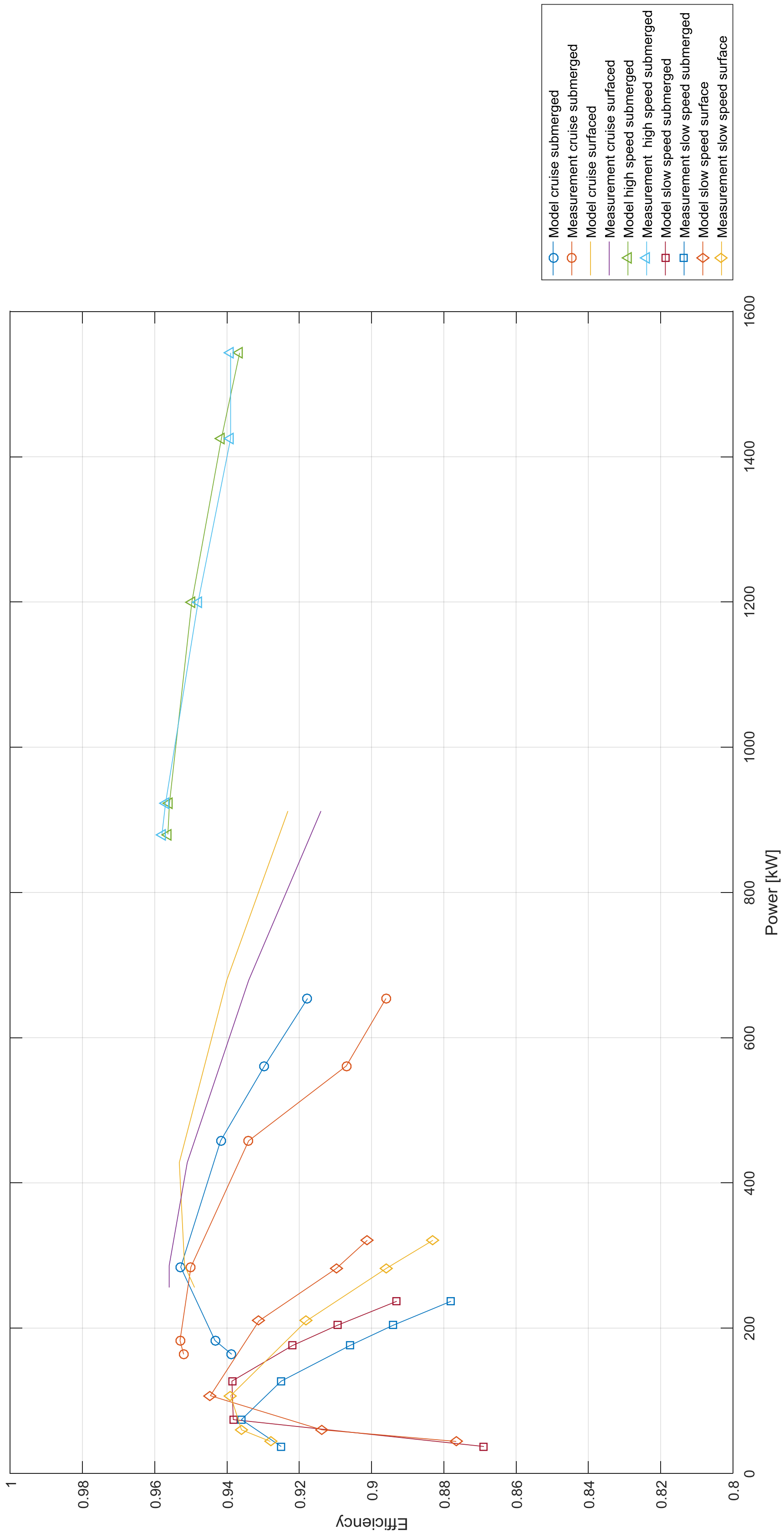

Figure 37 Modelled and measured efficiency

5.5 Rotor dimension prediction mission profile

This chapter elaborates on the dimensions of the propulsion motor expressed in volume and weight. The dimensions of the propulsion motor are a function of the required power output. The first principle dimension prediction is described by D. Stapersma and P. de Vos [21]. The idea behind first principle dimension prediction is that the dimensioning of the propulsion motor, and other electric machines, can be estimated by sizing the core of the machine to the required power output using first principles. The core consists out of primary and secondary elements. The machine dimensions can be obtained by multiplying the core dimensions, times a correction factor. The correction factor is obtained using regression analysis. This process is illustrated in Figure 38.

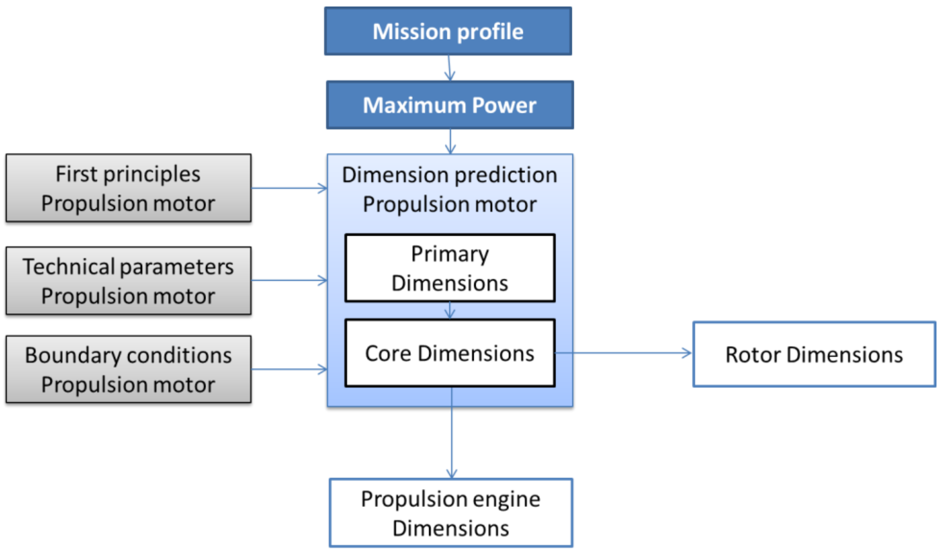

Figure 38 Process of prediction machine dimensions and rotor dimensions based on first principles

The rotor of the propulsion motor is the primary element of the motor. Electrical energy is converted to mechanical energy in the rotor. The dimensions of the rotor are a function of the operational requirements. The operational requirement that determine the propulsion motor size is the maximum power demand at a defined number of revolutions, which correspond with the number of revolutions of the propeller as there is no gearbox is involved in the system layout. The revolution and power are obtained from equation 2-7.

5.5.1 Primary dimensions

The basic equation that relates power output to angular speed and torque is given in 5-17. T Is the torque in Nm, ω is the angular speed in rad/s and n is the rate of rotation is rev/s. For electromotor is the torque expressed as the electromotive force times the radius of the rotor. The electromotive force is the Lorentz force that acts on the current carrying conductors in the rotor. Resulting in a force. P. de Vos [21] states that the electromotive force can be represented as a shear stress. The current carrying conductors are evenly spread over the rotor circumferential area, and therefor is this area considered. Using this relation results in equation 5-17.

$$P = T \cdot \omega = T \cdot n \cdot 2\pi \qquad \text{5-17}$$

$$T = EMF \cdot \frac{D_R}{2} = \tau_R \cdot A_R \cdot \frac{D_R}{2} = 2 \cdot \tau_R \cdot V_R \qquad \text{5-18}$$

$$n = \frac{v_t}{\pi \cdot D_R} \tag{5-19}$$

The area of the rotor is a function of the rotor diameter and length. The relation between those variables is defined in 5-21. This relation enables to play with the dimensions, while keeping the other terms constant. A long slender motor could deliver the same output power as a short big diameter motor.

$$\lambda_R = \frac{L_R}{D_R} \tag{5-20}$$

$$P = \pi \cdot \tau_R \cdot v_t \cdot D_R \cdot L_R = \pi^2 \cdot n \cdot D_R^2 \cdot L_R \cdot \tau_R \tag{5-21}$$

The shear stress can be calculated with the available data. The output power of the propulsion motor is divided by the number of armatures in the motor as both motor partitions deliver the same work. This technical parameter is assumed to be constant for the propulsion motors of the different required power outputs. The diameter and length of the rotor are obtained from the 5-16.

$$\tau_R = \frac{P/Z_a}{\pi^2 \cdot n \cdot D_R^2 \cdot L_R} = \frac{4000/2}{\pi^2 \cdot 3.3 \cdot 2.0^2 \cdot 1.44} = 11 \left[\frac{kN}{m^2}\right] \tag{5-22}$$

The dimension of the rotor for a constant diameter and the same shear stress is calculated in equation 5-23. The length of the rotor is usually extended at a constant diameter. The verified model is designed for higher power output than the nominal power output required for the assumed mission profile. The dimensions for the propulsion motor for the mission profile are determined with first principle dimension prediction. According to mission profile is the maximum output power 3600 kW at 19 knots. According to equation 2-7 is the rate of rotation 3.3 rps. The resulting rotor length is 1.3 meter according to 5-23.

$$L_R = \frac{P/Z_a}{\pi^2 \cdot n \cdot D_R^2 \cdot \tau_R} = \frac{3600/2}{\pi^2 \cdot 3.3 \cdot 2.0^2 \cdot 11} = 1.3\ [m] \tag{5-23}$$

5.5.2 Rotor dimensions performance model

The rotor dimensions that are obtained with the first principle dimension prediction model are input for the propulsion motor performance model for 3600 kW output.

Table 6 Rotor dimensions corresponding to the mission profile

Symbol	Value	Value	Unit	Description	Source
A_d	$L_R \cdot D_R$	$1.3 \cdot 2$	m^2	area cross section d-axis	
A_q	$L_R \cdot D_R$	$1.3 \cdot 2$	m^2	area cross section q-axis	
l_d	5.0	5.0	m	Magnetic length in d-direction	
l_{yq}	D_R	2	m	Effective length q-axis	
l_{yrd}	D_R	2	m	Effective length d axis	
dd		0.0105	m	Airgap length on the d-axis	[28]
dq		0.0148	m	Airgap length on the q-axis	[28]

5.6 Operational capabilities

The MEM on board is speed controlled with the shunt field controller. The controller has a limited output, resulting in a limited power output. The propulsion motor is switched in series and parallel, and the batteries are switched in series and parallel to extend the operational area of the propulsion motor. The switching moments are based on the limits of the shunt field controller and the optimum efficiency. This chapter elaborates on the operational capabilities of the propulsion motor with the derived parameters.

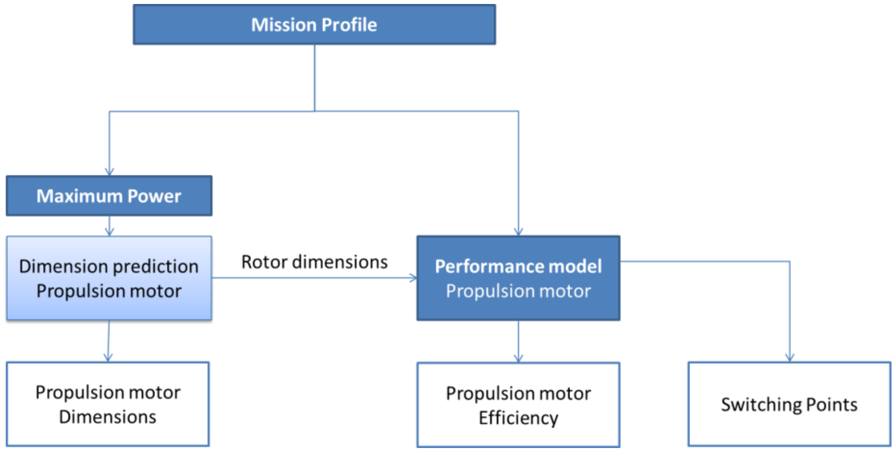

Figure 39 Switching points MEM

There are 4 modes of operations as stated in chapter 5.3. The limitations of the slow speed, cruise speed and high speed modes of operations are first analysed, followed by the dead-slow speed mode, which operates in a different way.

5.6.1 Slow speed mode of operation

In the slow speed mode of operation are the batteries switched in parallel and the armatures switched in series. The armature voltage of is than half of the battery voltage. The battery voltage is around 400 [V].

The armature current increases for an increasing power demand at constant armature voltage. The controlling variable, the shunt current, decreases. The armature current, shunt current and load and efficiency is illustrated in Figure 40.

The efficiency has an optimum. The optimum is a result of the losses due to the armature and shunt currents as explained in chapter 5.2.1 Propulsion motor efficiency. The contribution of the shunt losses are at first dominant, as the armature current becomes larger the armature losses increase.

Around 100 rpm the value shunt current is zero, and the shunt current cannot further decrease. The propulsion motor cannot be controlled at higher propulsor speeds. If higher speeds are desired the system switches into the cruise speed settings.

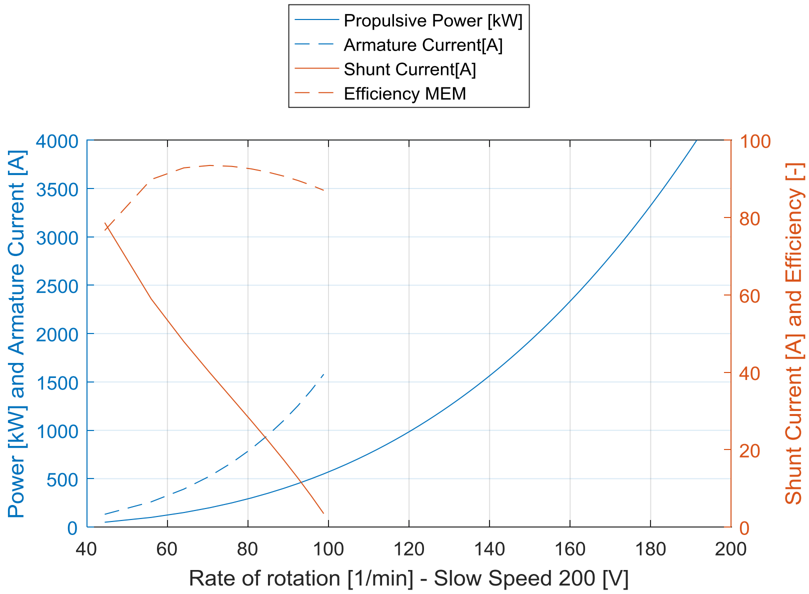

Figure 40 Slow speed settings

5.6.2 Cruise speed mode of operation

In the cruise speed mode of operation are the batteries and armatures switched in parallel. The armature voltage is around 400 [V]. The operational area of this mode of operation is shifted to higher rates of rotation compared to the slow speed settings.

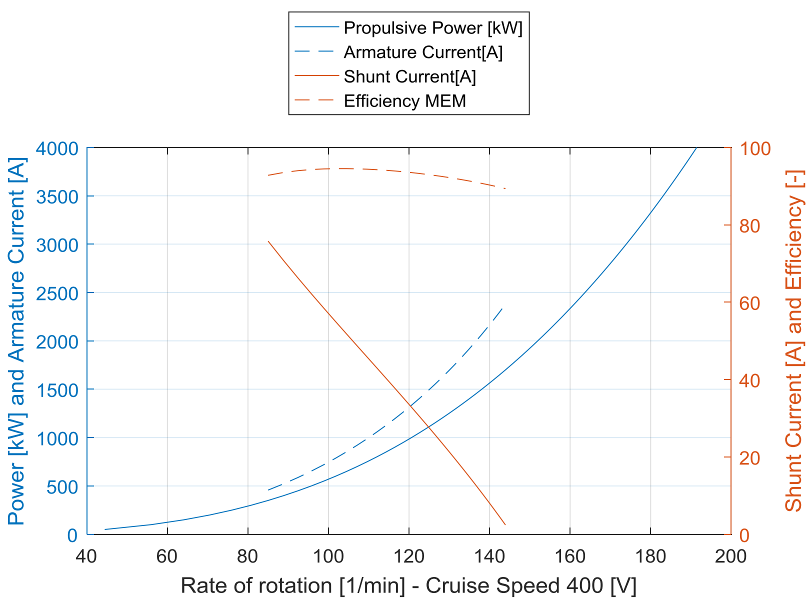

Figure 41 Cruise speed settings

5.6.3 High speed mode of operation

At the high speed settings is the armature voltage equal to twice the battery voltage. The armature voltage is around 800 [V].

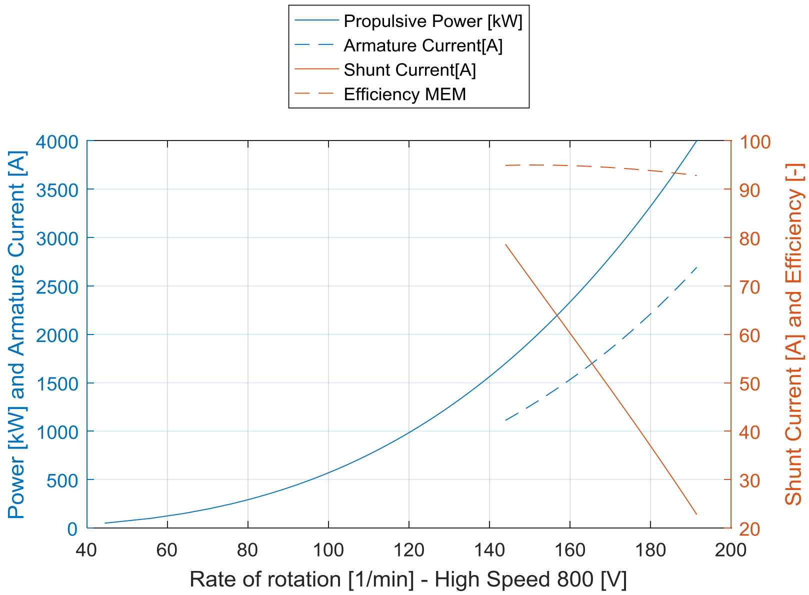

Figure 42 High speed settings

5.6.4 Switchboard settings

Switchboard settings are the powers at which the batteries and armatures switch in series or parallel. There are two switching points, representing the three modes of operation. The switchboard settings are optimized for optimum propulsion motor efficiency. The different modes of operation are plotted in Figure 43.

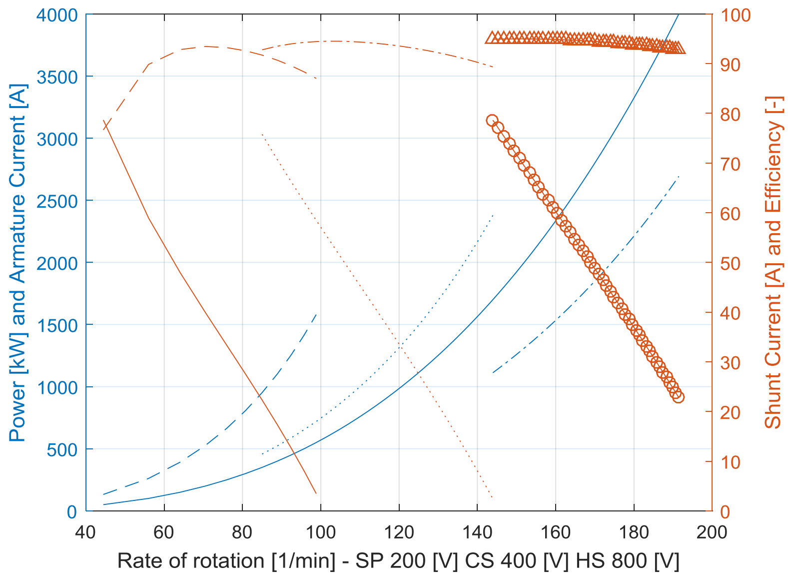

Figure 43 Modes of operation

The two switch points are at 90 and 140 rpm, respectively 400 kW and 1200 kW brake power. Up to 400 [kW] are the battery setting values 0.5 and the armature settings 0.5. The setting represents the slow speed switch settings. The batteries are switched in parallel, and the armatures are switched in series. As the armatures are switched in series, the voltage over the armatures is half of the battery voltage. The batteries are switched in parallel, so the batteries deliver both of the total required discharge current.

At 400 [kW] is the second switching point. This point represents the cruise speed switch settings. The batteries are switched in parallel and armatures are switched in parallel. The voltage supplied to the armatures is the voltage of one battery. The discharge current of the MEM is divided over two batteries. So the battery setting is 0.5.

At 1200 [kW] is the switching from cruise speed to high speed. The batteries are switched in series, and the armatures are switched in series. The armature setting is two, because the voltage to the MEM is twice the battery voltage. The battery settings are one because the each battery has to deliver the current of the two MEM halves.

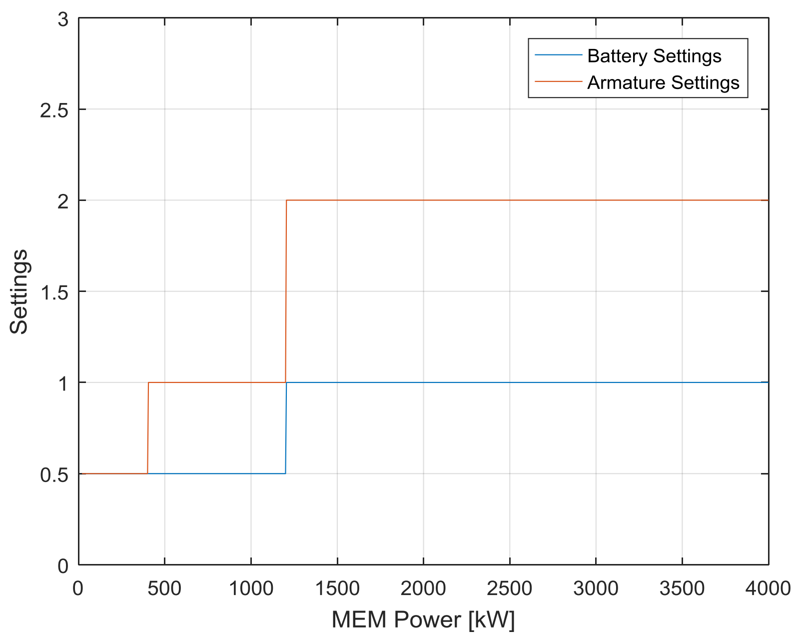

Figure 44 Switching points

5.7 Discharge currents

The combined switchboard settings and load characteristics lead ultimately to the armature current as function of the set power and available voltage. The relation is plotted in Figure 45. The armature current is the discharge current acting on the batteries. The influence of the shunt currents can be neglected.

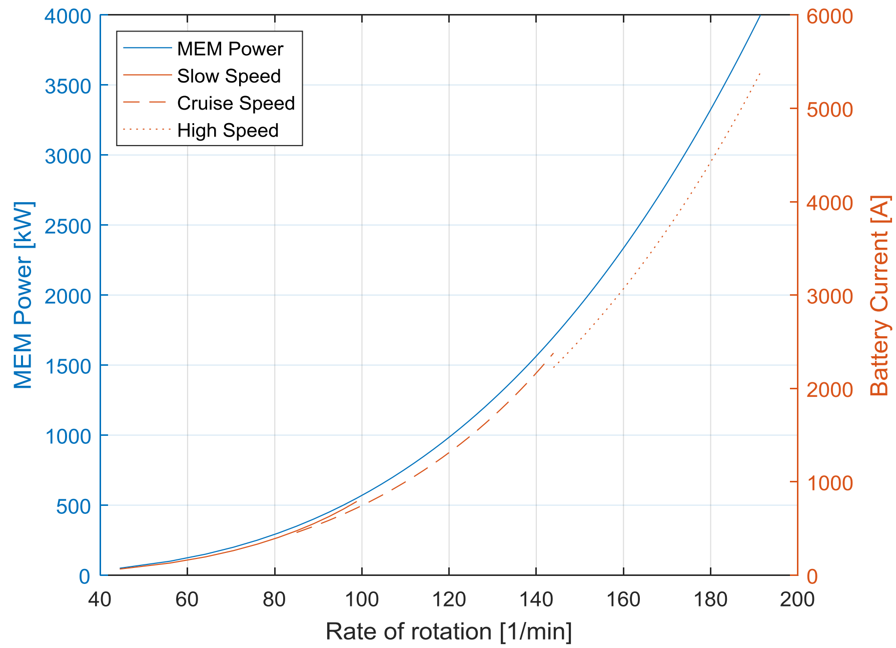

Figure 45 Armature current as function of the set power

The values of the armature current are based on an armature voltage of 200 V for the slow speed setting, 400 V for the cruise speed settings, and 800 V for the high speed settings. The armature voltage decreases during discharging. The result is an increased armature current. Figure 46 illustrates the armature current as function of the armature voltage and set power. The set power is according the ships resistance equation 2-8. On the vertical axis is the delivered brake power of the propulsion motor, with two armatures. The horizontal axis is the available battery voltage. The current is illustrated in the colours corresponding to their amplitude.

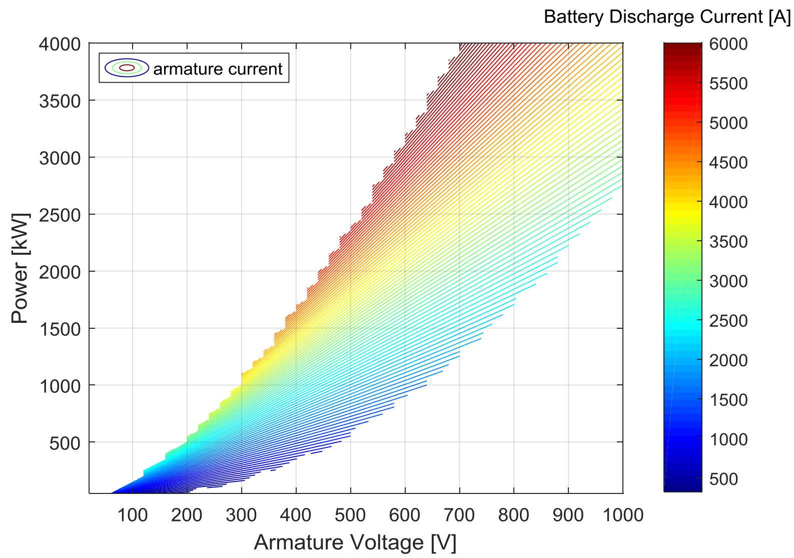

Figure 46 Armature current as function of power and voltage

The figure also illustrates the operational area of the propulsion model. The chopper is a mechanical device that has a limited output voltage. The output current is limited of 0 [A] up to 80 [A]. These limitations are taken into account for the PID-controller.

The effect of the controller limitations is clearly visible at high available voltages and low power demands. At low power demands, and higher voltages is the controller limited by the upper limit, 80 [A]. At the higher powers for lower voltages is the controller limited to the lower limit of 0 [A]. The values of the shunt field current are illustrated in Figure 47. The empty spaces are area's where the propulsion motor cannot operate. The switching of the batteries and armatures in series and parallel can prevent the propulsion motor to operate in these areas.

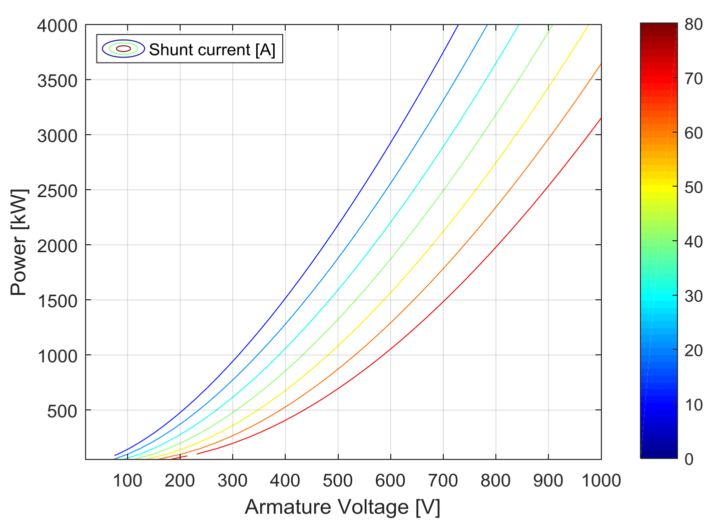

Figure 47 Shunt field current [A]

5.7.1 Dead slow speed

The dead slow speed setting differs from the other modes of operation. The chopper between the batteries and armatures works like a variable voltage supply in the dead-slow mode of operation. In the slow, cruise and high modes of operation is this chopper not used. The chopper is too noisy when it is switching the high currents during the slow, cruise and high speeds.

In contrast to the slow, cruise and high speed modes of operation is the dead slow speed not generic modelled. The settings are optimized for the two requested power outputs, 18 kW and 40 kW.

5.7.1.1 18 kW Power demand

The 18 kW power demand corresponds to the set dead-slow speed set in the mission profile during the surveillance and attack phase. The simulation results show a narrow voltage range where the propulsion motor can deliver the requested output power. The narrow range of the high efficiency illustrates the need of a voltage regulator between the batteries and the MEM. The voltage is acceptable in a range between 40 and 100 [V]. The optimum efficiency at the slow speed, 18 [kW] propulsive power, given in the mission profile is 88%. The battery voltage of the charged batteries is dependent on the number of cells per battery and the battery cell voltage. The optimum battery voltage is 50 [V]. The armature current is held constant at 24 [A]. See

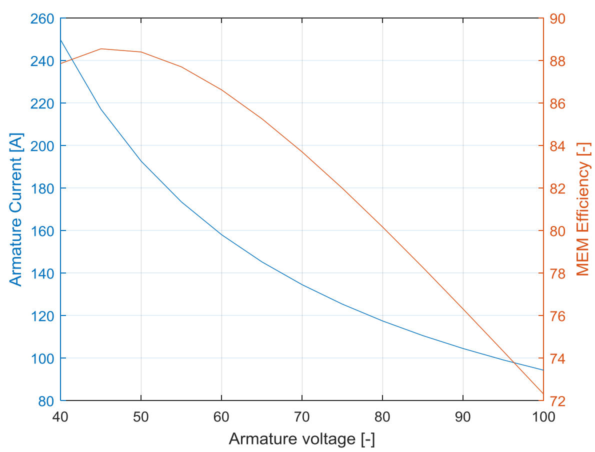

Figure 48 Efficiency and discharge current at 18 kW propulsive power

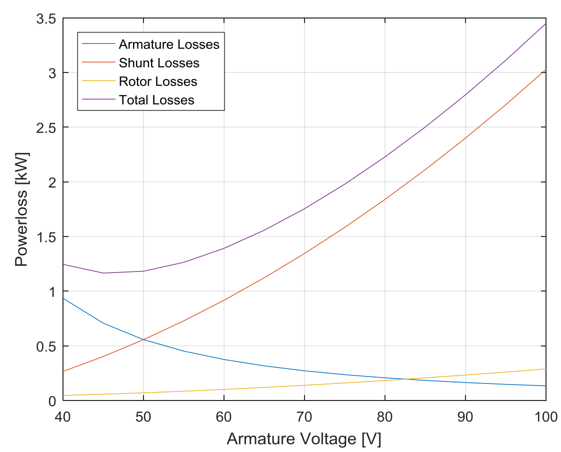

Figure 49 Power losses 18 kW

$$P_{EL} = Z_a \cdot U_a \cdot I_a = 2 \cdot 45 \cdot 220 = 19.8\ [kW] \quad \text{5-24}$$

$$\eta = \frac{P_{MEM}}{P_{EL}} = \frac{18.0}{19.8} = 0.91 = 91\%$$

$$I_a = \frac{P_{Armature}}{2 \cdot U_{batt}} = \frac{19.8}{2 \cdot 400} = 24\ [A]$$

5.7.1.2 40 kW power demand

The 40 kW power demand corresponds to the set dead-slow speed set in the mission profile during covert transit 1. The armature current is computed as 53 [A]. See equation 5-25.

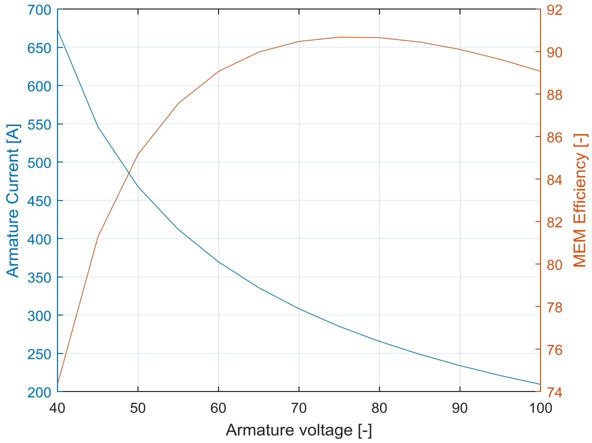

Figure 50 Efficiency and discharge current at 18 kW propulsive power

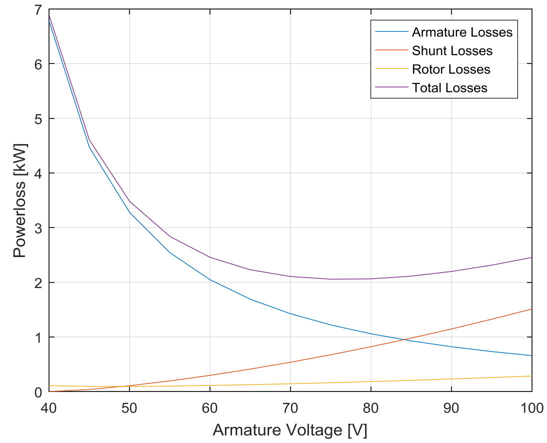

Figure 51 Power losses 18 kW

$$P_{EL} = Z_a \cdot U_a \cdot I_a = 2 \cdot 80 \cdot 265 = 42.4\ [kW]$$

$$\eta = \frac{P_{MEM}}{P_{EL}} = \frac{40.0}{42.4} = 0.93 = 93\% \qquad \text{5-25}$$

$$I_{cell} = \frac{P_{Armature}}{2 \cdot U_{batt}} = \frac{42.4}{2 \cdot 400} = 53\ [A]$$

5.8 Sizing the machine

The sizing of the total machine is the size of the core multiplied with an additional term. The term is a correction factor. It corrects the core size of the motor to the total dimensions of the motor. The additional term is obtained from data of suppliers. A database for DC machines is created, consisting data of one manufacturer; *HOLEC*. Unfortunately data of submarine propulsion motors is limited. Another type of submarine propulsion motor is added to verify the method. This type of machine is a permanent magnet (PM) type. As the first principle dimension prediction is generic, the method is also applicable to other types of electric machinery.

The results of the propulsion motor dimensioning are illustrated in Figure 52. The circles in this figure illustrate the two DC propulsion motors, the stars represent the PM. The colour of the circles and stars correspond to the length/diameter lines in Figure 52. The correction factors for the length and diameter make that the lines are a perfect fit. The correction factors for the length are 1.5 and for the diameter 1.3 for the DC and the PM motor.

It is clearly visible that the motors do fit the corresponding coloured lines for the DC and PM motors. There is however a significant deviation for the PM 1700 kW propulsion motor. The machine dimensions are smaller than calculated. This can be explained by a higher maximum air gap flux density as calculated in resulting in higher shear stress in equation 5-22.

Another interesting aspect is the ratio between rotor length and diameter. The DC motor diameter is limited to a radial speed of 25 m/s. Higher speeds may damage the rotor windings. The line with solutions stops for the DC machines in Figure 52, the limit of 25 m/s is exceeded. The PM motor does not have this limitation as the rotor of a PM machine has no windings on the rotor, but permanent magnets. This allows higher circumferential speeds. Resulting in larger rotor diameter for the same motor speed.

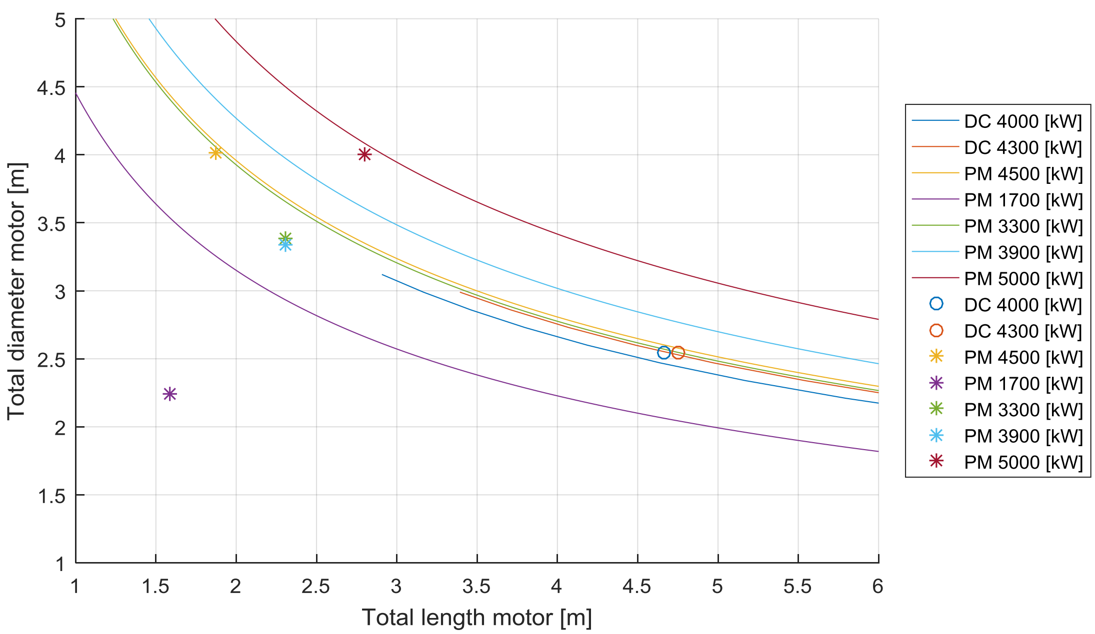

Figure 52 diameter of the propulsion motor as function of the length for constant volume

With the correction factors determined, the machine size of the 3600 [kW] motor can be estimated as illustrated in Figure 53. This motor is required for the given mission profile. The star in the figure is the arbitrarily chosen propulsion motor. Resulting in a total diameter of 2.6 [m] and a total motor length of 3.9 [m].

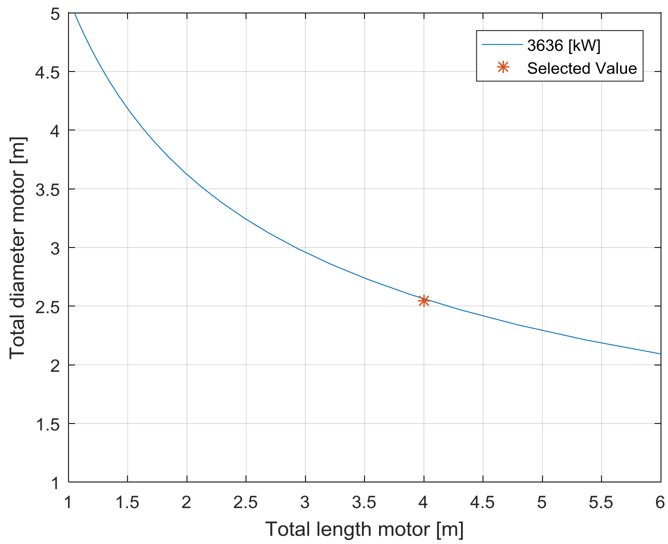

Figure 53 motor dimensions 3600 kW

The dimensions of the propulsion motors are the outsides of the external dimensions excluding the mounted coolers, choppers or frequency converters. The propulsion motors have resistors mounted on top, and the PM has frequency converters on top. The data of the motors is included in ANNEX E Propulsion motor dimensions.

5.8.1 Weight of the machine

The weight of the machine is related to the machine density. The machine density is expressed as the mass of the machine divided by the volume of the machine. The variations is length, width and height of the machine do not affect the mass of the machine as the volume of the machine is constant.

The mass of the motor is calculated as the volume of the motor times a motor density. The energy density is 2500 [kg/m^3] for the PM, the density is 2800 [kg/m^3] for DC machines. This value is obtained by comparing different motor data. The difference between the PM and DC machines can be explained by the materials used in the machine. The copper used in the DC compound machines is heavier than the rare magnets materials.

$$P = \pi^2 \cdot n \cdot D_R^2 \cdot L_R \cdot \tau_r$$

$$m_{motor} = V_{motor} \cdot \rho_{motor} = \frac{\pi}{4} \cdot D_R^2 \cdot f_d \cdot L_R \cdot f_l \cdot \rho_{motor}$$

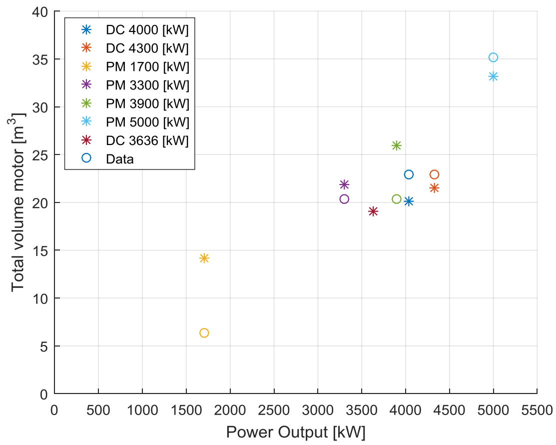

Figure 54 Volume of the motor

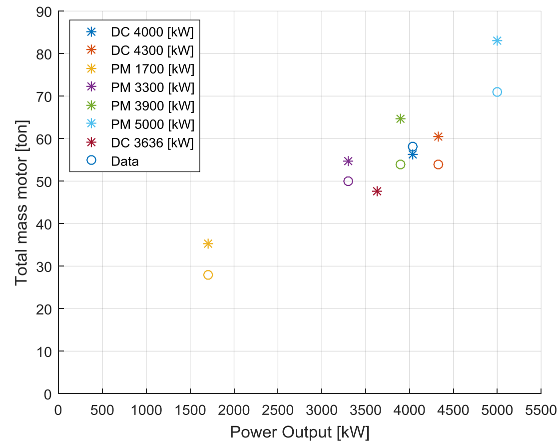

Figure 55 Weight of the motor

5.9 Propulsion motor efficiency and dimensions

The propulsion motor is dimensioned for the maximum defined power output at a defined rate of rotation. The mass, volume and efficiency as function of the assumed mission profile is captured in Table 7.

Table 7 DC- Compound properties for the assumed mission profile

DC-Compound 2 armatures	Mass [ton]	Volume [m³]	Efficiency
3600 [kW] Brake Power	48	19	Max. 95%

5.10 Conclusion

The propulsion motor performance is modelled in a performance model. This first principle model is based on the first and second law of Maxwell. The model is extended with a motor controller. The motor controller uses the shunt field to control the power output.

The model with controller is verified with available measurements of the manufacturer. The available measurements contain 30 measurement points. There are two types of measurements. (1) Measurements of constant power at varying battery voltages and (2) varying powers for constant battery voltages. The simulated armature current fits the available measurements perfect. The efficiency fits good perfect, within a margin of 2%. At lower power output is the error 4%.

It can be concluded that the propulsion motor performance model is a good representation of the propulsion motor. The model can be used for the propulsion plant simulations. The model is generic, and so it can be concluded that it is not only valid for the measured data points, but for the total power range over the total voltage range.

The measurement data is obtained from a 4000 [kW] propulsion motor. The required propulsion motor for the assumed mission profile is 3600 [kW]. It is assumed that all the motor parameters are constant except for the rotor dimensions. The rotor dimensions of the 4000 [kW] propulsion motor have been decreased with a prediction model, based on first principles, to the predicted size of the 3600 [kW] propulsion motor rotor. The performance model with controller, motor parameters and the calculated rotor dimensions is used to obtain the armature currents and to simulate the propulsion motor efficiency.

The calculated rotor dimensions have been used as starting point for the overall MEM dimensions, expressed in mass and volume. The rotor dimensions are assumed to be the core dimensions of the propulsion motor. Those core dimensions are multiplied with a correction factor to obtain the mass and volume of the MEM. The correction factor is obtained with regression analyse. The generic approach for the first principle predicting the dimensions of the propulsion motor is applicable and valid for the submarine propulsion motors of different types. The technical parameter used in the method is the shear stress acting on the rotor. This technical parameter is obtained by means of the available data of a propulsion motor, and a method based on the industry standards used in the construction of the rotor. The result is the mass and volume of the propulsion motor.

6 Battery performance model and dimensions

6.1 Introduction

For the prediction of the performance of batteries is a mathematical model required. The performances of interest are the capacity, the cell voltage and the battery efficiency. The model that is used for the prediction of the performances is the battery model of D. Stapersma [22]. The mathematical model is developed as a model for design calculations.

This chapter elaborates on the usability of the model for lead-acid and lithium-ion energy storage technology. The first subchapter elaborates on the theoretical model, the second chapter verifies the lead-acid model, and the third subchapter verifies the lithium-ion model.

The relation between the performance and the dimensions is the battery cell mass. The battery cell capacity is to be a function of the cell mass. As the cell mass increases the capacity of the cell increases: larger cells have more stored energy. The volume of the battery is assumed to be a function of the mass. The factor between the mass and volume is the battery density. The battery density is obtained from an unclassified battery cell.

6.2 Battery cell performance model

A complete description of the battery performance is obtained when the following functional dependencies are specified [22]:

- Battery capacity as function of the discharge current;
- Open cell voltage as function of pseudo discharge state;
- Pseudo resistance as function of pseudo discharge state.

These equations together form the performance model of a battery cell, as illustrated in Figure 56. The following subchapters elaborate on the functional dependencies as mentioned above.

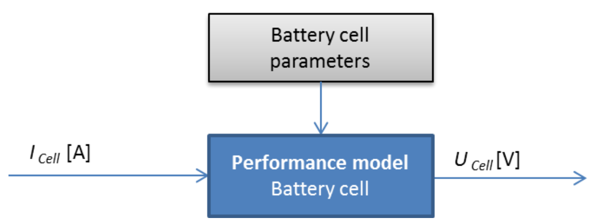

Figure 56 performance model battery cell

6.2.1 Discharge capacity as function of the discharge current

The capacity of a cell is expressed as the total quantity of electricity involved in the electrochemical reaction and is defined in terms of coulombs or ampere-hours. The change in ampere-hour in the battery cell is by definition:

$$dQ = I \cdot dt \;\rightarrow\; Q = \int_0^t I \cdot dt \tag{6-1}$$

The available charge; Q_{end} $[\mathrm{Coulomb}]$ is the electric current flow in Ampere $[\mathrm{A}]$ over a period of time. The delivered charge over the maximum time is also known as the capacity, C_t $[\mathrm{Ah}]$.

$$Q_{end} = \int_0^{t_{end}} I \cdot dt = C_t \quad and\; C_t = f(I_{end}) \tag{6-2}$$

The real discharge state of a battery state can be defined as the ratio of the ampere hours that left the cell and its maximum capacity at zero current C_∞. This is stated in equation 6-3. $x = 0$ Represents a full battery and $x = 1$ is related to an empty battery.

$$x = real\ discharge\ state = \frac{delived\ capacity}{maximum\ capacity} \quad 6\text{-}3$$

$$x = \frac{Q}{C_\infty} = \frac{\int_0^t I \cdot dt}{C_\infty}$$

As the capacity is a function of the discharge current a new term is introduced, the pseudo discharge state. The pseudo discharge state is defined as the delivered capacity divided by the available capacity at the momentous current.

$$y = pseudo\ discharge\ state = \frac{deliverd\ capacity}{instantaneous\ capacity} \quad 6\text{-}4$$

$$y = \frac{Q}{C_t(I)} = \frac{\int_0^t I \cdot dt}{C_t(I)}$$

$$x_{end} = \frac{Q_{end}}{C_\infty} = \frac{C_t}{C_\infty} \quad 6\text{-}5$$

6.2.1.1 Battery parameters

The input for the capacity as function of the current is data obtained from manufacturers. Data that is related to long, C_∞, medium, C_5, and short, C_0, discharge times what corresponds with respectively low, medium and high discharge currents. The lowercase *c* denotes the specific capacity in [Ah\kg], the uppercase C denotes the battery cell capacity.

$$C_\infty = c_\infty \cdot m \quad 6\text{-}6$$

$$C_5 = c_5 \cdot m \quad 6\text{-}7$$

$$C_0 = c_0 \cdot m \quad 6\text{-}8$$

The coefficient α shapes the minimum value of C_t i.e. at high discharge current say, in 1.2 hours. The coefficient β is the fraction of discharge capacity in 5 hours divided, by the maximum discharge capacity.

$$\alpha = \frac{C_0}{C_\infty} = \frac{c_0 \cdot m}{c_\infty \cdot m} \quad 6\text{-}9$$

$$\beta = \frac{C_5}{C_\infty} = \frac{c_5 \cdot m}{c_\infty \cdot m} \quad 6\text{-}10$$

τ_{char} Is the characteristic discharge time in hours for the 5 hour fraction. τ Is the discharge time in hours.

$$\tau_{char} = \left(\frac{1-\alpha}{\beta-\alpha}\right) \quad 6\text{-}11$$

$$\tau = t_5 \cdot \ln(\tau_{char}) \qquad \text{6-12}$$

$$I_{char} = \frac{C_5}{5 \cdot \ln\left(\frac{1-\alpha}{\beta-\alpha}\right)} \qquad \text{6-13}$$

Equation 6-14 is the expression for the battery cell capacity in relation to the discharge current.

$$C_t(I) = C_\infty \left(\alpha + \alpha \cdot e^{-\left(\frac{I_{in}}{I_{char}}\right)}\right) \qquad \text{6-14}$$

6.2.2 Open cell voltage as function of pseudo discharge state

The open cell voltage during discharge is a function of the pseudo discharge state. The parameters a and b prescribing the open voltages at respectively 70% and 100%. The determination of the parameters a and b is profound elaborated in “Theory and model for battery charging and discharging”. [22]

$$U_0(y) = U_0(0) \cdot (1 - a \cdot y - b \cdot y^e) \qquad \text{6-15}$$

The open cell voltage during charge is comparable to the cell voltage during discharge.

$$\widetilde{U_0}(y) = \widetilde{U_0}(0) \cdot \left(1 - \tilde{a} \cdot y - \tilde{b} \cdot y^{\tilde{e}}\right) \qquad \text{6-16}$$

6.2.3 Pseudo resistance as function of pseudo discharge state

The internal cell resistance is a function of the pseudo discharge state. The fit function consists of two parameters. The increase of the internal cell resistance, at increasing is expressed by the term c. c Is the total resistance increase over the available capacity. For submarine batteries is 30% an acceptable value at constant discharge rate. The value d is a fit factor that influences the steepness of the tail of the function. $R_i(0)$ Is the resistance when the battery is fully loaded.

$$R_i(y) = R_i(0) \cdot (1 + c \cdot y^d) \qquad \text{6-17}$$

$$c = \frac{R_i(1.0)}{R_i(0.0)} - 1 \qquad \text{6-18}$$

$$d = \frac{\ln\left(\frac{R_i(0.7)}{R_i(0.0)}\right) - \ln(c)}{\ln(0.7)} \qquad \text{6-19}$$

6.3 Verification battery model for lead-acid

The equations stated in chapter 6.2 are combined in a performance model. The input is the current, the output is the cell voltage corresponding to the current. The current can be a charging current or discharging current. Discharging is associated with a positive current, charging is associated with a negative current.

The model is verified with data of the MORAY Battery. The battery is manufactured by *VARTA*. The cell type is UR12. The mass of the cell is 530 [kg]. The parameters for the verification of the lead-acid battery cells are stated in Table 8.

Table 8 Battery cell parameters

Symbol	Value	Unit	Description	Source
m	530	kg	Battery mass	VARTA
c_∞	24.5	Ah/kg	Capacity at 100 h discharge time	VARTA
c_5	17.7	Ah/kg	Capacity at 5 h discharge time	VARTA
c_0	13.6	Ah/kg	Capacity at 1.2 h discharge time	VARTA
$U_0(0.0)$	2.09	V	Open cell voltage fully charged	VARTA
$U_0(0.7)$	1.95	V	Open cell voltage at 0.7	VARTA
$U_0(1.0)$	1.75	V	Open cell voltage fully discharged	VARTA
e	16	-	Fit function tail	Assumed & Fit
$R_i(0.0)$	0.042	µOhm	Cell resistance voltage fully charged	VARTA & Fit
c	30	%	Increase of resistance	Assumed increase acc. [22]

The performance simulation of the battery cell used to verify the model is illustrated in Figure 57. The input is the discharge current and the battery parameters. The model is limited for the maximum allowable state of discharge. The maximum depth of discharge is taken as the pseudo discharge state equal to 1, i.e. the battery is fully discharged for the given discharge current. The initial depth of discharge is taken as 0, i.e. the battery is fully loaded. The discharge current varies over a range between 130 up to 6000 [A]. The maximum discharge current is equal to the armature current of the propulsion motor. The simulation stops if the set maximum depth of discharge is equal to the pseudo state of discharge. The elapsed time is defined as the total discharge time.

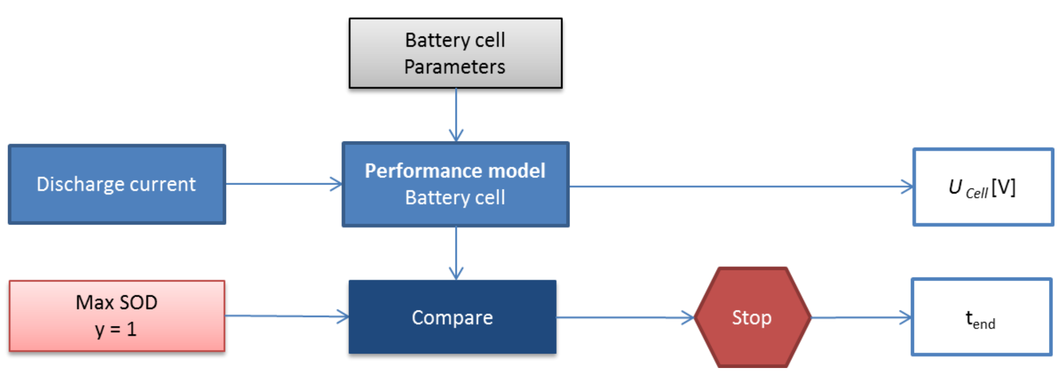

Figure 57 Verification performance model

6.3.1.1 Results verification

The results of the simulation are stated in Table 9. The first column represents the discharge current. The second and third column represent the discharge times. Respectively the data of the manufacturer and the results of the simulation. The fourth column represents the error between the manufacturer and the model. From the table it can be concluded that model is accurate enough to simulate the discharge time as function of a constant discharge current.

Table 9 Results discharge time simulation

I [A]	t [h] Data	t [h] Model	Error
130	100	97.0	3.0 %
249	50	49.3	1.2 %
570	20	20.2	-1.0 %
1050	10	10.0	-1.0 %
1880	5	4.99	0.2 %
2840	3	3.00	0.7 %
3950	2	2.01	1.0 %
5050	1.5	1.51	2.0 %
5900	1.25	1.27	1.6 %

Figure 58 illustrates the discharge time given by the manufacturer, and from the simulation at defined discharge currents. The lines in Figure 58 are lines of constant discharge currents. The labels of the figure are the pseudo depth of discharge and the open cell voltages. The dots in the figure are the voltages given by the manufacturer of the cells. The currents in the legend correspond to the discharge currents stated in Table 9. The voltage of the battery during charging is illustrated in Figure 59. The battery voltage is higher due to hysteresis effects [22]. Data of the manufacturer is not added as it was not available.

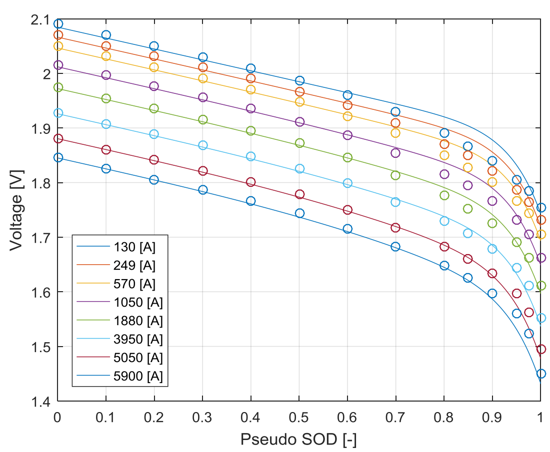

Figure 58 Cell voltage as function of the pseudo discharge state – Discharging

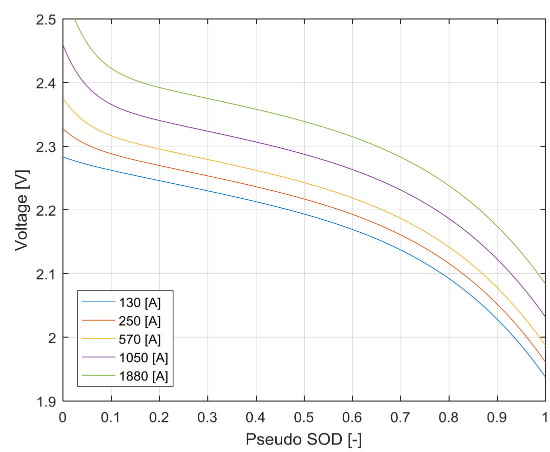

Figure 59 Cell voltage as function of the pseudo discharge state – Charging

Figure 60 illustrates the battery capacity as function of the discharge current. The line is the modelled capacity, the circles are the data obtained from the manufacturer. It can be concluded that the standalone model is a good representation of the behaviour of a real battery cell. The discharge times and the voltages as function of the discharge state match within a maximum deviation of 3 %.

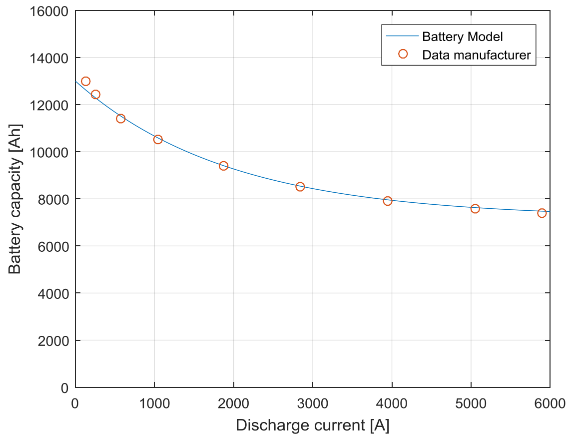

Figure 60 Battery capacity as function of discharge current

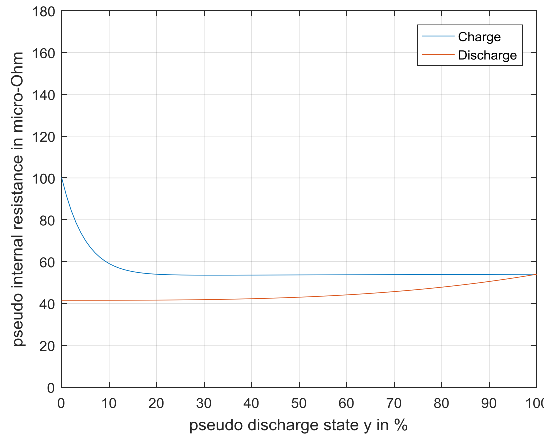

Figure 61 pseudo internal resistance as function of pseudo discharge state

6.4 Verification battery model for lithium-ion

This subchapter elaborates on the verification of the battery model for lithium-ion battery cells. The lithium-ion battery cells are the energy storage components in concept system configuration B. Verification justifies the use of the model.

Table 10 Lithium battery cell parameters

Symbol	Value	Unit	Description	Source
m	4.2	kg	Battery mass	KOKAM
c_∞	51.0	Ah/kg	Capacity at 100 h discharge time	KOKAM
c_5	47.6	Ah/kg	Capacity at 5 h discharge time	KOKAM
c_0	45	Ah/kg	Capacity at 1.2 h discharge time	KOKAM
$U_0(0.0)$	4.2	V	Open cell voltage fully charged	KOKAM
$U_0(0.7)$	3.7	V	Open cell voltage at 0.7	KOKAM
$U_0(1.0)$	3.0	V	Open cell voltage fully discharged	KOKAM

Table 11 Lithium-ion cell dimension properties

Cell type	Length [mm]	Width [mm]	Thickness [mm]	Volume [L]	Mass [kg]
SLPB14060330	327	464	14	2.12	4.2

6.4.1 Discharging

The available cell voltage data as function of the pseudo depth of discharge and discharge current is illustrated in Figure 62. The obtained simulation results of the performance model are represented in Figure 63. The cell capacities and discharge current are obtained from the manufacturer. The internal resistance is adjusted to fit simulation fit the given data. The simulated voltage can be considered a straight line up to 0.9 SOD, where the given data prescribes a dip around 40% relative capacity. This error is considered as not to be significant. The capacity as function of the discharge current is illustrated in Figure 64. The simulation do fit the data points of the manufacturer.

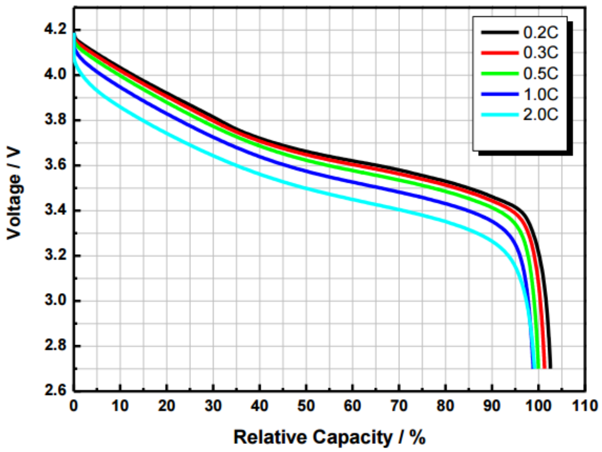

Figure 62 Cell voltage according to the manufacturer as function of the pseudo depth of discharge [15]

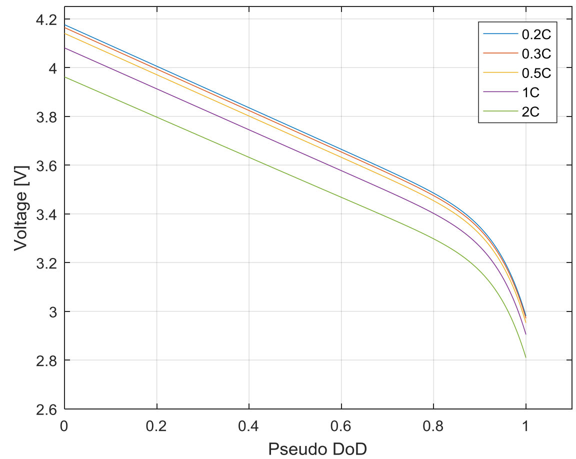

Figure 63 Modelled cell voltage as function of the pseudeo depth of discharge

The maximum charge current of the specified battery cell is 1C, corresponding to 200 A per cell up to the open cell voltage when fully charged of 4.2 V.

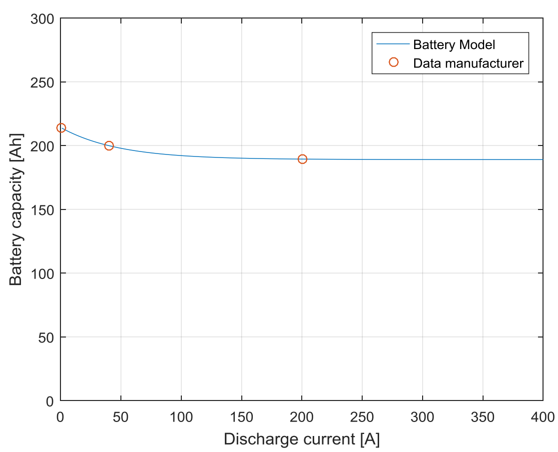

Figure 64 Cell capacity as function of the discharge current

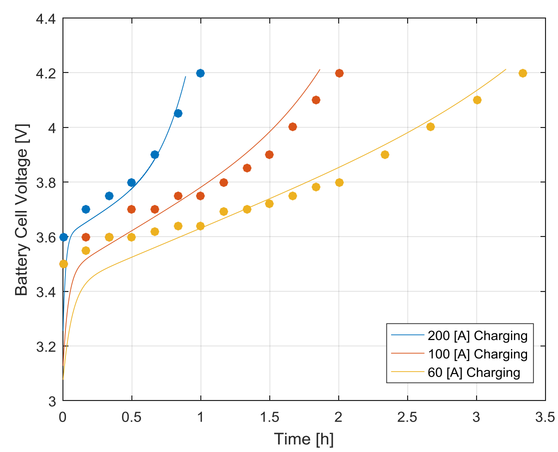

Figure 65 Battery voltage as function of time during constant charging

6.5 Comparison battery types

The batteries are compared on a very high level in the energy density plot in Figure 10. From the figure it was concluded that the energy densities; expressed in Watthour per litre and Watthour per kilogram, are higher for lithium-ion batteries compared to lead-acid batteries. The maximum discharge current per cell is however not taken into account. The maximum lithium-ion discharge current is limited to 400 [A] for the used cell [15], where the lead-acid cell discharge current is limited to 6000 [A] [29]. This subchapter elaborates on the comparison between the cells on a deeper level than the energy density plot in Figure 10, based on the battery models described in the previous chapters.

Figure 66 illustrates the battery cell capacity, expressed in Ampere-hour as function of the discharge current in Ampere. This figure is a combination of Figure 60 and Figure 64. The lead-acid battery is the VARTA UR 12 battery cell, the Li-ion battery is the single KOKAM cell. It is clearly visible that the lead-acid battery contains more capacity. The Li-ion cell is hardly visible in the left bottom corner. Besides the capacity, is the maximum discharge current of the lead-acid battery 6000 [A], a significant higher value compared to the lithium-ion cell, that is limited to 400 [A]. It is however not hard to understand that the lead-acid battery contains more capacity as the used battery cell mass is a 530 [kg] and the lithium-ion cell mass is a 4.2 [kg]. A better comparison is the comparison per unit of mass. The capacity per unit of mass is illustrated in Figure 67. Per unit of mass is the capacity of the li-ion cell twice the capacity of the lead-acid cell.

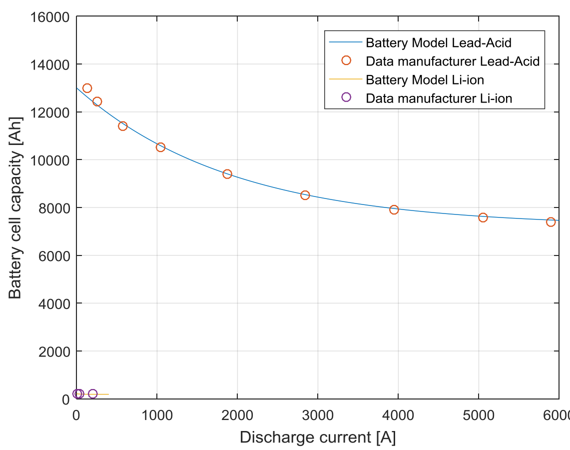

Figure 66 Battery cell capacity in [Ah]

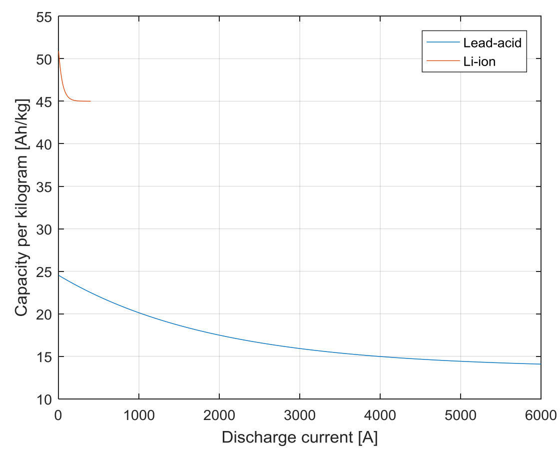

Figure 67 Battery cell capacity in [Ah/kg]

The maximum discharge current for lithium-ion cells can be increased by switching cells in parallel. By adding a second cell in parallel, the maximum discharge current doubles to a value of 800 [A]. Doubling to 4 cells in parallel results in a maximum discharge current of 1600 [A]. Besides the doubling of the discharge current is the capacity doubled.

The capacity for the parallel switched lithium-ion cells is expressed by equation 6-20. This equation is based on equation 6-14. The values are illustrated in Figure 68.

$$C_t(I) = C_\infty \left(\alpha + \alpha \cdot e^{-\left(\frac{I_{in}}{I_{char}}\right)} \right) \qquad \text{ref 6-14}$$

$$C_t(I) = C_\infty \cdot n_{parallel} \cdot \left(\alpha + \alpha \cdot e^{-\left(\frac{\frac{I_{in}}{n_{parallel}}}{I_{char}}\right)} \right) \qquad (6\text{-}20)$$

The capacity of the lead acid battery cell (VARTA UR 12), is compared to the lithium-ion battery cell. The lithium-ion battery cells are switched in parallel of 40, up to 70 cells. The simulation results show the steep decrease of capacity of the lead-acid cell as function of the discharge current. At low discharge currents is the capacity of the lead-acid cell equal to 60 cells in parallel. But at high discharge currents is the capacity as low as 40 cells.

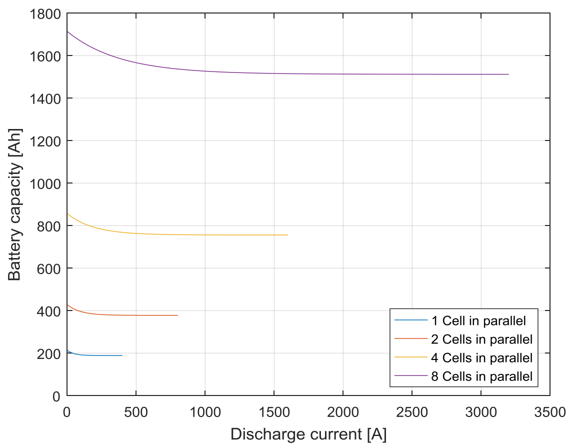

Figure 68 Lithium-ion cells in parallel

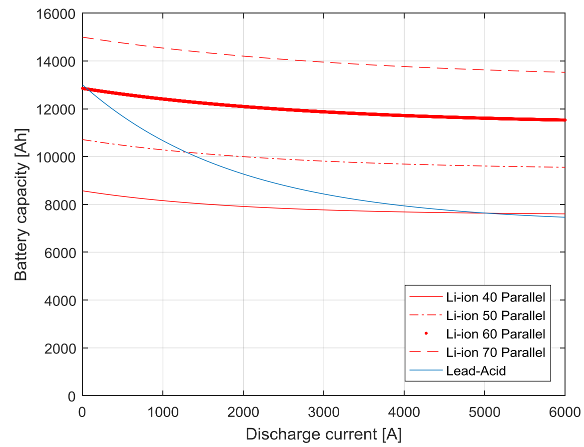

Figure 69 Lithium-ion and Lead-Acid

6.5.1 Normalized mass and normalized volume

The comparison of lead-acid and lithium-ion battery cells is normalized to equal weight and volume. The packing of the lithium-ion cells into a module is significant as discussed in section 3.4 and illustrated in Figure 70. The packing factor for volume, 1.6, must be multiplied with the volume of the cells. The packing correction factor for the mass, 1.3, must be multiplied with the mass of the cells.

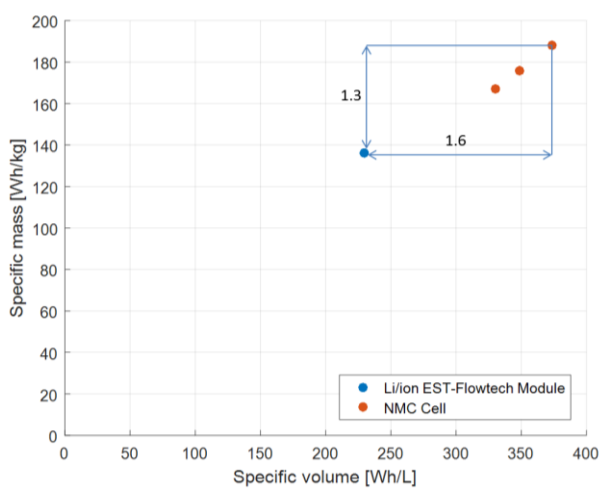

Figure 70 Correction factors

The cell properties are defined in Table 11 Lithium-ion cell dimension properties. The cell volume is 2.12 litres and has a mass of 4.2 kg. The packing factor for the volume is the specific mass of the cell divided by the specific mass of the cell module. This results in a packing correction factor of 1.6. The packing factor for mass is calculated in the same way as volume. The packing correction factor is 1.3.

$$n_{nor.mass} = \frac{m_{cell\ lead}}{m_{cell\ li-ion} \cdot f_{mass\ correction}} = \frac{530}{4.2 \cdot 1.3} = 97 \qquad \text{6-21}$$

$$n_{nor.volume} = \frac{V_{cell\ lead}}{V_{cell\ li-ion} \cdot f_{volume\ correction}} = \frac{0.20}{2.12 \cdot 10^{-3} \cdot 1.6} = 59 \qquad \text{6-22}$$

The lead-acid cell capacity, the lithium-ion battery capacity with normalized mass, and the lithium-ion battery capacity for normalized volume are plotted in Figure 71. The normalized mass configuration has the highest capacity over the total discharge range. The shape of the capacity of the normalized volume is the same as the shape of the normalized mass. According to the simulation is the capacity for lead-acid higher at for discharge currents lower than 200 [A].

The capacity can also been expressed in watt-hours. The difference between watt-hours and Ampere-hours is the multiplication with battery voltage. The battery voltage of the lithium ion battery cell is higher compared to a lithium-ion cell as illustrated in Figure 58 and Figure 63. Combining the capacity in Ampere-hours and the battery voltage results the watt-hour capacity. This is plotted in Figure 72. The battery capacity for the normalized volume is now higher for all discharge currents.

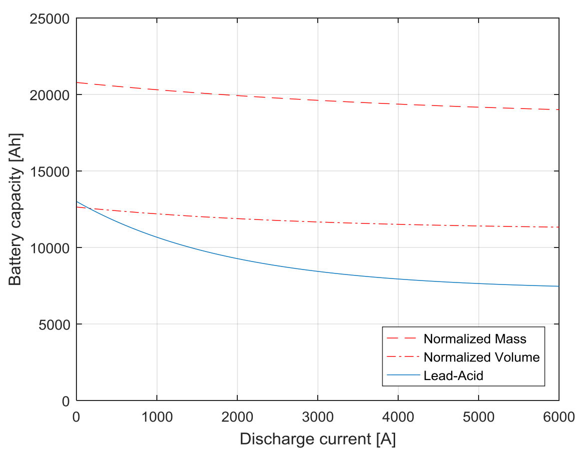

Figure 71 Battery capacity in Ampere-hour as function of the discharge current

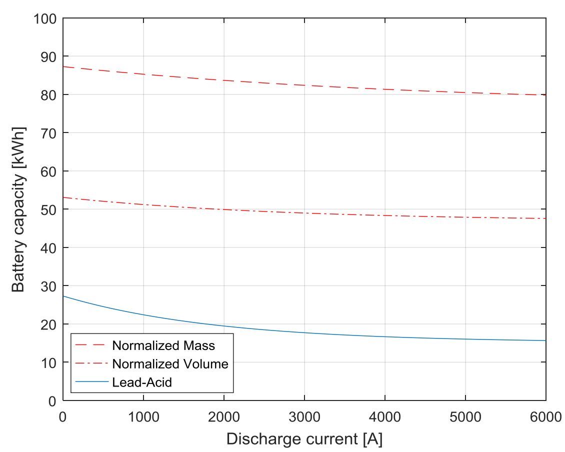

Figure 72 Battery capacity in kWh as function of the discharge current

6.5.2 Analyse

The illustrated results in Figure 71 and Figure 72 contain uncertainties. The lead-acid battery cell parameters are obtained from a battery from 1992, since than the battery technology became better, resulting in higher storage capabilities. Those data is classified and therefore not used in the research. The lithium-ion technology on the other hand is the newest technology with the latest available data. The intersection is assumed to shift to higher discharge currents.

Another uncertainty is the applied packing factor. This factor is obtained in a technical meeting with EST-Flowtech. The packing factor has however a significant influence on the total mass and volume. The used packing factor is for an air-cooled system. A water-cooled system could have a higher packing factor. The result of a higher packing factor is a lower number of cells in parallel, as calculated in equation 6-22. This results in a lower capacity. The difference in capacity, expressed in watthours, is such that the lithium-ion battery cell is preferred.

6.6 Conclusion

For the performance prediction of a battery cells is a performance model used. The mathematical model of D. Stapersma accurately describes the performance and is therefore useful for the propulsion plant design. Available discharge times and voltages over the total discharge range obtained from the manufacturer can be reproduced with the battery parameters. These constants are supplied by the manufacturer. The model is valid for lithium-ion and lead-acid batteries, as verified in subchapters 0 and 6.4. The battery cell performance during charging is also verified. These performances are required for the concept configuration power plant performance during snorting.

The lead-acid battery that is used to verify the performance model is optimized for submarine specific applications. Large cells of 530 kilograms containing large discharge capacities. A disadvantage of the lead-acid technology is the capacity at higher discharge currents. The cells have the highest energy storage capacity at low discharge currents, but are less effective at higher discharge currents. The available cell capacity is strongly dependent on the discharge current. The capacity is almost halved for the submarine specific battery cell. The capacity of lithium-ion battery technology is less dependent on the discharge current, an advantage during high propulsive power demands.

The disadvantage of the lithium-ion battery cells is that they are not capable of delivering the high discharge currents required for the high propulsive power of 6000 [A]. Besides, the cell mass is limited, resulting in a limited stored capacity per cell. The solution is switching the cells in parallel to deliver the high currents and to store the required capacity.

When the cells are switched in parallel, and the packing factor for mass and volume is taking into account, the lead-acid and lithium-ion cells can be compared. The stored energy as function of the discharge current is illustrated in Figure 71. The simulation results show that at very low discharge currents, lower than 200 [A] the lead-acid cell stores more energy than the lithium-ion cell for a normalized volume. At higher discharge currents the lithium-ion cell performs better, for normalized volume and mass. If the capacity is expressed in Watthours, the lithium-ion cell stores more energy for the normalized mass and normalized volume. It can be concluded in advance, based on the found results that for the assumed mission profile the lithium-ion battery cells require less mass and volume compared to lead-acid battery technology.

The absolute mass, containing the required energy to fulfil the mission can be obtained with simulations, using the battery cell and propulsion motor performance models.

7 Diesel generator performance model and dimensions

7.1 Introduction

The generator output power is dependent on the defined indiscretion ratio. The generator power is calculated for the specific mission profile. The required generator power is the input for the dimensioning of the generator and diesel engine. This chapter elaborates on the diesel generator set dimensioning and optimization with respect to mass and volume.

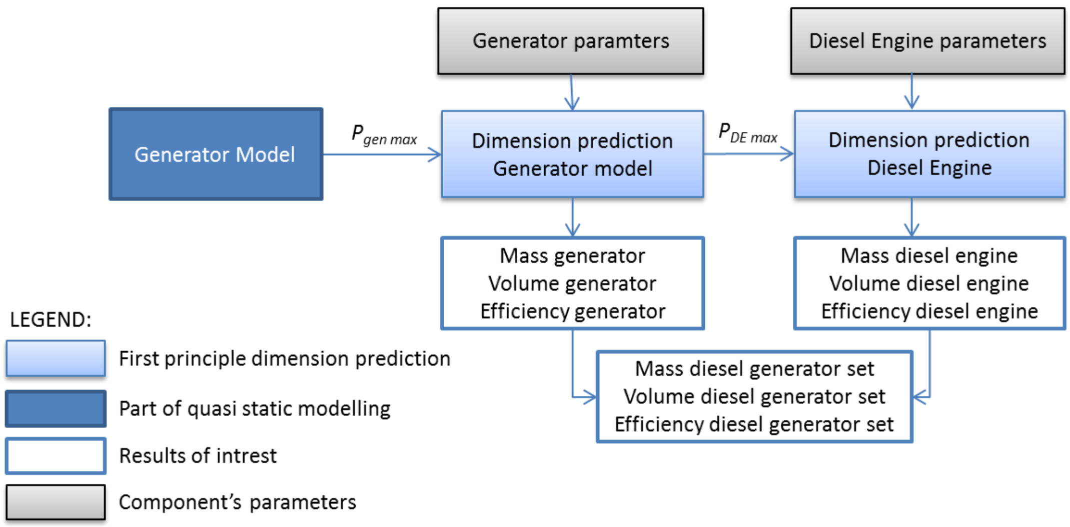

Figure 73 Diesel generator set dimensioning

7.2 Diesel generator set performance model

A diesel generator performance model is assumed not to be necessary. The diesel engines are running at constant power. The maximum constant power output. The load is not changing, the efficiency is assumed to be constant.

7.3 First principle dimensioning generator

The input for the generator component dimensioning is the generator output power. The sizing of the generator set is done using a scaling method described in the book: Electric machines, Drives, and Power Systems by Theodore Wildi [30]. The scaling of power output of the synchronous machines has an effect on the efficiency, mass, volume and costs. A small AC synchronous generator is taken as the initial generator. This generator can be scaled while remaining the technical constants; the numbers of poles, number of slots and speed of rotation, current and flux densities in the various parts of the machine; stator teeth, air gap and core.

The scale factor is expressed by the factor f. The volume of the motor is a multiplication of the area of the motor times the length. This is a cubic formula, the volume of the motor is scaled with a factor f^3. The mass of the generator is a function of the volume. The mass and the losses are therefore also scaled with a factor f^3.

$$m_{gen} = m_{ini} \cdot f^3 \qquad \text{7-1}$$

$$V_{gen} = V_{ini} \cdot f^3 \qquad \text{7-2}$$

The slots of the machine are a factor f wider and f deeper. As a result the cross section of the conductor is scaled with a factor f^2. A larger machine results in a larger allowable current, when the maximum current density is constant, the current is a function of the area and therefore scalable with a factor f^2. The generated voltage per conductor is expressed in equation 7-3.

$$E = B \cdot l \cdot v \tag{7-3}$$

The flux density is assumed to be constant. The length is scaled with a factor f. The speed of rotation is constant, so the peripheral speed of the conductor trough the magnetic field is increased with a factor f.

$$E_{scaled} = B \cdot f \cdot l \cdot f \cdot v = f^2 \cdot B \cdot l \cdot v \tag{7-4}$$

The power output is the result of multiplying the voltage and current.

$$P_{scaled} = E_{scaled} \cdot I_{scaled} = f^2 \cdot E \cdot f^2 \cdot I = f^4 \cdot E \cdot I \tag{7-5}$$

The scaled efficiency can be calculated by:

$$\eta_{scaled} = \frac{P_{out_{scaled}}}{P_{in_{scaled}}} = \eta \cdot \left(\frac{f^4}{f^3 + f^4}\right) = \eta \cdot \left(\frac{f}{f+1}\right) \tag{7-6}$$

The results of the scaling are compared with data of manufacturers. The data is obtained of multiple manufacturers, and a varying range of power. The blue dots in Figure 74 and Figure 75 are the data points. Three coloured dots are the initial generators. The lines are the scaling lines of the initial generators.

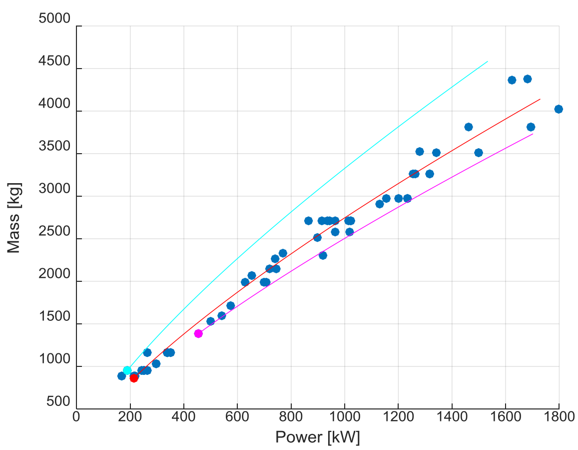

Figure 74 Power versus mass generators

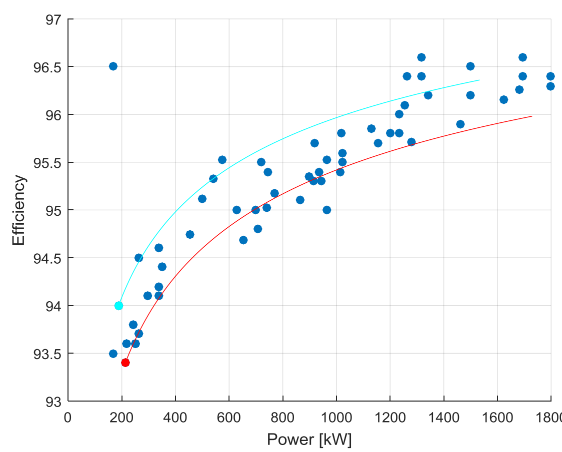

Figure 75 Power versus efficiency generators

It can be concluded that the methodology of scaling an initial generator while remaining the technical constants the same results in accurate results. The required diesel engine power is obtained by dividing the required generator power by the generator efficiency. The required diesel engine power is the input for the dimensioning of the diesel motor. The used generator efficiency is 95%. Besides the generator efficiency is the conversion of AC to DC taken into account. This value is assumed to be 92%.

7.4 First principle diesel engine dimensioning

Sizing the diesel engine for a submarine application is the same as the sizing of surfaced marine diesel engines. The invention of the snorting system increased the main objective of a submarine, stealth, but has a significant effect on the performance.

Due to power density and relative robustness against exhaust gas backpressure, most modern submarine diesel engine designs employ high-speed four stroke engines. An interesting aspect of the diesel engine, especially in submarine applications, is the charging of the cylinder. The charge of air is pre-compressed by a compressor before entering the cylinder. The supply air to the cylinder consists of three parts, the first part is the air drawn into the cylinder during the inlet stroke by the movement of the piston, this is called the induction. The second part is filling up of the cylinder during the equalizing of the cylinder pressure and the inlet receiver while only the inlet vale is open; and therefor this mechanism is called pressurizing. And the third part is the scavenging of the cylinder while both in-, and exhaust valves are open. [31] Especially the pressurization and the scavenging require the compressor.

The static backpressure has an influence on the *blow down and gas exhaust* stroke and *scavenging stroke*. As the backpressure increases more power is required to expel the gases out of the cylinder. The pressure ratios across the turbocharger compressor and turbine decrease, reducing mass flow of air through these components and thus the available air in the cylinder. At the same time, the fuel flow must increase to provide extra power necessary to overcome the increased pumping losses while maintaining a constant brake power output. As a result the specific fuel consumption increases above that for an engine operating in atmospheric conditions [32]. The high back pressure is responsible for the power drop of the engine under submerged conditions.

7.4.1 Submarine diesel engine technical parameters

The predicting of diesel engine dimensions using first principle relationships consists out of two main steps. First, the core of the engine has to be sized to the required power output and speed. Second, making use of core dimensions a range can be estimated for the size of the total engine using regression analysis. [21] The challenge for submarine diesel engine sizing is that there are just a few diesel engine manufactures. Those manufactures are not willing to share information or the information is outdated. The only recent information is of MTU. Therefor MTU data are used.

The submarine diesel engine performance parameters are obtained from the available output power and the knowledge that the core of the machine is constructed out of 4000M73. [33]

Table 12 marine diesel engine technical parameters 4000M73

Symbol	Description	Value	Unit	Source
$\boldsymbol{p_{me}}$	Mean effective pressure	22.5	bar	-
$\boldsymbol{c_m}$	Mean piston speed	12.5	m/s	-
$\boldsymbol{L_s}$	Stroke length	0.19	m	MTU
$\boldsymbol{D_B}$	Bore diameter	0.17	m	MTU
$\boldsymbol{\lambda_s}$	Stroke to bore ratio	1.12	-	MTU
$\boldsymbol{n}$	Revolutions per second	32.8	rev/s	MTU
$\boldsymbol{k}$	4-stroke diesel engine	2	-	MTU

The length and diameter of the bore of the 4000M73 are used. This results in the same stroke to bore ratio. The output power and the revolutions per second of the submarine diesel engines are known. [33]

The mean piston speed and the mean effective pressure can be derived. As stated in equation 7-7 and 7-8. [4]

$$P_B = 1300\ kW$$

$$N = 1800\ rpm \rightarrow 30\ rps$$

$$c_m = 2 \cdot L_s \cdot N = 2 \cdot 0.19 \cdot 30 = 11.40\ m/s \tag{7-7}$$

$$p_{me} = \frac{32 \cdot\ P_B}{\pi} \cdot \frac{\lambda_s^2}{c_m^3} \cdot \frac{N^2 \cdot k}{i} = 16.8\ bar \tag{7-8}$$

The submarine diesel engine performance parameters are stated in Table 13. Those parameters are used to determine the core size of the diesel engines.

Table 13 submarine diesel engine technical parameters

Symbol	Description	Value	Unit	Source
p_{me}	Mean effective pressure	16.8	bar	-
c_m	Mean piston speed	11.4	m/s	-
L_s	Stroke length	0.19	m	MTU
D_B	Bore diameter	0.17	m	MTU
λ_s	Stroke to bore ratio	1.12	-	MTU
n	Revolutions per second	30.0	rev/s	MTU
k	4-stroke diesel engine	2	-	MTU

The performance parameters of the submarine engine are plotted against the marine diesel intended for surface operation in Figure 76. The performance parameters of the diesel engines have been obtained from technical datasheets of the supplier. In propulsion motors with the highest performance parameters are diesel engines with a low average load factor.

The load factor is the amount of load and the amount of time the generator set is operating at that load. One of the important steps in sizing generator sets for any application is to determine the application’s average load factor. Understanding this parameter is essential not only for proper power system sizing but also for operability and reliability. [34] The engines with the low load factor are designed for sprint power, where the high load engines are more conservative, designed for long endurance. The submarine diesel engine is designed as a more conservative engine. The submarine diesel engines have high load factors. The diesel engine is only running at maximum power output, to reduce the snorting time.

In Figure 76 illustrates two submarine diesel engines; 396 SE84 and MTU Submarine. The 396 SE84 is an older design of MTU. This type will be replaced by the MTU submarine engine. There have been improvements in the performance parameters. This results in a higher power output within the same space. The most recent development in submarine diesel engine technology is the exhaust gas turbo charging in combination with a waste gate. The dynamic effects caused by the waves working on the turbo are reduced. MTU uses the 4000 series as a basis for the submarine engine [35]. As for all predecessor submarine engine designs, submarine specific components are developed to meet the demanding operating conditions on board of submarines. The M73 components are used as the basis for the core of the motor.

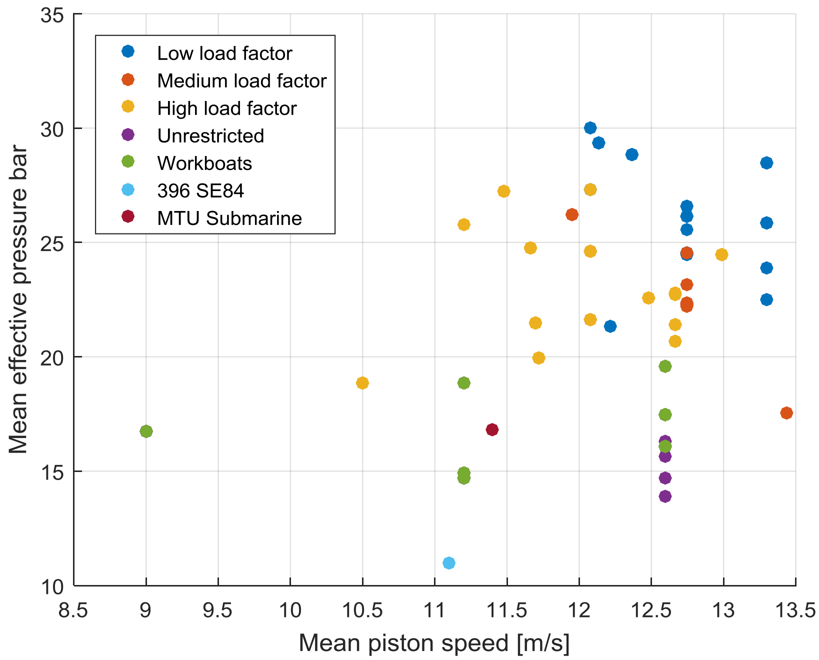

Figure 76 Mean effective pressure plotted against mean pistion speed

The parameters of the MTU submarine diesel engine have been used to predict the dimensions of the diesel engine generator set as function of the assumed mission profile.

7.4.2 Dimension prediction submarine diesel engine

The performance parameters of the diesel engine have been obtained in the previous chapters. Those performance parameters are used to size the core of the diesel engine.

7.4.2.1 Sizing the core

The brake power can be expressed in terms of mean effective pressure [4], mean piston speed, bore to stroke ration, λ_s , and rate of rotation. This equation can be rewritten to express the number of cylinders as function of the brake power. The parameters used in the equation are stated in Table 13.

$$P_{B\ Diesel} = \frac{P_{gen}}{\eta_{gen} \cdot \eta_{conv}} = \frac{\pi}{32} \cdot p_{me} \cdot \frac{c_m^3}{\lambda_s^2} \cdot \frac{i}{n^2 \cdot k} \qquad \text{7-9}$$

$$i = \frac{P_{gen}}{\eta_{gen} \cdot \eta_{conv}} \cdot \left(\frac{32 \cdot n^2 \cdot k \cdot \lambda_s^2}{\pi \cdot p_{me} \cdot c_m^3}\right) \qquad \text{7-10}$$

The calculated number of cylinders is the input for the dimensioning of the core diesel engines. The core dimension is the input for the total volume and mass of the diesel engine(s).

7.4.2.2 Length of the core

The core length of the motor is the number of cylinders times the bore diameter. For V-shaped engines the core length is divided by two. [21]

$$L_{core} = \frac{i}{2} \cdot D_B$$

7.4.2.3 Width of the core

The construction type, ct, is 0 for the trunk piston type and 1 for crosshead type engines. Current submarine engines do not make use of a crosshead. Crosshead type constructions are used in large 2-stroke low speed diesel engines to minimize sideways forces on the piston. The width of the core is calculated in equation 7-11. The derivation of the equation is stated in the work of P. de Vos. [21].

$$W_{core} = 2 \cdot \max\left(\left(\frac{L_s}{2} + (1+ct)\cdot L_s\right)\cdot sin\left(\frac{\alpha}{2}\right) + \frac{D_B}{2}\cdot cos\left(\frac{\alpha}{2}\right); L_s\right) \quad \text{7-11}$$

$$W_{core} = 2 \cdot \max\left(\left(\frac{0.19}{2} + (1+0)\cdot 0.19\right)\cdot sin\left(\frac{90}{2}\right) + \frac{0.17}{2}\cdot cos\left(\frac{90}{2}\right); 0.19\right) = 0.523\ [m]$$

7.4.2.4 Height of the core

The height of the core can be calculated with equation 7-12. [21]:

$$H_{core} = \frac{L_s}{2} \cdot \max\left(\left(\frac{L_s}{2} + (1+ct)\cdot L_s\right)\cdot cos\left(\frac{\alpha}{2}\right) + \frac{D_B}{2}\cdot sin\left(\frac{\alpha}{2}\right); \frac{L_s}{2}\right) \quad \text{7-12}$$

$$H_{core} = \frac{0.19}{2} + \max\left(\left(\frac{0.19}{2} + (1+0)\cdot 0.19\right)\cdot cos\left(\frac{90}{2}\right) + \frac{0.17}{2}\cdot sin\left(\frac{90}{2}\right); \frac{0.19}{2}\right) = 0.357\ [m]$$

7.4.2.5 Sizing the machine

The sizing of the machine is the multiplication of the calculated core, times the correction ratio. The correction factor are illustrated in Figure 77 Core length vs overall length ratio, Figure 78 Core length vs overall length ratio and Figure 79 Core height vs overall height ratio.

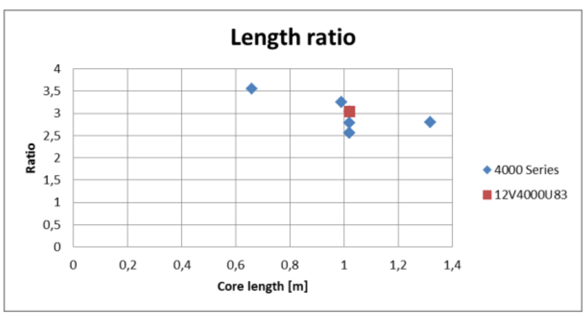

Figure 77 Core length vs overall length ratio

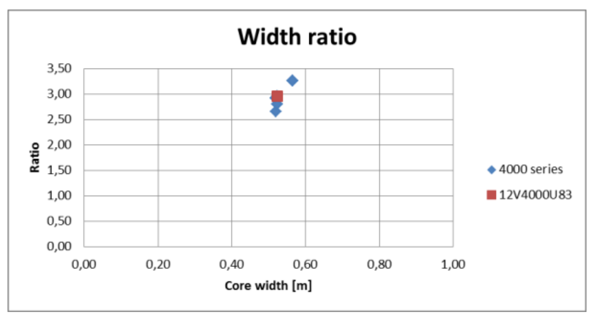

Figure 78 Core length vs overall length ratio

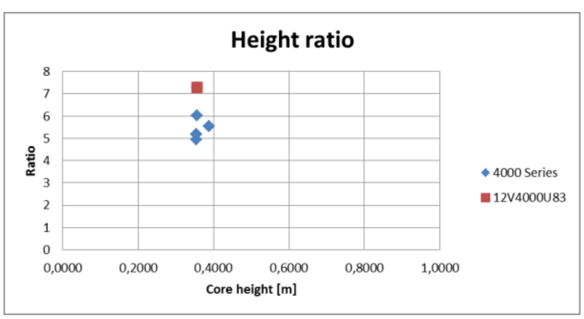

Figure 79 Core height vs overall height ratio

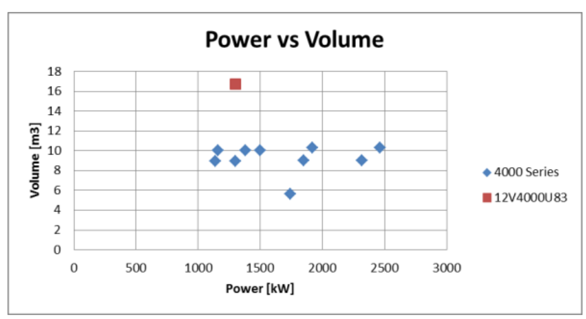

Figure 80 Power vs volume

The length and width ratios are comparable with that of surfaced marine diesel engines. Which makes sense, the U83 diesel motor is an assembly of the M70 and M73 types. The height ratio has a deviation.

This deviation is caused by the exhaust gas collection vessel on top of the diesel engine. The result is a much higher volume compared to marine surface diesel engines.

The dispersion in Figure 80 in volume as function of power is caused by the load factors. The volumes are relatively constant as function of the power output. The higher power outputs are from the engines with a low load factor.

MTU is working on a V12 submarine diesel engine. It is assumed that the submarine line will be extended with a six, eight and 16 cylinder engine. The parameters and the correction ratios can be used to predict the size of the engines.

Table 14Submarine diesel volume engine prediction

	6 Cylinder	8 Cylinder	12 Cylinder	16 Cylinder
Core length	0.51 $[m]$	0.68 $[m]$	1.02 $[m]$	1.36 $[m]$
Core Length correction	3.5	3.3	3.2	2.8
Total length	1.8$[m]$	2.2$[m]$	3.3 $[m]$	3.8 $[m]$
Core width	0.523 $[m]$	0.523 $[m]$	0.523 $[m]$	0.523 $[m]$
Core width correction	3	3	3	3
Total width	1.5 $[m]$	1.5 $[m]$	1.5 $[m]$	1.5 $[m]$
Core height	0.357 $[m]$	0.357 $[m]$	0.357 $[m]$	0.357 $[m]$
Core height correction	7	7	7	7
Total height	2.5$[m]$	2.5$[m]$	2.5$[m]$	2.5$[m]$
Volume	6.75 $[m^3]$	8.25 $[m^3]$	12.76 $[m^3]$	14.25 $[m^3]$

7.4.3 Weight of the diesel engine

The weight of the standard 4000 series is available and of the weight of a 12V4000 submarine motor. The weight of the submarine diesel engine is 1.5 times the weight of the standard diesel engine. The weight of the other types is available and corrected with the factor 1.5 for the conversion to a submarine diesel engine.

Table 15Submarine diesel engine mass prediction

	6 Cylinder	8 Cylinder	12 Cylinder	16 Cylinder
Mass surface propulsion motor	4000 kg	4700 kg [36]	6600 kg [36]	8000 kg [36]
Correction submarine equipment			1.5	
Added mass equipment	2000 $[kg]$	2350 $[kg]$	3300 kg	4000 $[kg]$
Total mass per engine incl. equipment	6000 $[kg]$	7050 $[kg]$	9900 $[kg]$ [33]	12000 $[kg]$

7.5 Diesel and generator dimensioning optimization

The combination of the generator dimensioning and the die diesel engine dimensioning results in the power generation system optimization. The mass of the scaled generator, diesel engine and the combined mass are plotted against the delivered generator power in Figure 81. The blue line is the diesel engine mass, the red line is the generator mass and the yellow line is the combined mass. In the figure is a 6 cylinder engine plotted. The steps are the increase of the number of engines, for 600 [kW] is one engine required, 700 [kW] requires 2 engines. In Figure 81 is the volume plotted against the generator power.

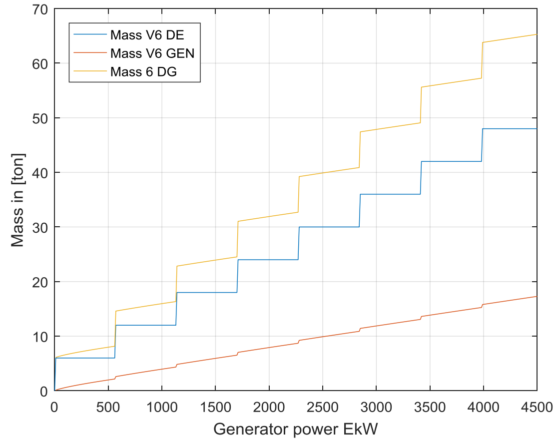

Figure 81 power generation mass plotted against generator output power

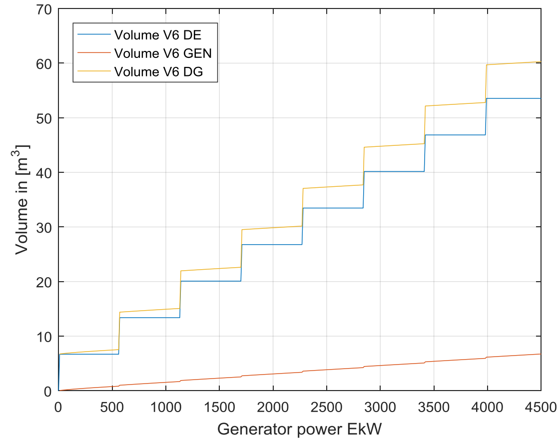

Figure 82 power generation volume plotted against generator output power

In Figure 83 is the mass of the diesel generator set plotted for a 6,8,12,16 cylinder diesel engine as function of the diesel generator. Figure 84 illustrates the volume of the diesel generator sets as function of the generator power. These dimension prediction models are used to determine the optimum diesel generator sets with respect to mass and volume.

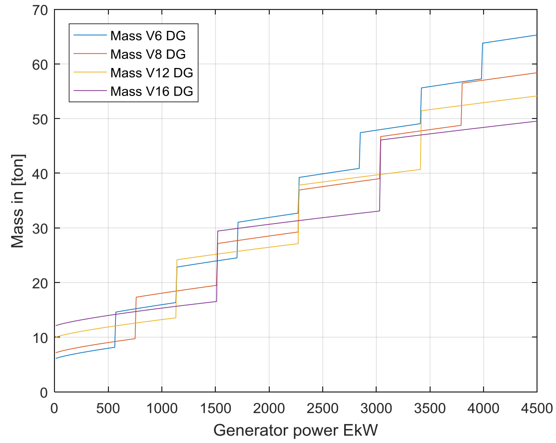

Figure 83 Mass of the diesel generator set as function of the generator output power

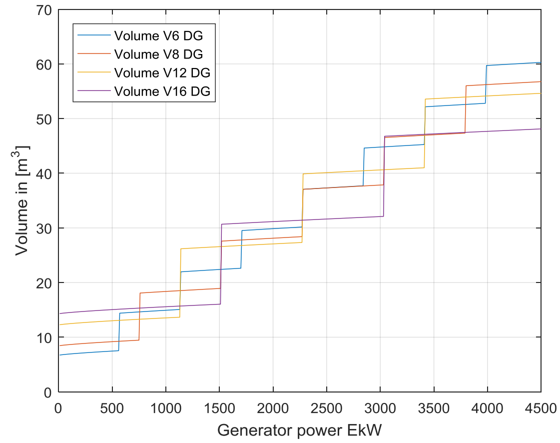

Figure 84 Volume of the diesel generator set as function of the generator output power

7.6 Conclusion

The volume and weight of the diesel generator set as function of the required generator power can be obtained with first principle dimension prediction.

The efficiency of the diesel generator set is assumed to be constant. According to the diesel engine manufacturer are the performance parameters of the submarine engine comparable to the performance parameters of the marine surface diesel engines with high load factors. The manufacturer (MTU) uses exhaust gas turbo charging in combination with a waste gate to optimize the performance parameters.

The performance parameters are used in the first principle dimension prediction modelling to predict the dimensions of the diesel generator set.

8 Propulsion plant configuration A

8.1 Introduction

The performance models of the propulsion motor and the battery cell have been verified in the previous chapters. It is concluded from numerical simulations and experimental results, that those models are good representations. Combining the two models and the switchboard settings results in the propulsion plant configuration A.

The model is used to dimension the batteries. The dimensions of the batteries are dependent on the battery properties and the set mission profile. The battery properties are defined as parameters. The relevant part of the mission profile for dimensioning the batteries is the surveillance and attack part of the mission. The surveillance and attack part of the mission is the longest part without recharging the batteries. An algorithm is used to find the optimum battery mass for the assumed mission profile, for the set parameters. The found optimum battery properties are used for the computing of the generator output power. The generator power is depended on the covert transit requirements set in the mission profile. The generator output is used to determine the weight and volume of the diesel generator set.

8.2 Propulsion plant model

The propulsion plant performance model during the deeply submerged operation is built with the performance models of the propulsion motor and the batteries. The input for the propulsion motor is the set propulsive power, at a defined rate of rotation, and the available battery voltage. The output of the model is the current that has to be supplied by the battery cells. The current required for propulsion motor and the current for the auxiliary systems is considered to be the total discharge current, acting on the batteries.

The switching of the batteries and propulsion motor in series and parallel is done in the switchboard (SWB). Besides the switching in series and parallel converts the SWB the total discharge current to the discharge current per cell. The discharge current per cell is the input for the performance model of the battery. The output of the battery cell performance model is the battery cell voltage. The battery cell voltage is input for the SWB. The SWB switches to the total battery output. The battery output is dependent on the cell voltage and battery settings; series or parallel. The propulsion plant model during deeply submerged operation is illustrated in Figure 85.

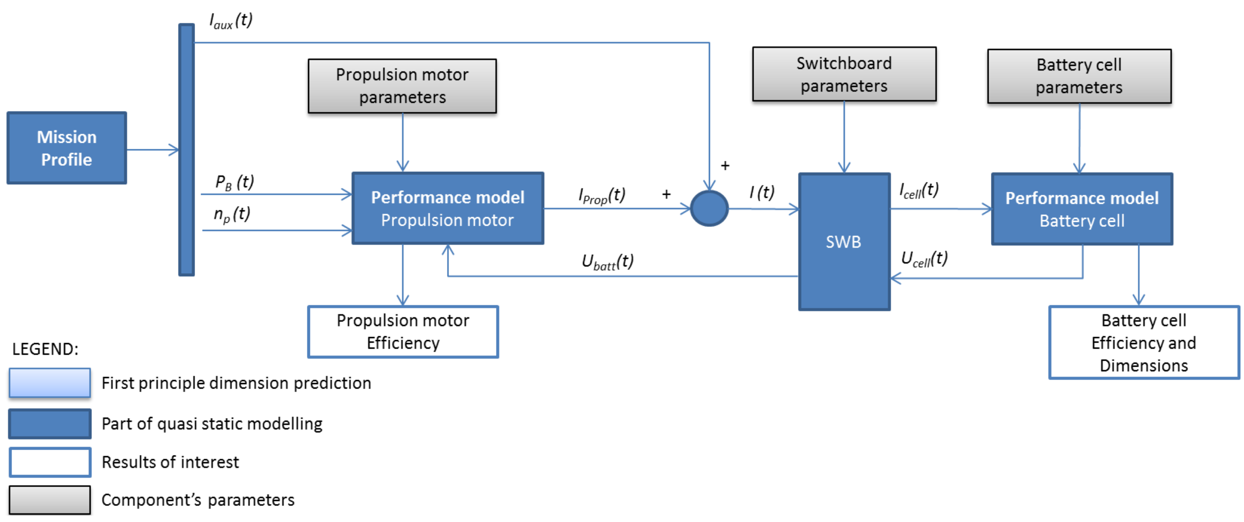

Figure 85 Propulsion system during submerged operation

8.3 Battery topology

The energy storage components consist of two batteries. The batteries consist of multiples cells as can been seen in Figure 86. The cells are connected in series to form a battery. The battery voltage is dependent on the number of battery cells in series.

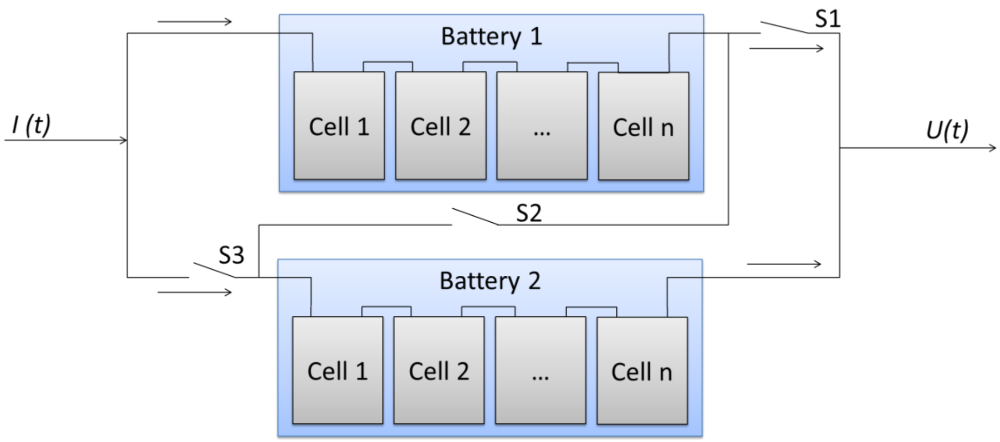

Figure 86 Battery topology lead-acid

The cells in the batteries are connected in series. The voltage of the battery is equal to the sum of the cells.

$$U_{bat1} = U_{b1\,cell1} + U_{b1\,cell2} + U_{b1\,cell3} + \cdots + U_{b1\,cell\,n} \qquad \text{8-1}$$

$$U_{bat2} = U_{b2\,cell1} + U_{b2\,cell2} + U_{b2\,cell3} + \cdots + U_{b2\,cell\,n}$$

The performance model of the battery cell represents a single cell. It is assumed that the cells in the battery have the same behaviour, independent of their position in the battery. Equation 8-1 becomes equation 8-2.

$$U_{bat1} = U_{cell} + U_{cell} + U_{cell} + \cdots + U_{cell} \qquad \text{8-2}$$

$$U_{bat2} = U_{cell} + U_{cell} + U_{cell} + \cdots + U_{cell}$$

The batteries can be either in parallel or series. Switch *S1* and *S3* closed, *S2* is open for parallel. And in series are switch *S2* closed and *S1* and *S3* open. The armature voltage and capacity then becomes:

$$U_{Bat\ parallel} = U_{bat1} = U_{bat2} \qquad \text{8-3}$$

$$C_{Bat\ parallel} = C_{bat1} + C_{bat2}$$

$$U_{Bat\ series} = U_{bat1} + U_{bat2} = 2 \cdot U_{bat1}$$

$$C_{Bat\ series} = C_{bat1} = C_{bat2} = C_{bat1}$$

8.4 Battery mass optimization algorithm

A battery mass optimization algorithm is used to find the optimum battery mass as function of the assumed mission profile.

8.4.1 Objective

The objective of the battery mass optimization algorithm is to find the optimum battery mass. The optimum battery mass is defined as the lowest battery cell mass that meets the set requirements. The requirements are set in the mission profile. The surveillance and attack (SA) part of the mission contain the requirements. This part of the mission is the longest period without recharging. The SA part of the mission is illustrated in Figure 87.

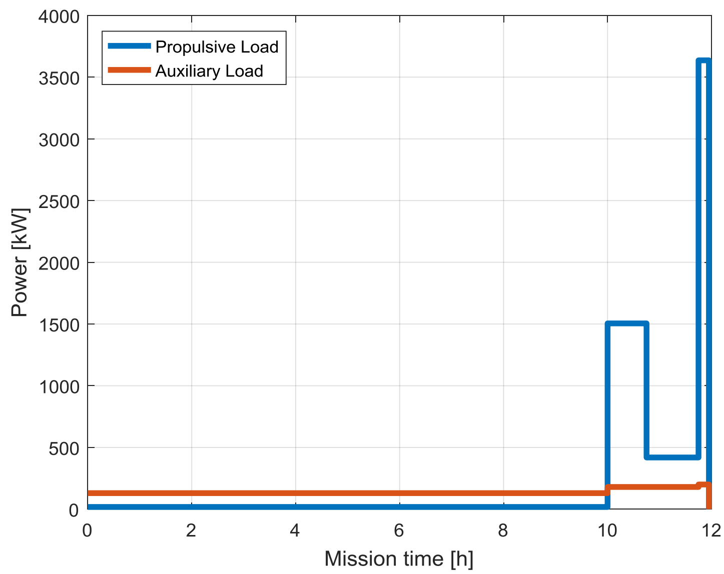

Figure 87 Assumed mission profile

8.4.2 Method

There are two variables in sizing the batteries. (1) The number of cells in series per battery and (2) the mass per cell. The number of cells in series defines the battery voltage and the mass per cell defines the cell capacity. These two variables cannot be seen separately as the discharge current is a function of the battery voltage.

The minimum number of cells in series is determined by the minimum required voltage of the propulsion motor for the maximum power output. The maximum power output of the propulsion motor is 3600 kW. The minimum required voltage for the power output is 680 [V] and is obtained from Figure 46. This results in a minimum number of cells of 326 for a battery cell voltage of 2.09 [V] [23]. The batteries are switched in series, so the minimum number of cells is 163 per battery. The maximum allowed MEM voltage is 882 [V] according to the manufacturer, resulting is a maximum of 210 cells in series per battery. The range of batteries is extended to investigate the influence of the number of cells in series. The maximum number of cells is taken as 240 cells in series per battery.

The capacity of the battery is a function of the discharge current as stated in equation 6-14. The parameters involved in equation 6-14 are related to the different cell capacities for high, medium, and low discharge current, related to α and β . And α and β are related to the mass as stated in equation 6-9 and 6-10.

$$C_t(I) = C_\infty \left(\alpha + \alpha \cdot e^{-\left(\frac{I}{I_{char}}\right)} \right)$$ ref(6-14)

$$I_{char} = \frac{C_5}{5 \cdot \ln\left(\frac{1-\alpha}{\beta-\alpha}\right)}$$ ref(6-13)

$$\alpha = \frac{C_0}{C_\infty} = \frac{c_0 \cdot m}{c_\infty \cdot m}$$ ref(6-96-10)

$$\beta = \frac{C_5}{C_\infty} = \frac{c_5 \cdot m}{c_\infty \cdot m}$$ ref(6-10)

The capacity of the cell is increased until the capacity is sufficient for the assumed mission profile, by increasing the mass of the cell by Δm.

$$m = m_{initial} + \Delta m$$

When the battery cell mass is obtained the number of cells is increased. This process is visualized in Figure 88 and Figure 89.

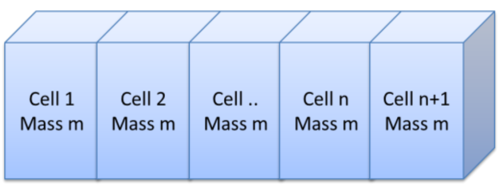

Figure 88 Number of cells *n* with mass *m*

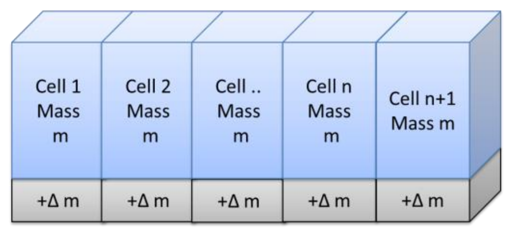

Figure 89 Cell mass increase by Δm

$$U_{bat} = U_{cell} \cdot n$$

$$C_t(I, m) = C_{cell}(I, m_{cell})$$

$$U_{bat} = U_{cell} \cdot n$$

$$C_t(I, m) = C_{cell}(I, (m_{cell} + \Delta m))$$

8.4.3 Simulation

The performance models of the propulsion motor and the battery model are used to simulated the performance and indicate if the capacity is sufficient. This is illustrated in Figure 90. There are three stop functions added to the performance model. The first stop function is the stop for exceeding the maximum pseudo depth of discharge. When the batteries are discharged the depth of discharge increases from the initial 0.2 to 1.0. When the value of 1.0 is reached the stop function is activated and the cell mass is increased.

The second stop function is activated when the propulsive power delivered by the model is lower than the set required power by the mission profile. The lower power is caused by the low battery voltage. The battery voltage is too low to maintain constant. A pre-set allowable error margin is integrated that allows an offset between the delivered propulsive power and the set propulsive power. This value is set at 80%.

The third stop function is activated if the simulation time is equal to the final time, the end time of the mission profile. When the set time is reached, the battery cell mass is a valid solution.

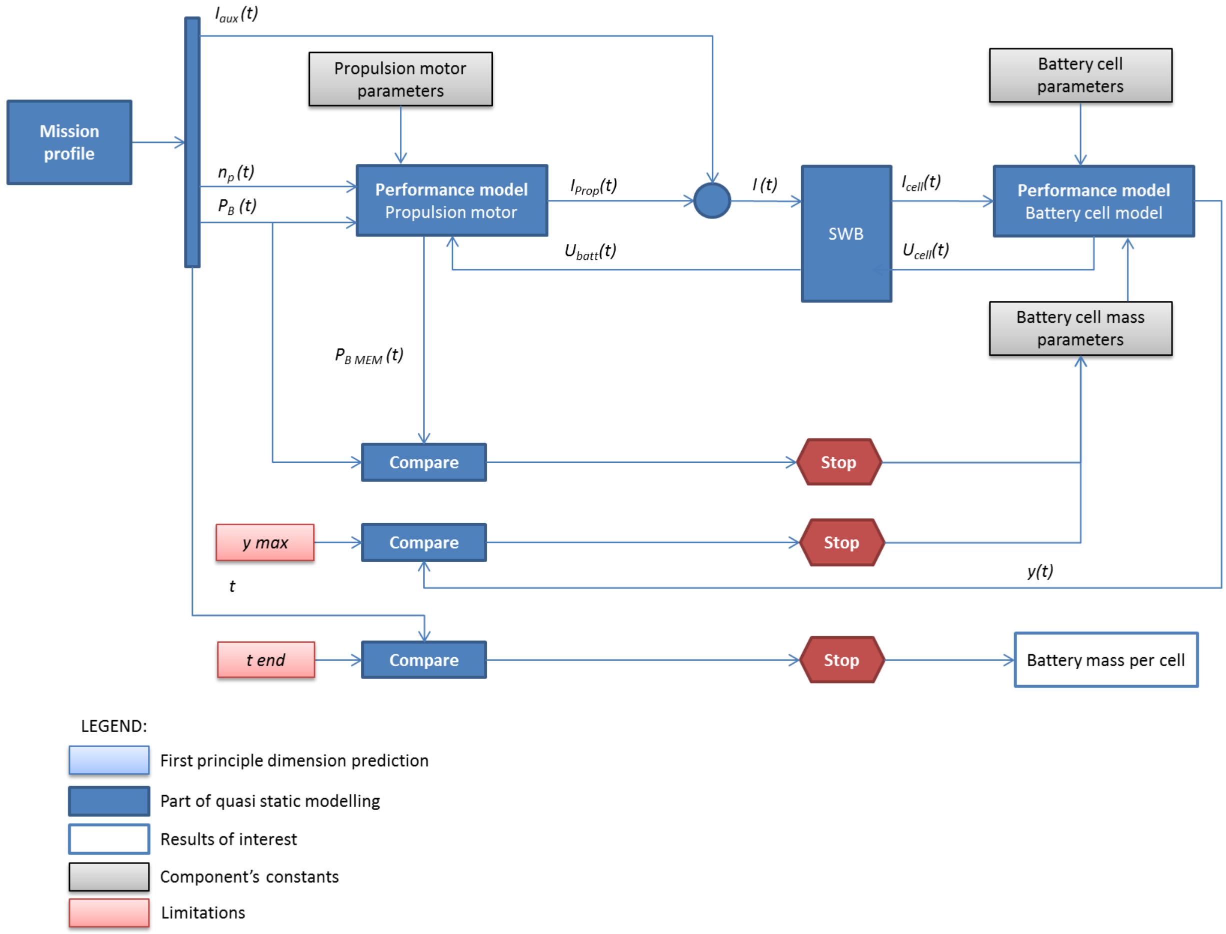

Figure 90 Battery mass optimization methodology

8.5 Results optimization

The results of the optimization are discussed in this chapter. Figure 91 is a plot of the found solutions of the algorithm. The figure illustrates the required mass per cell as function of the number of cells in series. As the number of cells increases, the required cell mass decreases. Increasing number of cells causes higher voltages. Higher voltages result in lower discharge currents. Lower discharge currents result in higher battery capacity, and therefore less battery mass. Figure 92 illustrates the mass per battery. The mass per battery is the cell mass, times the number of cells.

The discontinuous result is remarkable. There is a nod in the solution at 223 cells in series. This nod is caused by the stop functions. At low cell numbers is the stop function for delivered power activated. The propulsion motor is not capable of delivering the required power at low voltages as described in chapter 5.6. At higher battery cells is the battery voltage high enough to deliver the required power but is the battery cell capacity the limiting factor.

Figure 93 illustrates the required mass as calculated and illustrated in Figure 91 and only the power limitation. Those values are indicated with the red line. As expected is the red line continuous.

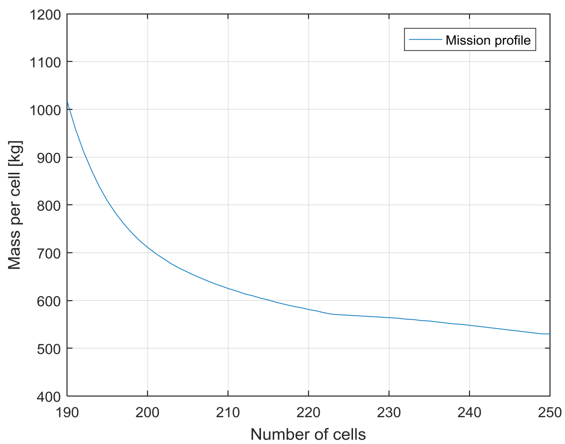

Figure 91 Optimization results [1]

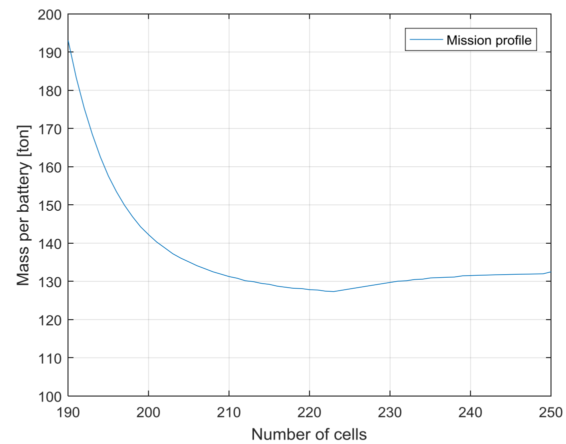

Figure 92 Optimization results [2]

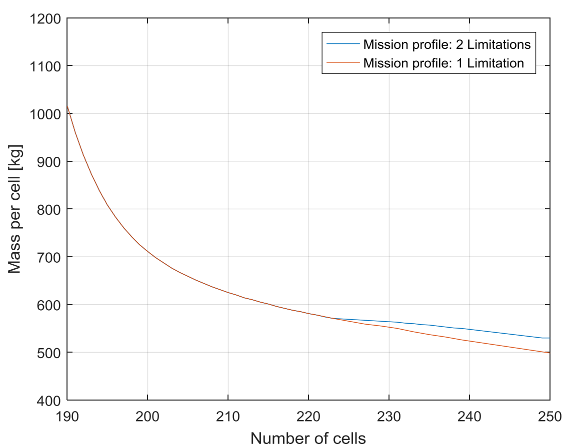

Figure 93 Optimization results [1]

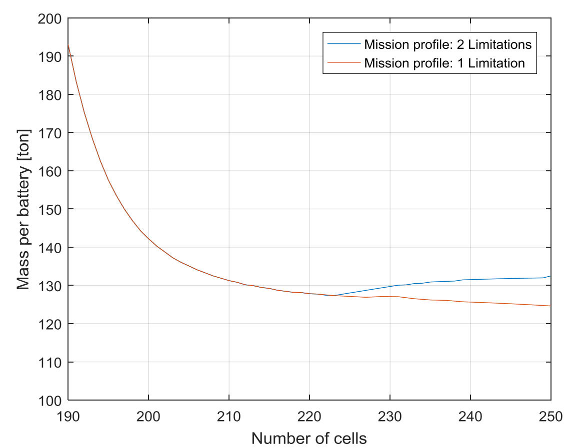

Figure 94 Optimization results [2]

8.5.1 Power requirements

Two conditions have been set. (1) The propulsive power may not be lower than 80% of the set power in the mission profile. And (2) the pseudo depth of discharge may not be higher than 1. 1 Indicates the battery is empty for the momentous discharge current.

The results of the simulation with the optimum battery settings are illustrated in the following figures. Figure 95 illustrates the set propulsive power and the and the simulated deliverd power bij the MEM. The densitiy of the circels illustrate the required calculation steps. The denser the more steps. The high peaks are caused by the PID controller. The peaks have a neglegible effect on the battery charge. It is clearly visible that the set mission profile is followed by the propulsion motor. Figure 96 illustrates the finale part of the mission profile. The deliverd power by the propulsion motor decreases steaply, but ends precisily within the 80% margin. It can be concluded that the power requires have been met.

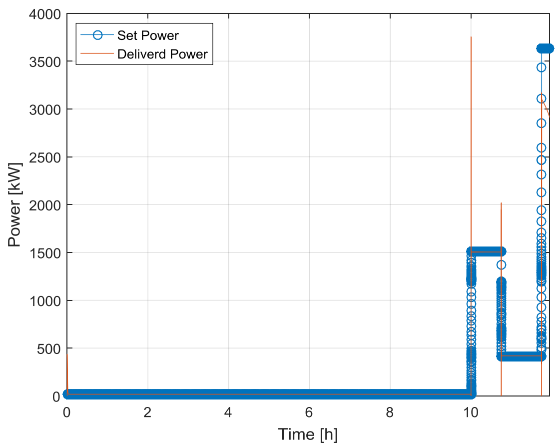

Figure 95 Set power and simulated power

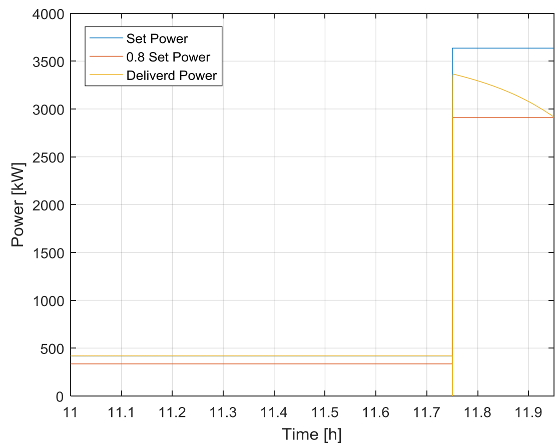

Figure 96 Set burst power and simulated power

8.5.1 Pseudo state of discharge

The pseudo state of discharge and the real state of charge of the battery cell is plotted in Figure 97. The maximum allowable pseudo state of discharge is 1, the battery is empty for the corresponding current. The maximum real state of discharge is not reached.

The battery cell voltage during the SA is plotted in Figure 98. The slope of the cell voltage decreases linear with the set power as the voltage a function is of the discharge current. At the end of the mission is the voltage decreasing non-linear as the voltage is decreasing non-linear around a pseudo depth of discharge. This is illustrated in Figure 58.The value of the voltage is dependent on the pseudo state of discharge as plotted in Figure 97.

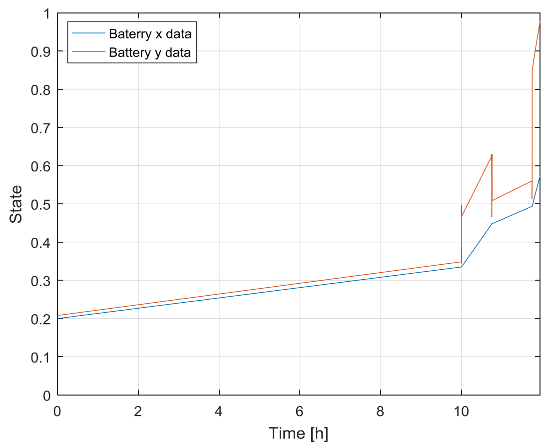

Figure 97 State of discharge(x) and pseudo discharge(y)

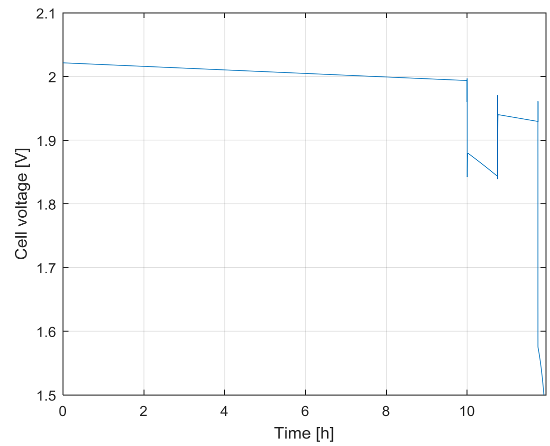

Figure 98 Battery cell voltage

The armature voltage and the discharge current per battery are plotted in time in Figure 99. The switching of the batteries and armature is clearly visible. These are the steps in the voltage. During the discharging decreases the battery cell voltage, as the SOC decreases. The result is a decreased battery voltage.

The simulated propulsion motor efficiency during SA part is plotted in Figure 100. The fat line, and the vertical lines from 10 hours and above are caused by the controller settings. It can be concluded that the optimum number of cells and mass per battery complies with the set requirements and is a valid solution.

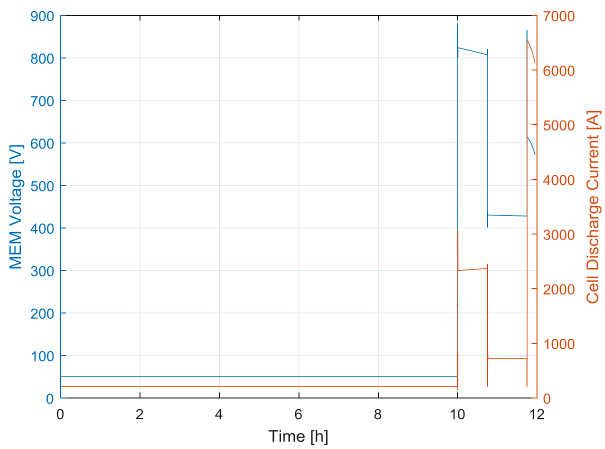

Figure 99 Armature voltage and current

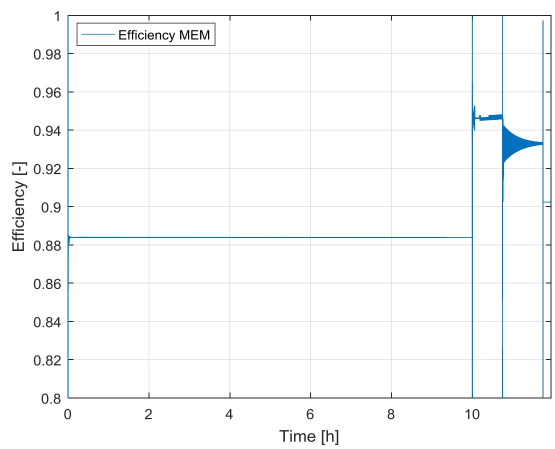

Figure 100 Propulsion motor efficiency

8.5.1 Volume

The given mission profile results in an optimum battery mass for 223 cells per battery and 571 kg per cell. Or 210 Cells per battery and 625 kg per cell is the optimum if the maximum propulsion voltage is taken into account.

The volume of the cells is assumed to be only a function of the mass. The moray battery is used as reference. The mass of the moray cell is 530 [kg] and volume is 0.20 [m³]. This results in an average cell density of 2650 [kg/ m³]. The required volume for the 223 cell layout is 96 [m³].

$$V_{cell} = \frac{m_{cell}}{\rho_{cell}} = \frac{571}{2650} = 0.22\ m^3 \quad (8\text{-}4)$$

$$V_{Battery} = 2 \cdot n_{cell} \cdot V_{cell} = 2 \cdot 223 \cdot 0.22 = 96\ m^3 \quad (8\text{-}5)$$

The volume for the 210-625 cell lay out is 99 [m³]. The results of the simulations and calculations are listed in Table 16.

Table 16 Results as function of the mission profile

	Battery Layout	Battery technology	Mass	Volume
Concept Conf. A	223-571	Lead-acid	282 ton	96 m^3
Concept Conf. A	210-625	Lead-acid	290 ton	99 m^3

8.5.1 Sensitivity analysis

The mass of the battery is increased to find the optimum battery mass for the assumed mission profile. The mass is increased without changing other battery parameters. A relevant parameter is the internal cell resistance. The increased mass leads to increased battery volumes and battery dimensions. The area and the height of the cell increase. The height of the battery cell is a property that is related to the internal cell resistance. Higher the cell dimensions results into a longer electrical path, results in a higher internal cell resistance.

An analysis is done to determine the effect of increased cell resistance on the loss on capacity, and there for the increase of mass, as the mass is a representation of the stored capacity. As starting point is the internal resistance of the MORAY cell of 530 kg chosen. This resistance is multiplied with a factor f that represents the increase. For f is a value between 0.1 and 0.4 used. Representing an increase of resistance between 10% and 40% per kilogram of increased mass, compared to the 530 kg lead-acid battery. This is mathematical represented by equation 8-6.

$$r_i = r_{ref} \cdot \left(1 + f \cdot \left(\frac{M_{Bat} - M_{ref}}{M_{ref}}\right)\right) \tag{8-6}$$

The result of the simulation is illustrated in Figure 101. The lines converge to one point, the reference mass. When the battery mass is equal to the reference mass is the internal resistance the same, independent of f.

$$r_i = r_{ref} \cdot \left(1 + f \cdot \left(\frac{M_{Bat} - M_{ref}}{M_{ref}}\right)\right) = r_{ref} \cdot \left(1 + f \cdot \left(\frac{530 - 530}{530}\right)\right) = r_{ref} \cdot 1 = r_i$$

Figure 101 illustrates the required mass per cell with increased cell resistance. At 210 cells is the increase 15 kg per cell, an increase of 4%. At 223 cells is the increase less than 1%. It can be concluded that increasing the internal resistance as function of the mass has not significant influence on the set battery mass.

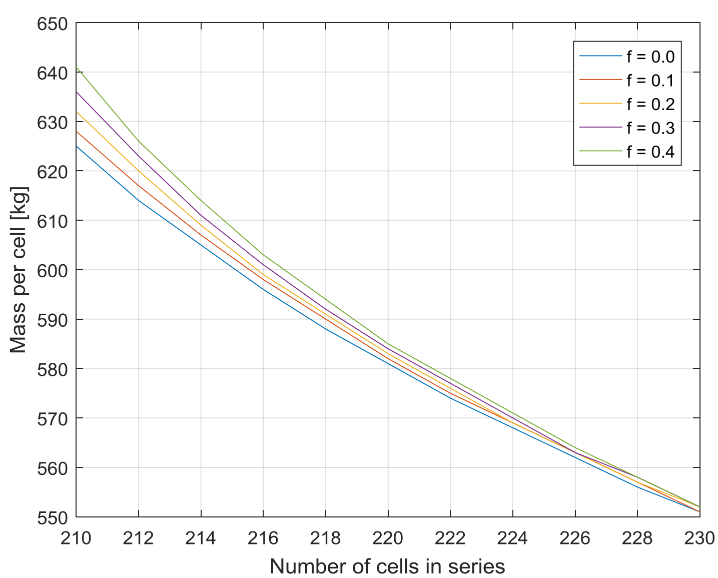

Figure 101 Effect of increased resistance as function of cell mass

8.6 Variation studies surveillance and attack

The generic propulsion plant model enables to variate the mission profile. Variation studies investigate the effect of the assumed mission profile on the mass and volume of the batteries. In addition, variations prove the possibility of changing the mission profile and the robustness of the optimization algorithm.

8.6.1 Mission profile variations

The first variation aims to illustrate the effect of the burst load. The different propulsion load variations are illustrated in Figure 102. The first profile is the mission profile as defined in Figure 2. The second profile is a mission profile with the burst at the beginning of the mission. The third mission is only a burst load.

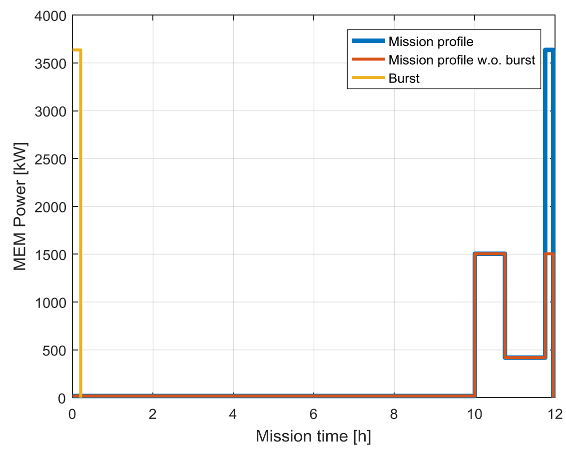

Figure 102 Mission profile variations

The results of the simulations are plotted in Figure 103 and Figure 104. The variations show the effect of the burst on the mass per cell as function of the number of cells. The line indicating the mission profile without burst is linear while the cell mass for the burst load non-linear is. This can be explained with Figure 60, the capacity as function of the discharge current. Lower number of cells result in lower battery voltages, resulting in higher discharge current and lower capacity per cell.

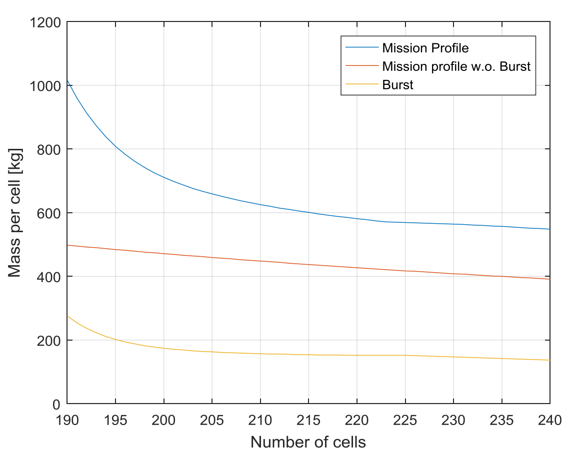

Figure 103 Mass per battery cell

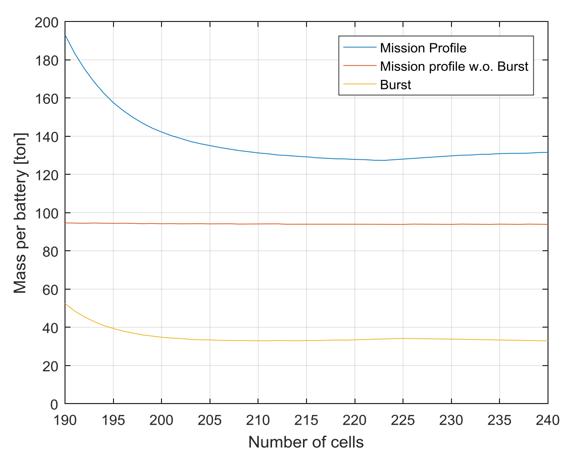

Figure 104 Mass per battery

8.6.2 Inverse mission profile

The inverse mission profile has the same composition and as the assumed mission profile. The difference is the position of the burst load. The burst load is in the inverse mission profile is at the beginning of the mission, instead of at the end. Figure 105 shows the mission profiles.

The battery masses as function of the number of cells are plotted in Figure 106. It is noticed that a lower mass is required for the inverse mission profile than for the normal mission profile even though the kilowatt-hour load is the same. This can be explained by the pseudo state of discharge of both mission profiles are illustrated in Figure 107.

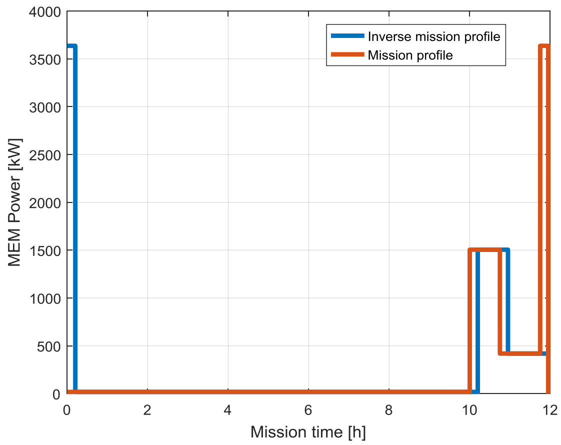

Figure 105 Mission profile and inverse mission profile

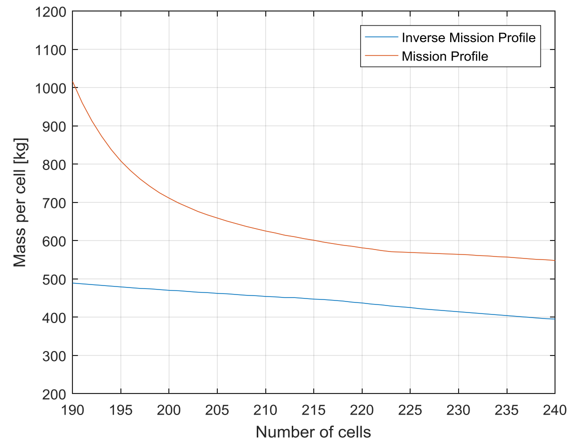

Figure 106 Results optimization

Both states start at 0.2, as stated in the boundary conditions. The high peak of the inverse mission profile rises to 0.5 and then drops back to 0.3. The pseudo discharge state is defined as the charge divided by the total capacity as function of the discharge current.

As the discharge current decreased just after the burst, C_t increases resulting in a drop of y. The normal mission profile has the peak at the end of the mission. So the peak hits $y = 1$ and the simulation is stopped as the maximum discharge state is reached.

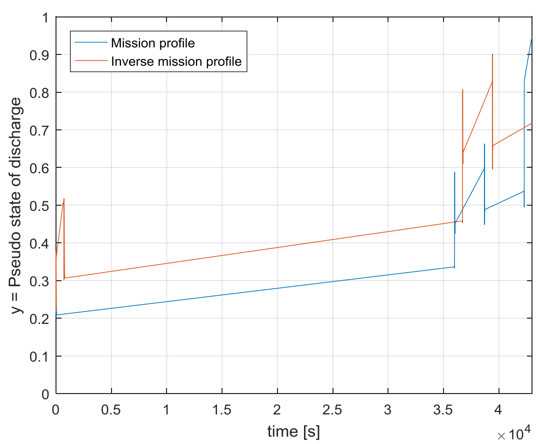

Figure 107 State of discharge and pseudo state of discharge

8.7 Charging lead-acid batteries

The generator(s) on board of a submarine are primarily responsible for charging the main batteries during snorting. The required generator output power is a function of the performance requirements set in the assumed mission profile.

The generator power is however limited to a maximum. The generator power is limited by maximum charge current. The charge current charges the batteries. During charging the battery voltage increases. The cells can be damaged if the maximum cell voltage is exceeded. The cell voltage during charging is a result of three factors. (1) The hysteresis losses during charging (2) The internal resistance times the charge current and (3) the increase of voltage as function of the SOC.

This chapter elaborates on the required generator power as function of the assumed mission profile taking into account the battery cell voltage.

8.7.1 Methodology

The methodology that is used to determine the generator output power is illustrated in Figure 108. The input is the mission profile. From the mission profile are the performance requirements obtained. These are the propulsive power and auxiliary power during the surfaced and snorting operation and the given indiscretion ratio. These requirements are the input for the propulsion plant performance model. The power is limited by the maximum cell voltage during charging. The cell voltage may not exceed 2.45 [V] [23]. The battery cell performance model is verified and can be used to simulate the cell voltage during the charging.

The calculated generator power is the input for; (1) the dimensioning of the generator and (2) the propulsion plant performance simulations. The propulsion plant performance is expressed in the efficiency during the covert transit.

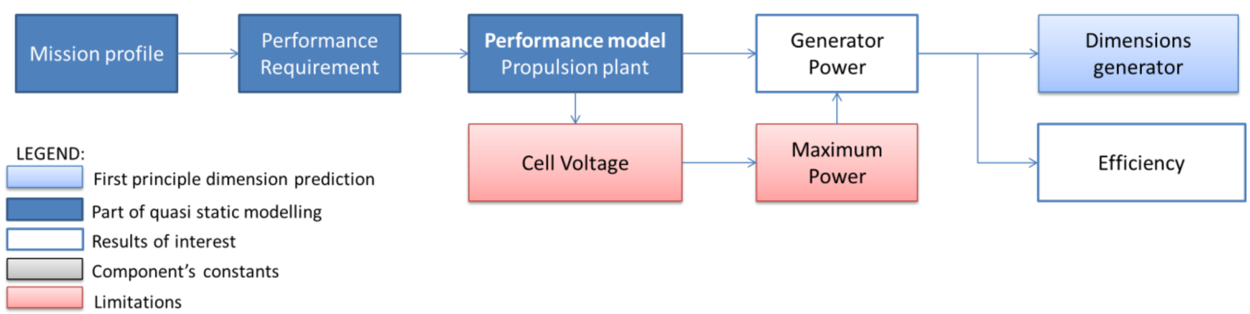

Figure 108 Generator power methodology

8.7.2 Charging process lead-acid

Charging process of a lead-acid is divided in three stages. The first charging stage is the constant power charging stage. The capacity is restored up to 80% of the battery cell capacity. The second stage is constant voltage charging. The charge current rapidly decreases to maintain constant voltage. The third stage is a constant charge current. The charging of the batteries during snorting operation is in the first charging stage. This is illustrated in Figure 109. During the convert transit varies the SOC of the batteries between 80% and 60%. This implies that the batteries are charged at constant power.

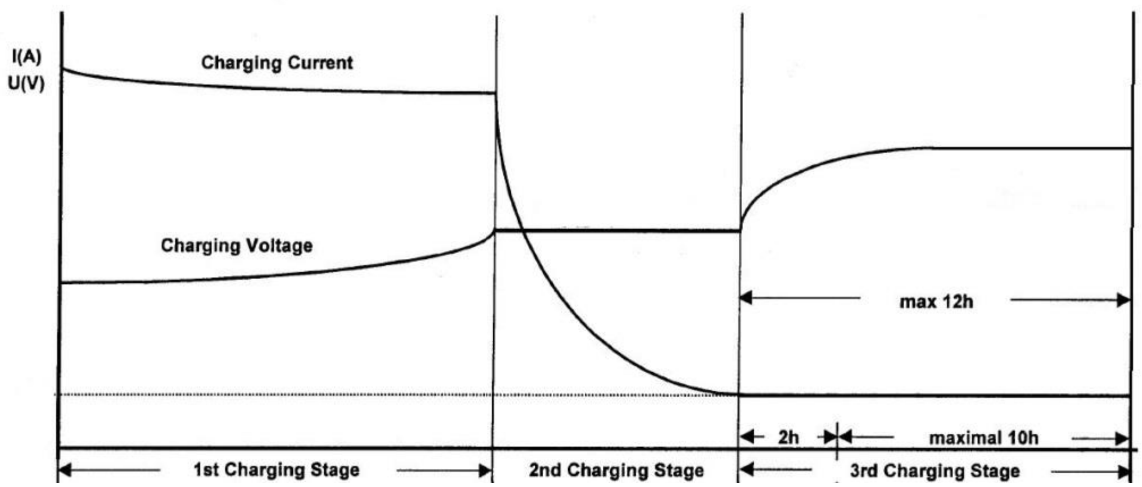

Figure 109 Charging phases [23]

8.7.3 Performance requirements charging

The generator performance requirements during the covert transit are defined in the mission profile. The mission profile defines the indiscretion ratio. The indiscretion ratio is the ratio between the submerged time and snorting time. The submerged time is the time between the snorting periods. Figure 110 illustrates the submerged and snorting time of covert transit 1. The submerged time has a propulsive load of 40 kW, and an auxiliary load of 180 kW. The propulsive load during snorting is 160 kW, the auxiliary load is 260 kW.

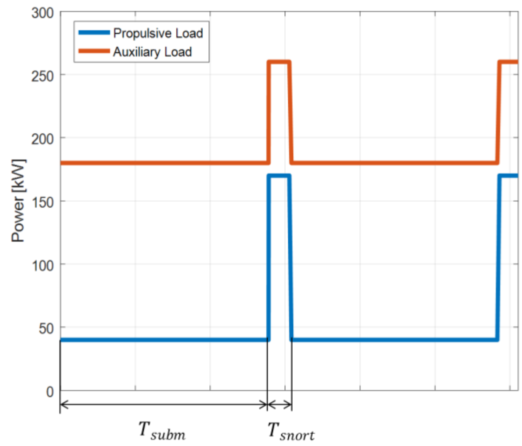

Figure 110 Submerged and snorting time for covert transit 1

The submerged time is dependent on the battery layout, the propulsive and auxiliary load, and the SOC range. The mission profile has a defined state of charge between 0.8 and 0.6. The batteries are drained between 80% and 60% during snorting. The deeply submerged time is obtained with simulations. The corresponding snorting time is computed with equation 8-7. Equation 8-7 is obtained by rearranging equation 2-1.

$$IR = \frac{T_{snort}}{T_{snort} + T_{subm}} \qquad \text{ref(2-1)}$$

$$T_{snort} = \frac{T_{subm} \cdot IR}{1 - IR} \qquad \text{8-7}$$

The snorting time is a function of the generator output power. Higher charge power result in shorter recharge times. The recharge time is considered to be the snorting time.

The assumed mission profile contains two covert transit periods. The transit periods differ in the indiscretion ratio and in propulsive power demand. The shape of the mission profiles is illustrated in Figure 111 and Figure 112. The assumed propulsive loads are defined in Table 17 and Table 18.

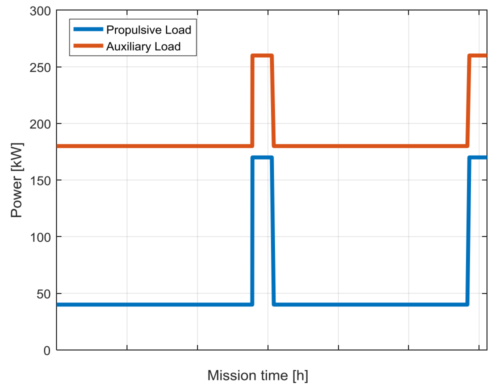

Figure 111 Power requirements covert period 1

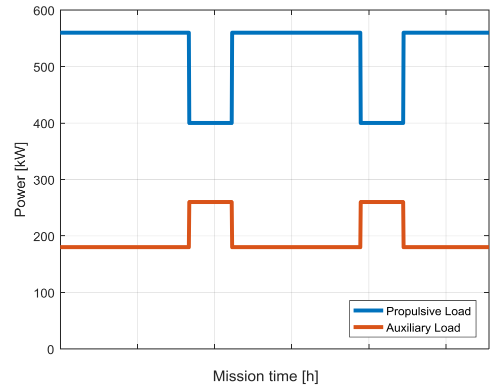

Figure 112 Power requirements covert period 2

Table 17 Requirements covert period 1

Requirements covert period 1			
Sub	Propulsive power	40	[kW]
Sub	Auxilairy power	180	[kW]
Snort	Propulsive power	170	[kW]
Snort	Auxiliary power	260	[kW]
IR	Indiscretion ratio	0.10	[-]

Table 18 Requirements covert period 2

Requirements covert period 2			
Sub	Propulsive power	560	[kW]
Sub	Auxilairy power	180	[kW]
Snort	Propulsive power	400	[kW]
Snort	Auxiliary power	260	[kW]
IR	Indiscretion ratio	0.28	[-]

The used battery layout is the optimized battery layout with respect to mass and volume; 210 cells in series and 625 kg per battery cell. The batteries SOD is increasing during this period for 0.2 to 0.4. The computed submerged times that correspond to the battery layout, and requirements are set Table 19. The propulsion plant is capable of delivering the set propulsive power and auxiliary power for a period of 18.84 hours for the settings of period 1, and 3.28 hours for covert period 2.

Table 19 Simulated submerged time

Submerged time	Simulation
Covert transit 1	18.84 [h]
Covert transit 2	3.28 [h]

The required snorting time required to meet the set indiscretion ratio for the simulated submerged time is calculated by rewriting equation using equation 8-8.

$$T_{snort} = \frac{T_{subm} \cdot IR}{1 - IR} = \frac{18.84 \cdot 0.1}{1 - 0.1} = 2.01\ hours \qquad \text{ref(8-7)}$$

Table 20 Required snorting time to meet the IR set in the mission profile

Required snorting time	Simulation
Covert transit 1	2.01 [h]
Covert transit 2	1.24 [h]

8.7.4 Required generator output power

The required generator output to charge the batteries within the defined period of time is obtained with simulations. The diesel engines convert the chemical energy into mechanical power and the generator converts the mechanical power into electric power. The available generator power, divided by the battery system voltage, U_{bat}, is the charge current I_{bat}. This is illustrated in Figure 113.

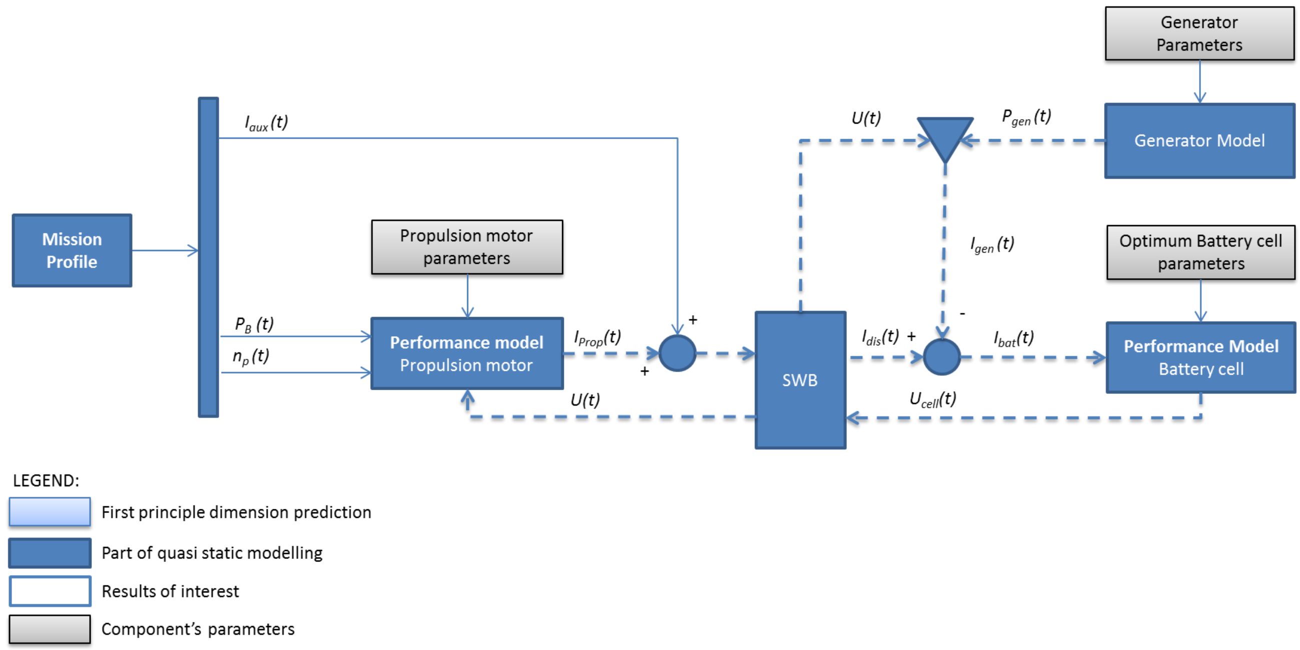

Figure 113 Propulsion plant performance model

The charge time as function of the generator power output power, with the constant propulsive and auxiliary loads are illustrated in Figure 114. The charge time decreases as the generator power increases. Increased generator power results in a higher charge current and a reduced charge time. It takes less long to charge the batteries up to 0.2 SOD from 0.4 SOD for covert transit 1 compared to covert transit 2. The current acting on the battery is defined as the discharge current minus the charge current. Note that the discharge current is indicated with the positive sign. The discharge current is higher for covert transit 2 compared to covert transit 1, resulting in a lower charge current and a longer charge time.

$$I_{bat}(t) = I_{dis}(t) - I_{charge}(t) \tag{8-8}$$

The charge time as function of the generator power and the required snorting times as defined in Table 20 are plotted in Figure 115. The blue lines correspond to covert transit 1, the red lines correspond to covert transit 2. The intersection of the charge times results in the required generator output power. The required generator power for covert transit 1 is 1900 [kW] and 3000 [kW] for covert transit 2. The obtained powers from the simulations are stated in Table 21.

Table 21 Generator power according the performance requirements

Required generator power	IR	Simulation
Covert transit 1	0.10	1900 kW
Covert transit 2	0.28	3000 kW

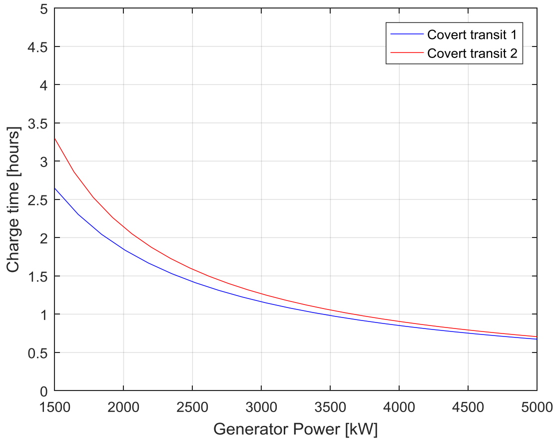

Figure 114 Charge time as function of the generator output power

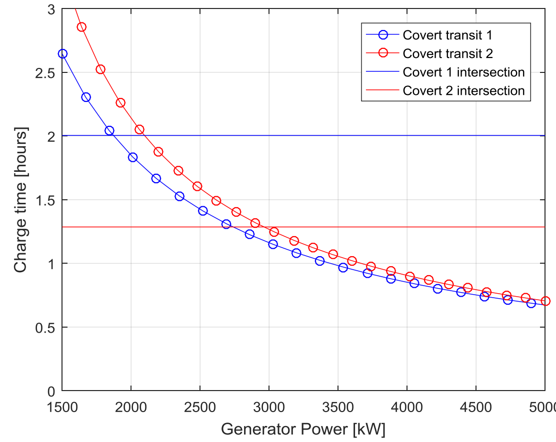

Figure 115 Solution according to the mission profile

The IR can also been directly expressed as function of the generator power for the defined covert periods. The submerged time is constant for the calculations, the charge time decrease. The result is a decreasing IR. The tangent of the indiscretion ratio is steep at lower charge powers and flattens out at higher generator power voltages. A doubling in the power results in a halving of the IR.

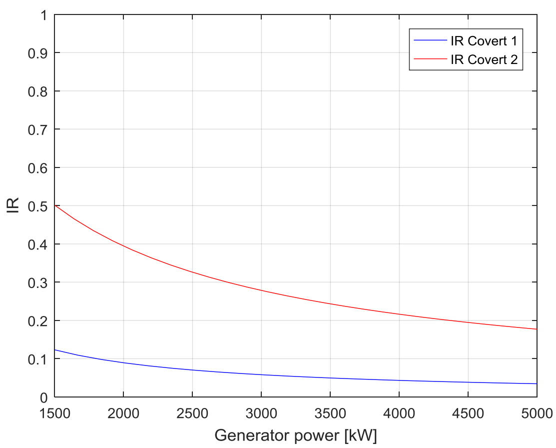

Figure 116 IR covert 1 and covert 2

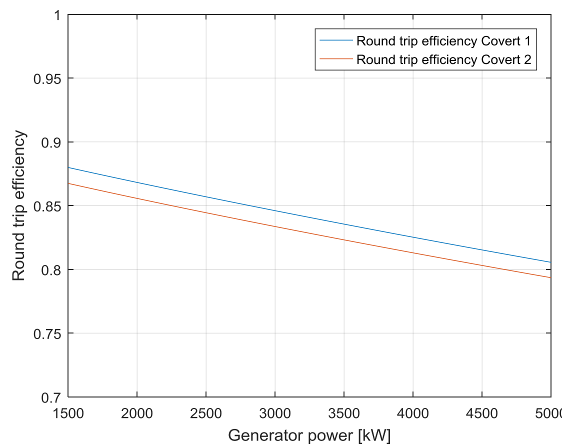

Figure 117 Round trip efficiency

The time simulations for the found solution are plotted in Figure 118 and Figure 119. Figure 118 illustrates the charge and discharge powers during covert transit 1. The discharge power is indicated with a blue area, the charge power is indicated with a red area. The first part is the submerged part; 40 [kW] propulsive power and 180 [kW] auxiliary power. After a period of 18.84 hours is the generator started. The generator output power is 1900 [kW]. At that moment the propulsive power is increased to 170 [kW] and 260 [kW] auxiliary power.

Figure 119 illustrates the cell voltage and the state of discharge during covert transit 1. The SOD increases from 0.2 to 0.4 in a period of 18.84 hours and is decreased to 0.2 in a period of 2.01 hours. It can be concluded that the generator output power of 1900 [kW] meets the requirements for covert transit 1. It can also be concluded that the battery voltage does not exceed the maximum battery voltage.

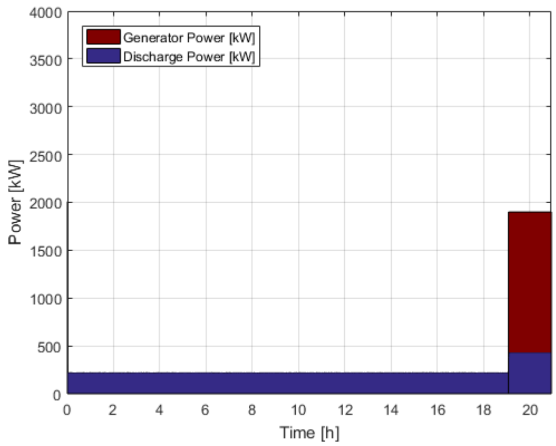

Figure 118 Representation of covert transit 1

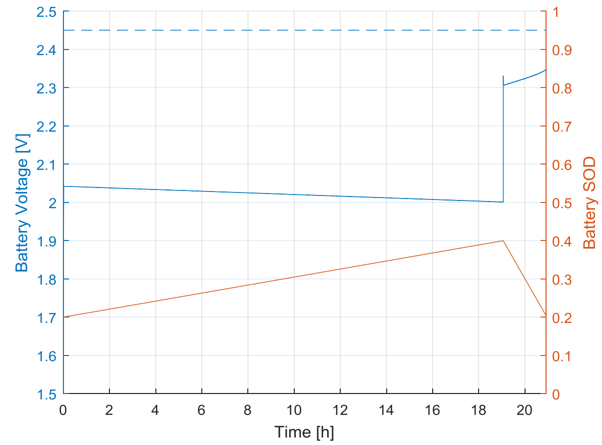

Figure 119 Battery voltage during covert transit 1: 1900 kW charging IR = 0.10

The time simulation results of covert transit 2 are plotted in Figure 120 and Figure 121. The computed generator power output meets the set requirements, and the battery cell voltage does not exceed the maximum cell voltage.

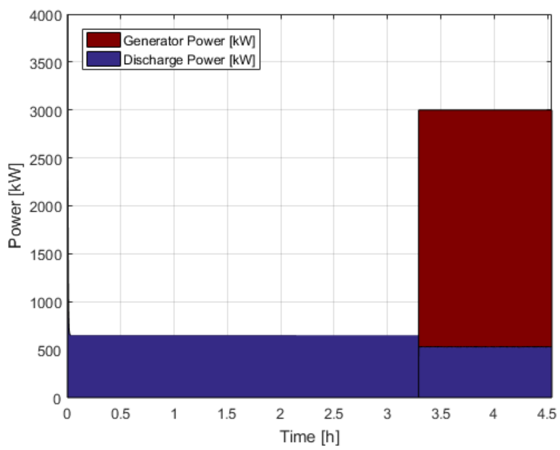

Figure 120 Representation of covert transit 2

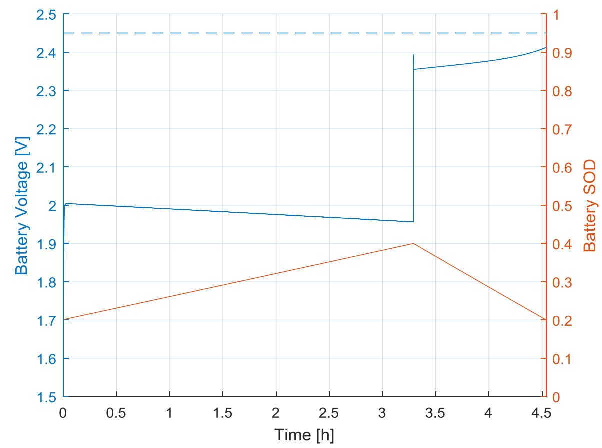

Figure 121 Battery voltage during covert transit 1: 3000 kW charging IR = 0.28

8.7.5 Verification

The results of the simulations have been compared to the results of another calculation methodology, available at *Nevesbu*. The power requirements are stated in Table 22 and illustrated in Figure 122. The propulsive power is constant during snorting and during submerged sailing. The auxiliary power is different for the submerged and snorting conditions.

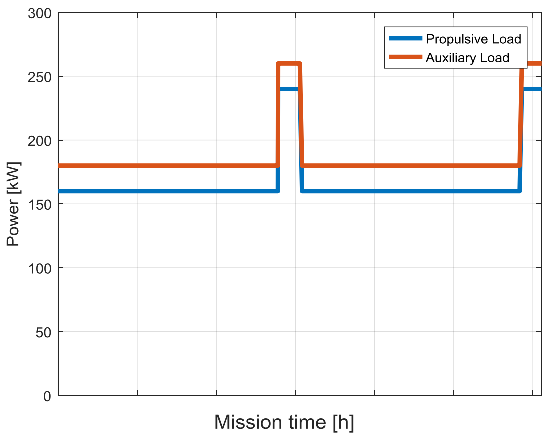

Figure 122 Requirements concept design

Table 22 Requirements concept design

Requirements concept design			
Sub	Propulsive power	160	[kW]
Sub	Auxilairy power	180	[kW]
Snort	Propulsive power	240	[kW]
Snort	Auxiliary power	260	[kW]
IR	Indiscretion ratio	0.13	[-]

The results of the simulation are captured in Figure 123. The required generator power to meet the defined indiscretion ratio is 2500 [kW]. The required installed diesel generator power is 2850 [kW], assuming a combined generator efficiency and AC/DC conversion of 87%. This efficiency is based on the generator efficiency of 95% [30] and the AC/DC conversion of 92% [4]. According to another calculation method that is available at *Nevesbu* is the required power to meet the requirements 3300 [kW], a deviation of 450 [kW]. It is not directly clear what caused the deviation. The difference might be caused by different boundary conditions and propulsion plant component parameters.

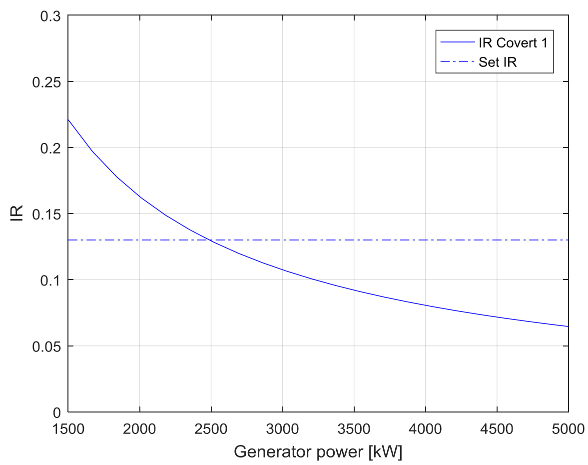

Figure 123 Sketch Design

8.8 Charge power limitations

The maximum charge power is limited by the cell voltage. The cell voltage may not exceed 2.45 Volt, this value is defined by the manufacturer. This subchapter elaborates on the maximum charge power.

A representation of the first charging stage is illustrated in Figure 124 [23]. The second and third charging stages are not relevant during the covert transit. The diesel engine will run at a maximum constant power to charge the batteries as fast as possible, without exceeding the gassing voltage. The battery cell voltage increases during charging. The charging current is decreasing during charging. The decrease is caused by an increasing battery cell voltage. The charge current is the generator output power divided by the battery voltage.

The assumed mission profile prescribes a SOC varying between 0.8 and 0.6. In an ideal situation is for constant power charging the cell voltage 2.45 at the end of charging. The charge time is than minimal for constant power charging. This is illustrated in Figure 124.

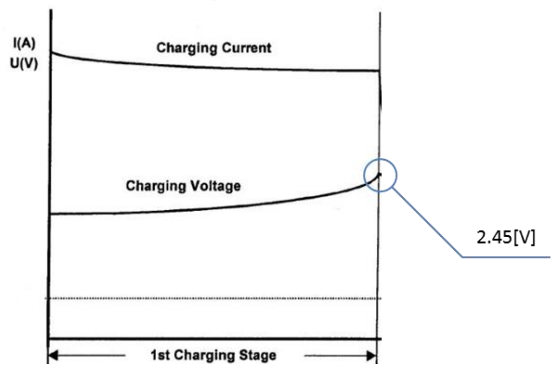

Figure 124 Illustration of the maximum voltage during constant power charging

The method used to find the maximum charge power is to calculate the battery voltage at the end of charging for the different charge powers. The end of charging is defined as 0.8 state of charge. The battery voltages and the IR are both a function of the generator output power. The performance requirements and the limitations are captured in one figure, Figure 125. On the left vertical axis is the IR plotted, on the right vertical axis is the battery voltage at the end of charging plotted. The continuous lines represent the properties of covert transit 1, the discontinuous lines represent the properties of covert transit 2.

The intersection of the maximum cell voltage and the cell voltages during charge indicates the maximum allowable charge power. The maximum charge power, is 3250 [kW] for covert transit 1, and 3500 [kW] for covert transit 2. At those generator output powers is the battery voltage 2.45 [V] at the end of charging.

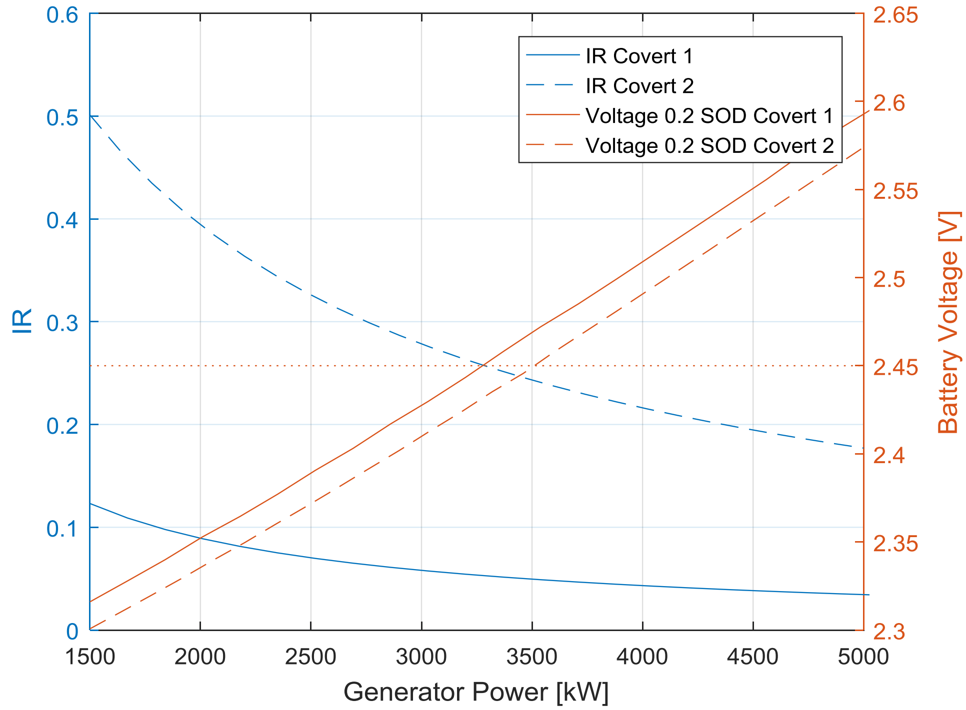

Figure 125 Cells in series 210 of 625 kg

Table 23 Covert transit generator performance requirements and limitations

Generator power	IR Set	Performance requirements	Limitation
Covert transit 1	0.10	1900 kW	3250 kW
Covert transit 2	0.28	3000 kW	3500 kW

The generator output power computed to meet the performance requirements is lower than the limiting generator power. It can be concluded that the maximum voltage is not exceeded during CT1 and CT2.

Figure 126 illustrates the battery voltage and the charge current during snorting. At the SOD value of 0.2 is the battery voltage at a maximum. Figure 127 illustrates the charge current and battery cell voltage during the snorting for the maximum charge power. At a SOD of 0.2 is the maximum battery voltage of 2.45 [V] reached. The discharge time is for both generator output powers the same, the charge time is shorter. This results in a lower IR.

The peak at the beginning of the charging is caused by the motor controller. The motor controller needs time to control the propulsion motors power output. The battery voltage rises immediately after the generator is started. Resulting in The change of the battery voltage has an influence on the power output.

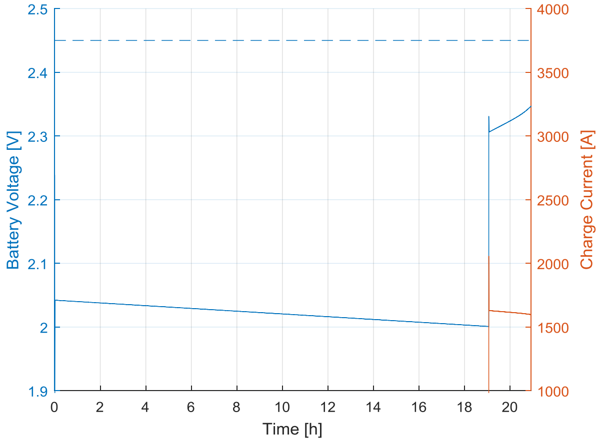

Figure 126 Battery voltage during covert and SOD for covert transit 1: 1900 kW charging IR =0.10

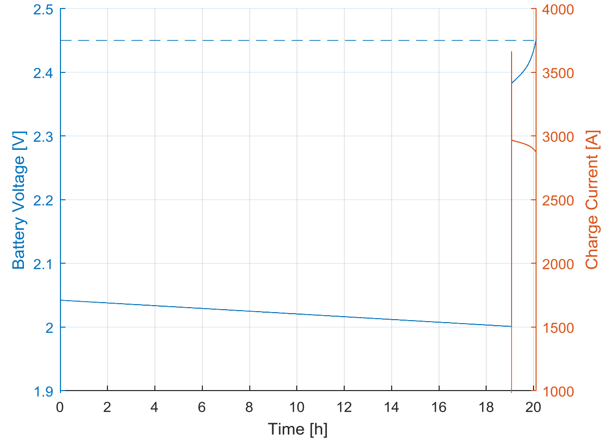

Figure 127 Battery voltage during covert transit 1: 3250 kW charging IR =0.05

The battery cell voltages and charge currents, for CT2, as function time are plotted in Figure 128 and Figure 129. The first part of the time simulation is a submerged sailing. The battery cell voltage decreases. At the time 3.28 [h] the battery capacity is 60%. The diesel generator set is started and the cell voltage increases. Figure 128 has an installed generator output power of 3000 kW. 3000 kW is computed to meet the set performance requirements.

The maximum generator output power is 3500 kW. The cell voltage at the end of charge is equal to the maximum cell voltage. The IR is reduced to 0.24.

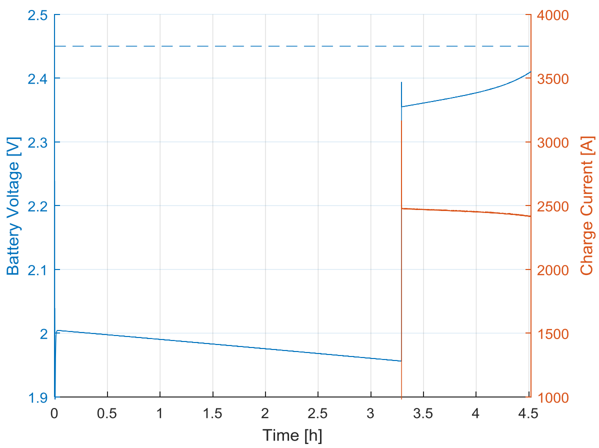

Figure 128 Battery cell voltage and current at 3000 kW constant power charge: IR =0.28

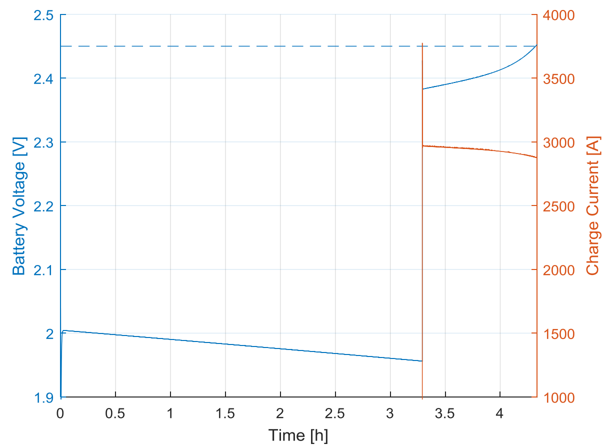

Figure 129 Battery cell voltage and current at 3500 kW constant power charge: IR = 0.24

8.9 Battery layout variations

The number of batteries does not affect the required generator output power to meet the indiscretion ratio. The optimization of the propulsion plant configuration A as function of an assumed mission profile can only be done for the battery mass. This is plotted in Figure 130 and Figure 131.

The number of cells in series and the mass per affects the deeply submerged time during the covert transit. This is not a requirement set in the mission profile. Besides the deeply submerged time do the number of affect the maximum generator power. The battery charge current is the generator power divided by the battery voltage. Higher battery voltages result in lower charge currents. Lower charge currents mean lower battery voltages and result in higher allowable generator powers.

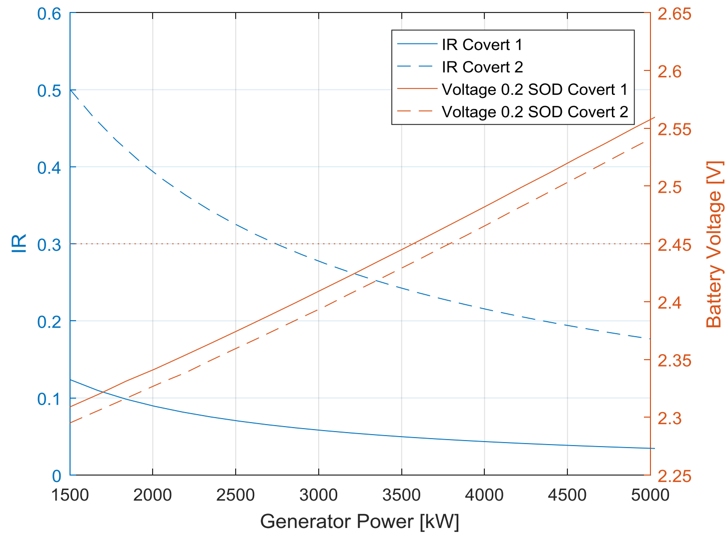

Figure 130 Cells in series 223 of 625 kg

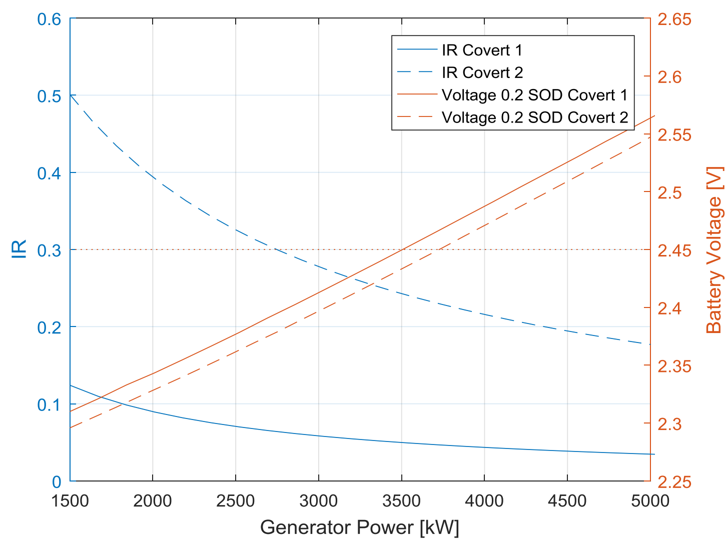

Figure 131 Cells in series 223 of 571 kg

8.10 Variation performance requirements

The charging requirements are set in the assumed mission profile. This chapter elaborates on the defined requirements.

8.10.1 SOC variation

The assumed mission profile prescribes a SOC during snorting varying between 0.8 and 0.6. The battery voltage is highly dependent on the SOC and therefor is the limitation highly dependent on the SOC. Figure 132 illustrates the cell voltages at the end of charging for 0.8 SOC and 0.7 SOC and the corresponding IR, both as function of the generator output power. A significantly lower cell voltage is reached for 0.7 SOC compared to 0.8 SOC at the end of charging. Or in other words, the intersection shifts to the right, enabling higher charge powers, and allowing higher charge powers without exceeding the maximum battery cell voltage.

The IR as function of the generator output power is the same. This is hardly visible in the plot, the lines lie on each other.

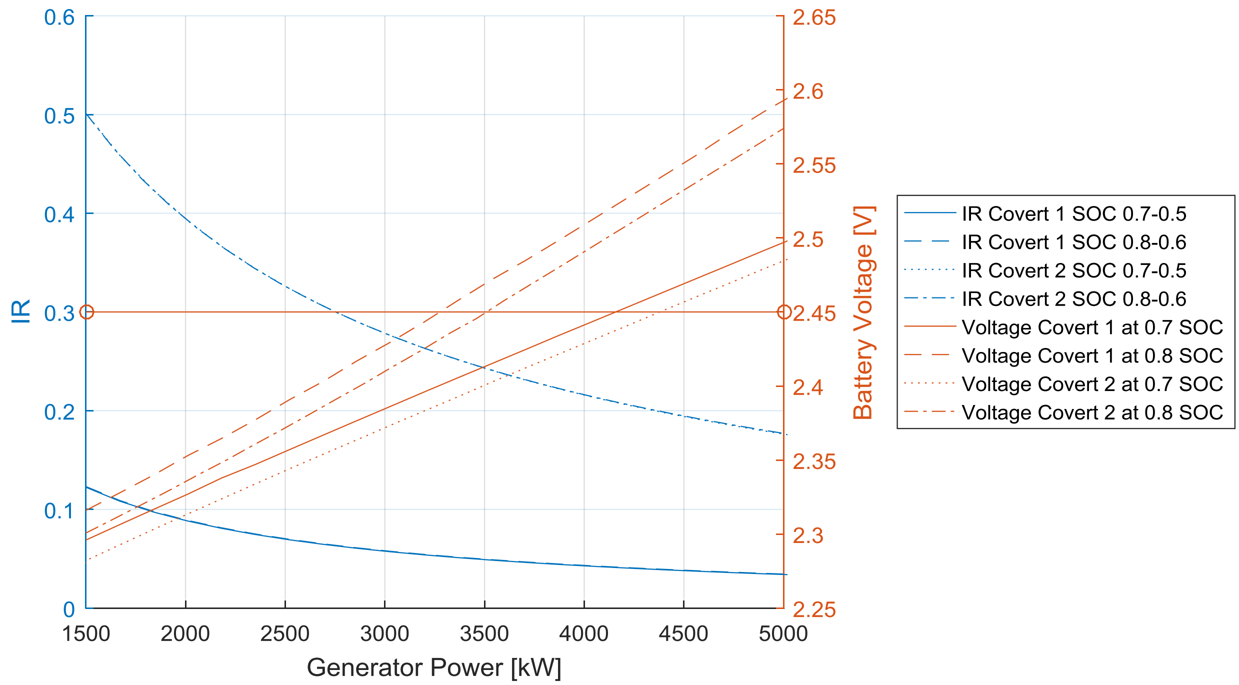

Figure 132 Battery cell voltage and IR as function of the generator output power for set auxiliary and propulsive power and 210 series and 625 kg

The figure shows that the effect of a set maximum state of charge can limit the generator output power. Table 24 summarizes the results of the simulation. It is clear that the generator output power limitation is dependent on the SOC. The IR as function of the generator power output is not changed for a changed SOC area.

Table 24 Required generator power

Generator power	IR Set	Required	Limitation (0.8 SOC)	IR MAX (0.8 SOC)	Limitation (0.7 SOC)	IR MAX (0.7 SOC)
Covert transit 1	0.10	1900 kW	3250 kW	0.05	4200 kW	0.04
Covert transit 2	0.28	3000 kW	3500 kW	0.24	4300 kW	0.22

8.10.2 Tactical snorting time

From a tactical point of view it is desired to snort for a period of maximum 20 minutes or snort until the maximum cell voltage [37]. The diesel engines are loud machines that disturb the passive sonar of the submarine resulting in a blind spot. To be sure whether there is no hostile submarine approaching, the snorting is interrupted to clear the area.

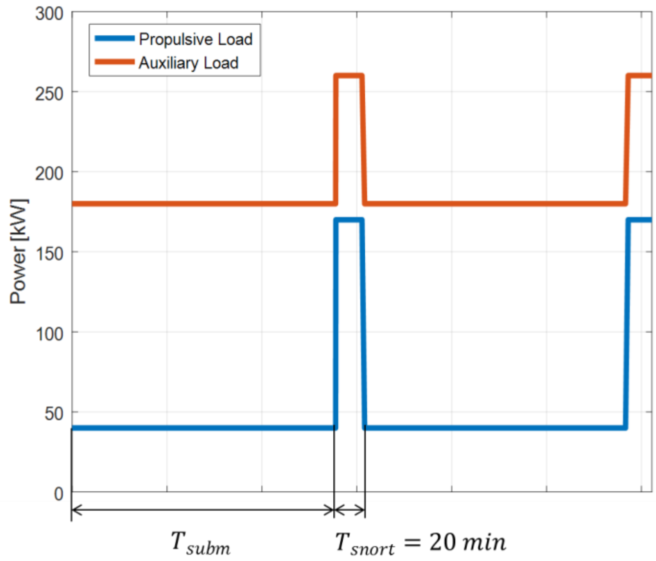

Figure 133 Set snorting period

The submerged time for 20 minutes snorting can be calculated with equation 8-9. The snorting time is 20 minutes and the IR is assumed to be the same for discharging between 0.8 and 0.6 SOC.

$$T_{subm\ 20\ \mathrm{min}} = \frac{\left(T_{snort\ 20\ \mathrm{min}} - IR_{20\ \mathrm{min}} \cdot T_{snort(20\ \mathrm{min})}\right)}{IR_{20\ \mathrm{min}}} \qquad \text{8-9}$$

$$IR_{0.8} = IR_{20\ \mathrm{min}} \qquad \text{8-10}$$

The indiscretion ratio corresponding to the generator output power for the different load conditions are obtained with simulations. The propulsive load conditions during the submerged sailing vary while the surfaced speed is assumed to be constant.

Figure 134 illustrates the SOD and battery cell voltage as function of time. Two methods of charging are illustrated. (1) The SOD between 0.2 and 0.4 and (2) the tactical charging of 20 minutes. The SOD is linearly increasing during the discharge as function of time. It can be concluded that assumption made in equation 8-9 holds and that the set snorting time does not affect the required generator output power.

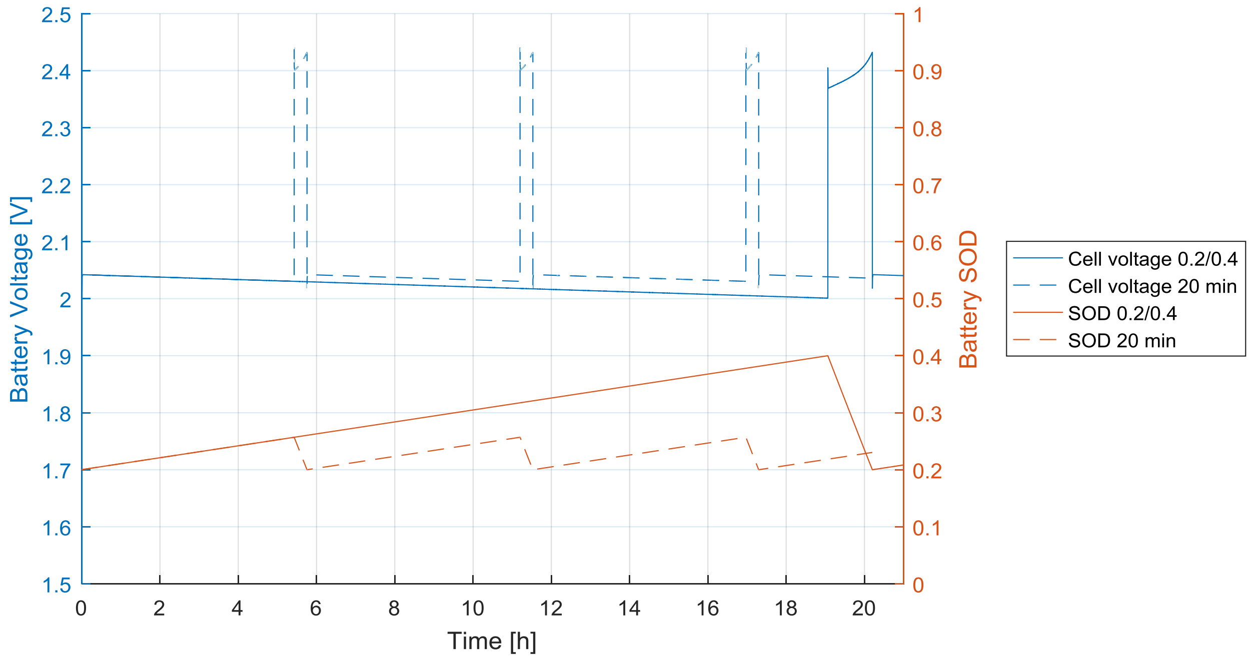

Figure 134 Covert transit 1

8.10.1 Optimization of the mission profile

The assumed mission profile defines two deeply submerged speeds in CT1 and CT2. Those are arbitrarily chosen. The propulsion motor performance model and the battery cell performance model enables to obtain the maximum deeply submerged range as function of the submarine speed. The technical parameters and the boundary conditions stated in the previous chapters are used.

The calculated submerged time is obtained with the performance models. The deeply submerged time and the deeply submerged speed results in a deeply submerged range. The submerged time is the time between 0.8 and 0.6 batteries SOC.

$$S_{Sub} = T_{subm\ 0.2} \cdot v_{sub} \qquad \text{8-11}$$

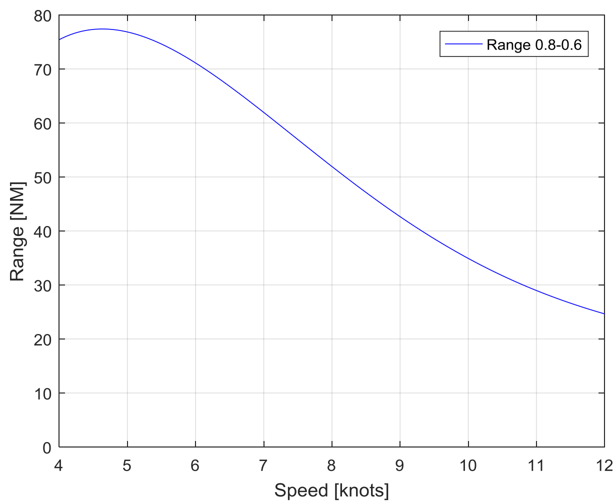

Figure 135 Range as function of submarine speed

Notable is the optimum range peak, as function of the submerged speed, for the three configurations. This peak is a result of the propulsive and auxiliary power demand. At low speeds is there a relatively long discharge time. The longer discharge time implies that the auxiliary power is delivered for a longer time. The energy consumed by the auxiliary systems cannot be used for the propulsion motor. After the peak is the range steeply decreasing. This is caused by the increased resistance. The required propulsive power as function of the set speed a third order function.

It can be concluded that the maximum range for a discharge between 0.8 and 0.6 battery state of charge is 78 nautical miles. The distance is achieved at a submarine speed of 4.7 knots.

8.11 Dimensioning diesel generator set

The required generator output power is calculated in chapter 8.7 0for concept configuration A. The required generator output power for concept configuration A is 3000 kW. This power can be delivered by multiple diesel generator set layouts. The diesel generator weight as function of the generator output power is plotted in Figure 136. The diesel generator volume is plotted in Figure 137. The realization of the figures is explained in chapter 7.5 Diesel and generator dimensioning optimization. The optimum result is the solution with two V16 diesel engines. The possible diesel generator layouts are listed in Table 25.

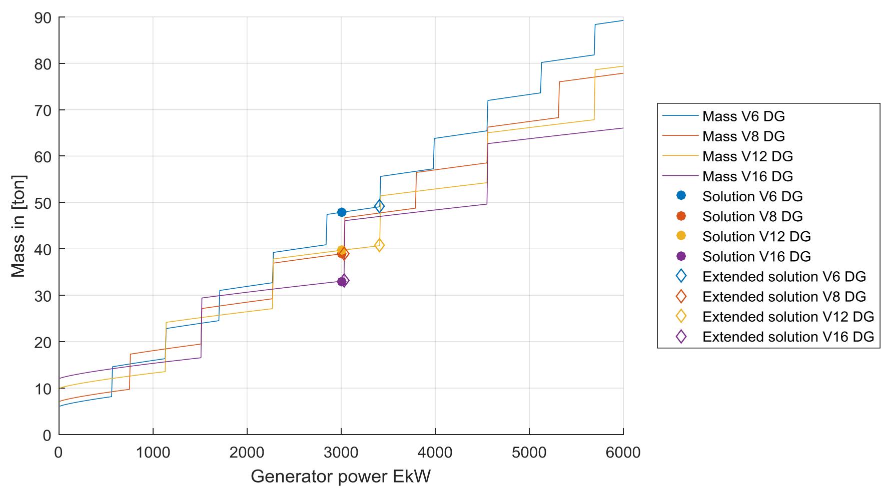

Figure 136 Diesel generator mass as function of generator power

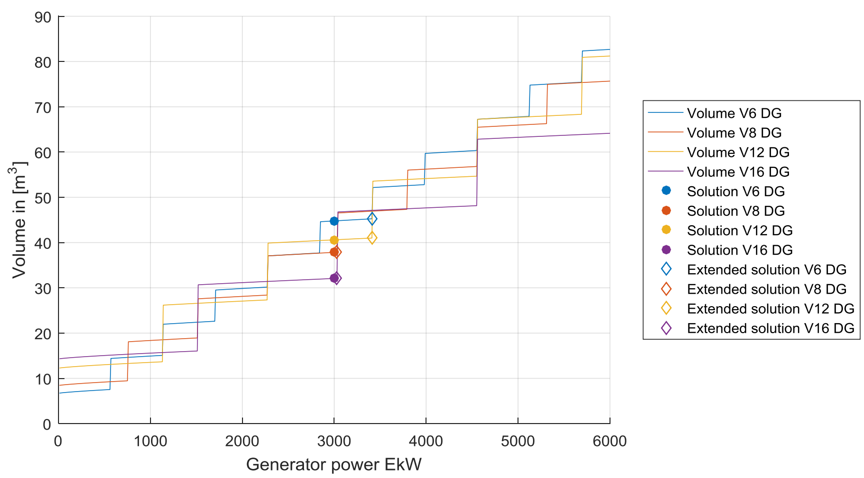

Figure 137 Diesel generator volume as function of generator power

Table 25 Solutions concept configuration A

Type	Power [EkW]	Brake Power [kW]	n.o. engines	Mass ton	Volume m³	max Power [EkW]	Mass ton	Volume m³
V6	3000	3400	6	48	45	3400	49	45
V8	3000	3400	4	39	48	3000	39	38
V12	3000	3400	3	40	41	3400	41	41
V16	**3000**	**3400**	**2**	**33**	**32**	**3000**	**33**	**32**

8.12 Propulsion plant efficiency

The propulsion plant efficiency during snorting is defined as the delivered propulsive and auxiliary power over the total period of time divided by the generator output power during the snorting period. The efficiency during the charging after the mission profile is stated in equation 8-12. Figure 138 is a graphical representation of the efficiency of covert transit 1. The blue area represents the discharge power of the propulsion and auxiliary load. The red area indicates the generator power. The discharge power divided by the charge power results in the snorting efficiency.

$$\eta_{snorting} = \frac{\int_0^{t_{sub}} (P_{MEM\ SUB} + P_{aux\ SUB}) dt_{sub} + \int_{t_{sub}}^{t_{snort}} (P_{MEM\ SNORT} + P_{aux\ SNORT}) \cdot dt_{snort}}{\int_{t_{sub}}^{t_{snort}} P_{GEN}\, dt_{snort}} \quad \text{8-12}$$

The efficiency is determined for the battery system of 210 cells and 625 kg per cell. The efficiency during the covert transit 1 for the 1900 [kW] generator power is 84%. The efficiency for 3000 [kW] charging is 84%.

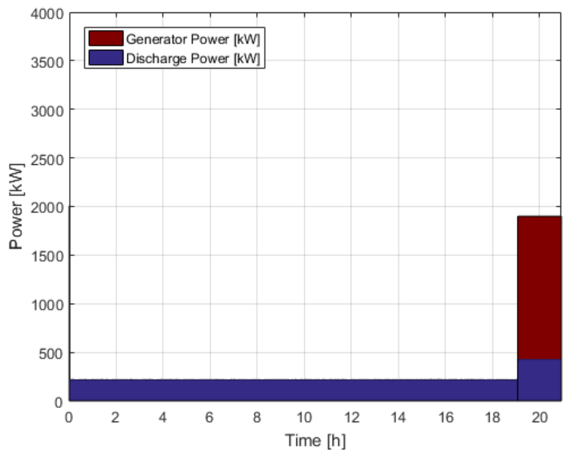

Figure 138 Representation of the efficiency calculation during covert transit 1

The efficiency of the propulsion plant is the efficiency of the propulsion motor, battery and diesel generator. The propulsion motor efficiency and battery efficiency are modelled in performance models. The diesel generator efficiency is assumed to be constant. The efficiency of the diesel engine is obtained with the data of the manufacturer. [33] The efficiency of the generator set is obtained from Figure 75.

$$\eta_{CT} = \eta_{snorting} \cdot \eta_e \cdot \eta_{gen} \cdot \eta_{conv} \quad \text{8-13}$$

8-14

$$\eta_e = \left(\frac{3.600.000}{sfc \cdot h^L}\right) = \left(\frac{3.600.000}{238 \cdot 42700}\right) = 0.35 \quad \text{8-15}$$

$$\eta_{gen} \cdot \eta_{conv} = 0.95 \cdot 0.92 = 0.87$$

8-16

The resulting efficiencies during the covert transit are

$$\eta_{CT1} = 0.84 \cdot 0.35 \cdot 0.95 \cdot 0.92 = 0.26 = 26\% \quad \text{ref. 8-13)}$$

$$\eta_{CT2} = 0.77 \cdot 0.35 \cdot 0.95 \cdot 0.92 = 0.24 = 24\% \quad \text{ref. (8-13)}$$

8.12.1 Fuel consumption covert transit 1

The required diesel fuel for the transit mission is obtained by simulations. The input is the generator output of 3000 [kW], the battery properties and SOD. The SOD varies between 0.2 and 0.4. The results of the simulation are illustrated in Figure 139. Total duration of period 1 is set at 470 hours.

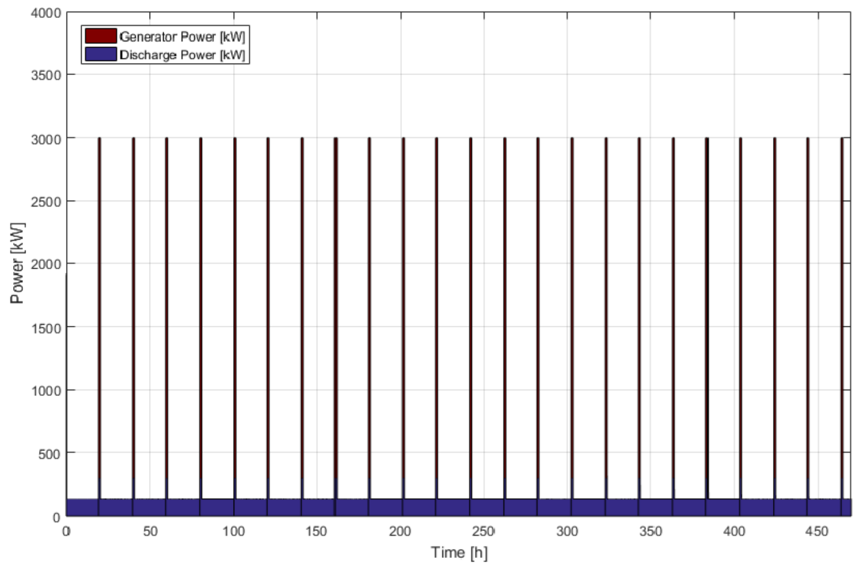

Figure 139 Generator power during covert transit 1

The required fuel mass is calculated as the time the generator is running times the specific fuel consumption of the diesel engine. This is defined in equation 8-17. The total power delivered by the generator during the mission is the integral over time of the generator power. The snorting time is obtained by dividing the total delivered power by the generator power as stated in equation 8-19. The resulting fuel mass of during covert transit 1 is 19 ton.

$$m_{fuel} = T_{snort} \cdot P_{generator} \cdot sfc \tag{8-17}$$

$$Q = \int_0^{t_{end}} P_{generator}\, dt \tag{8-18}$$

$$T_{snorting} = \frac{Q}{P_{generator}} \tag{8-19}$$

$$m_{fuel} = 26.2 \cdot 3000 \cdot 238 = 19\ ton \qquad \text{Ref. 8-17}$$

The indiscretion ratio is the simulated snorting time, divided by the total mission time.

$$IR = \frac{T_{snort\ simulated}}{T_{snort\ defined} + T_{submerged\ defined}} = \frac{26.2}{470} = 0.056$$

8.12.1 Fuel consumption covert transit 2

The total fuel mass during cover transit 2 is 26 ton.

$$m_{fuel} = 36.2 \cdot 3000 \cdot 238 = 25.9\ ton$$

The indiscretion ratio is obtained by simulations as 0.27.

$$IR = \frac{T_{snort\ simulated}}{T_{snort\ defined} + T_{submerged\ defined}} = \frac{36.2}{135} = 0.27$$

8.12.1 Overt transit

The overt transit, illustrated in Figure 2, indicated with OT1 and OT2 have the same power load, the resulting required power is 705 [kW]. Resulting in a total required diesel storage tank of 88 ton. According to the energy flow diagram (EFD) in Figure 5 is the battery not used during the overt transit. The efficiency of the batteries does not have to be taken into account. A simulation is not required.

$$P_{load} = P_{aux} + P_B = P_{aux} + \frac{P_D}{\eta_s} = 200 + \frac{500}{0.99} = 705\ [kW]$$

$$\frac{P_{load}}{\eta_{gen} \cdot \eta_{conv}} = \frac{P_{load}}{0.95 \cdot 0.92} = 810\ [kW]$$

The diesel engine efficiency according to MTU with the 5% error margin is 238 [gr/kWh].

$$m_{fuel\ overt} = 810\ [kW] \cdot (260 + 230)[h] \cdot (238)\left[\frac{g}{kWh}\right] = 94.5 \cdot 10^6\ [g] = 95\ ton$$

8.12.2 Summary

Table 26 summarizes the efficiency and fuel consumption of the concept configuration A during the assumed mission profile.

Table 26 Efficiency and fuel consumption during the assumed mission profile

	Generator power [kW]	Transit	IR Set [-]	IR Sim. [-]	Time [h]	Efficiency [-]	Efficiency [-]	Fuel Mass [ton]
Concept Conf. A	810	OT	-	-	490	-	-	95
	3000	CT1	0.10	0.056	470	84%	26%	19
	3000	CT2	0.28	0.270	135	77%	24%	31
Total								**145**

8.13 Conclusion concept propulsion plant configuration A

The concept configuration propulsion plant A can be modelled by combining the performance model of the propulsion motor battery cell. This enables to simulate the performance of the concept propulsion plant during the surveillance and attack part of the mission.

An algorithm is used to find the optimum mass and volume of the battery. The algorithm calculates for all the possible number of cells the corresponding mass per cell. The solution found by the algorithm has to meet three requirements. (1) The delivered power by the propulsion motors are within a defined error of the set power. (2) The maximum pseudo depth of discharge of the battery cell may not be exceeded. (3) The simulation time has to be equal to the set time.

The result of the algorithm is an optimum number of 223 per battery, with a corresponding cell mass of 571 kg per cell. The total mass of the batteries is 257 ton. The corresponding volume is 97 m^3. The MORAY design has 210 cells per battery and 530 [kg] per cell. The number of cells is based on the maximum allowable propulsion voltage. Increasing the maximum allowable voltage of the propulsion motor would increase the endurance of the submarine at higher speeds. For a limited system voltage of 882 V is the corresponding to 210 cells per battery and a mass 625 [kg] so a total mass of 262 ton and 99 [m^3] for the assumed mission profile. The difference between the optimum battery mass, and the battery mass limited to the maximum propulsion motor voltage is 3% or 5 ton.

The algorithm will always find a solution for a given number of cells if the number of cells is able to deliver the required voltage to be able to be in the operating field of the propulsion motor. The disadvantage of this solution is that battery sizes may become unrealistically large and not constructible. The solution found is a theoretical solution and gives an indication of the required battery mass. This theoretical approach does not take into account the possible batteries on the market.

The mission profile is an assumed profile, it is an example, the propulsion plant performance model is generic and capable of following al the mission profiles as input. The variations in the mission profile show the high dependency of the battery system layout. Despite the specific character of the mission profile, the simulation shows an optimum cell mass, in the range of 200 cells up to 240 cells. The burst and the position of the burst in the mission profile have a major influence on the mass. The maximum allowable motor voltage limits the design. It is recommend adding more realistic mission profiles to explore whether there is a trend in the operational requirements.

There are inaccuracies in the models and the method of increasing the battery cell capacity while keeping the other parameters constant. By increasing the cell capacity, the cell size is increased. As the cell size increases the cell resistance will increase as the current has to travel a longer distance trough the battery. And vice-versa the battery cell resistance would decrease for smaller batteries than the battery resistance obtained from the MORAY battery. This effect is not taken into account. Simulations with increasing resistance as function of the cell mass have been executed to indicate the sensitivity of the model and the effect on the cell mass. The increase in resistance of 40% results in 5 kg more cell mass required for 223 cells in series, and 15 kg for 210 cells in series. This effect needs to be taken into account.

The batteries are charged at constant power during snorting operation. The batteries are drained during the submerged part of the covert transit and charged during the snorting part of the transit. This is repeated until the set covert transit time is reached. The batteries are recharging at constant power. The power is delivered by diesel generator set(s). The required generator output power is obtained by performance simulations.

The performance requirements consist of three parts. (1) The propulsive and auxiliary power during snorting and submerged parts of the covert transit. (2) The indiscretion ratio during the covert transit. (3a) Set state of discharge during the covert transit of (3b) the maximum charge time. The maximum charge time is set for tactical reasons. During snorting operation is a blind spot created on the radar. Allowing hostile submarines approaching from the rear. The boundary conditions are the optimized battery-layout and computed MEM properties. The properties are defined in the parameter files.

The charging power is limited by the cell voltage. The generator power is however limited to a maximum. The generator power is limited by maximum charge current. The charge current charges the batteries. The battery voltage increases during charging. The cells can be damaged if the maximum cell voltage is exceeded.

The number of cells in series per batteries does not affect the required generator output power to meet the indiscretion ratio. The number of cells and the mass per affect the deeply submerged time during the covert transit and the maximum charge power.

The result of the simulation is a generator output power of 1900 kW for convert transit 1 (CT1), and a required generator power of 3000 kW for covert transit 2 (CT2). The highest generator power is leading from design perspective, resulting in a generator power of 3000 kW. The 3000 kW generator output power is also used to charge the batteries during CT1. The maximum allowable generator power, for constant power charging up to 80% SOC, is 3250 kW for covert transit 1 and 3500 kW for covert transit 2. The IR is respectively 0.05 and 0.24. It can be concluded that for approaches, 3a and 3b the calculated generator power is the same.

The assumed mission profile defines two deeply submerged speeds in CT1 and CT2. Those are arbitrarily chosen. The propulsion motor performance model and the battery cell performance model enables to obtain the maximum deeply submerged range as function of the submarine speed. It can be concluded that the maximum range for a discharge between 0.8 and 0.6 battery state of charge is 78 nautical miles. The distance is achieved at a submarine speed of 4.7 knots.

The efficiency during the covert transit is defined as the energy used by the propulsion motor and auxiliary users during the submerged and snorting part of the covert transit divided by the power output of the generator for the duration of the snorting period. The efficiency of the propulsion plant during CT1 is 84%. This is the result of the propulsion motor and battery efficiency. The efficiency can be explained by the propulsion motor efficiency (93%), combined with the battery efficiency (85%). When the diesel generator set efficiency is taken into account is the efficiency 26%. The efficiency during CT2 is 77%. The propulsive power is higher resulting in higher required currents and a higher power loss. The propulsion plant efficiency, including the diesel generator set is 24%. The required diesel fuel storage capacity to meet the mission requirements is 145 ton.

9 Propulsion plant configuration B

9.1 Introduction

This chapter elaborates on the battery dimensioning and generator output power for propulsion plant configuration B as function of the assumed mission profile. The same methodology is used as for concept propulsion plant configuration A. The first part is the optimization of the lithium-ion batteries for the assumed mission profile. The second part is the determination of the generator output power.

9.2 Battery topology

The topology of the Lithium-ion batteries is comparable to the lead-acid batteries. Two batteries can be switched in series or parallel to supply the required voltage to the propulsion motor. The lead-acid batteries consist of cells where the Lithium-ion batteries consist of cell packs. The cell packs contain cells. This is illustrated in Figure 140.

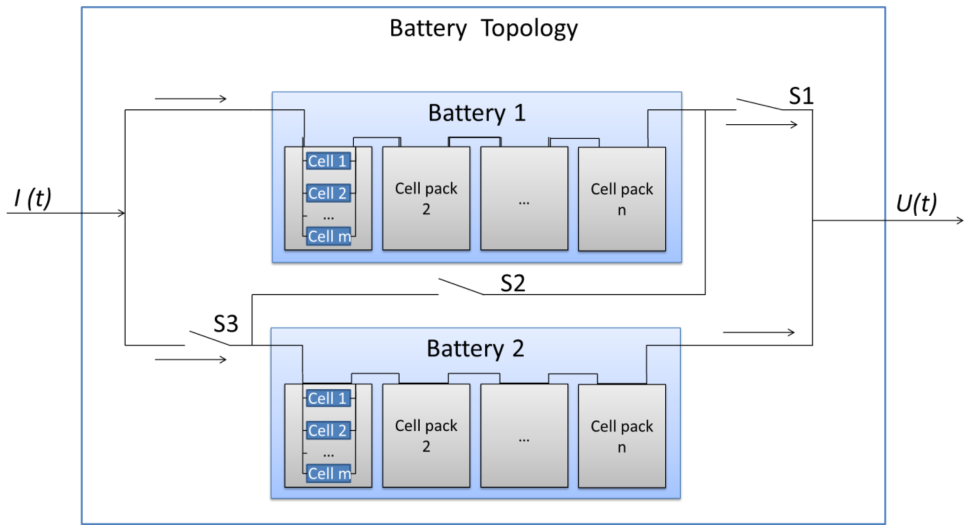

Figure 140 Battery topology Lithium-ion

The cell packs in the batteries are connected in series. The voltage of the battery is equal to the sum of the cell packs.

$$U_{bat1} = U_{b1\ cell\ pack\ 1} + U_{b1\ cell\ pack\ 2} + \cdots + U_{b1\ cell\ pack\ n} \qquad 9\text{-}1$$

$$U_{bat2} = U_{b2\ cell\ pack\ 1} + U_{b2\ cell\ pack\ 2} + \cdots + U_{b2\ cell\ pack\ n}$$

The performance model of the battery cell represents a single cell. It is assumed that the cells in the cell pack have the same behaviour, this is described in equation 9-2. It is also assumed that the cells in the different cell packs have the same behaviour as described in equation 9-2.

$$U_{b1\ cell\ pack\ 1} = U_{cell\ 1} = U_{cell\ 2} = \cdots = U_{cell\ m} \qquad 9\text{-}2$$

$$U_{b1\ cell\ pack\ 1} = U_{b1\ cell\ pack\ 2} = \ldots = U_{b1\ cell\ pack\ n} \qquad 9\text{-}3$$

9.3 Battery mass optimization algorithm

The optimum battery mass method is the comparable to the lead-acid technology optimization. The difference is the increasing of capacity. The lead-acid optimization algorithm increases the battery cell mass when the capacity is insufficient. The additional cell mass contains energy that is added to the initial cell energy up to the point where the stored energy capacity is sufficient for the submerged part of the mission profile. The lithium-ion cell mass cannot be increased. The largest cells on the market are around 5 kg. The cell chemistry and stability do not allow the increase of the cell. The algorithm increases the number of cells in parallel to increase the capacity. Through this the battery voltage remains the same while the battery capacity is increased. This is illustrated in Figure 141 and Figure 142.

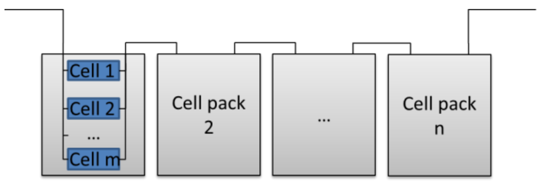

Figure 141 Battery construction

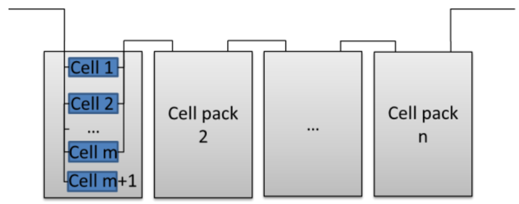

Figure 142 Increased capacity

$$U = U_{cell} \cdot n_{cell\ pack}$$

$$C = C_{cell} \cdot m_{cell\ series} = (c \cdot m_{cell\ mass}) \cdot m_{parallel}$$

$$U = U_{cell} \cdot n_{cell\ pack}$$

$$C = (c \cdot m_{cell\ mass}) \cdot (n_{cell\ series} + 1)$$

The number of cell packs is increased and the loop algorithm is started again, as illustrated in Figure 143 and Figure 144.

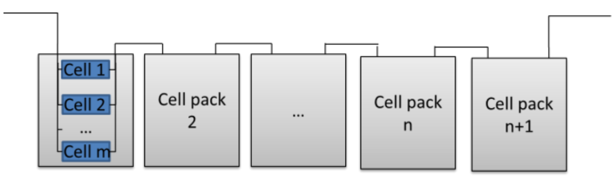

Figure 143 Battery construction with increased cell pack

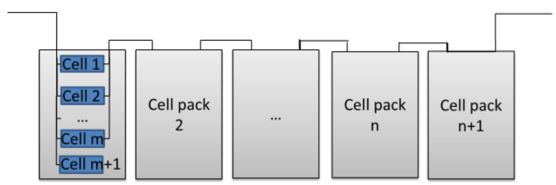

Figure 144 increased cell pack and capacity

$$U = U_{cell} \cdot (n_{cell\ pack} + 1)$$

$$C = C_{cell} \cdot m_{cell\ series}$$

$$U = U_{cell} \cdot (n_{cell\ pack} + 1)$$

$$C = C_{cell} \cdot (m_{cell\ series} + 1)$$

9.4 Battery mass prediction results

The result of the optimization is plotted in Figure 145. On the horizontal axis is the number of cells in series, on the vertical axis is the number of cells in parallel. The various lines are different mission profiles. The mission profiles are described in chapter 8.6.1. The increase of cells in series results in in a nonlinear decrease of number of cells in parallel for the mission profile. The increased number of cells in parallel has two effects. The first effect is that the discharge current is divided by the number of cells in parallel, resulting in a lower discharge current per cell and there for a longer discharge time. The second effect is an increased cell capacity as the cell capacity is a function of the discharge current. The bumpy line is caused by the stepwise increase per cells.

The total number of cells is the number of cells in series, times the number of cells in parallel times the number of batteries. The total number of cells is reasonably constant as can be seen in Figure 146 can be explained by the fact that the cell capacity a function is of discharge current. The optimum number of cells is constant from 105 cells in series and 40 cells in parallel. The battery voltage is equal to the 882 [V] when fully charged and switched in series.

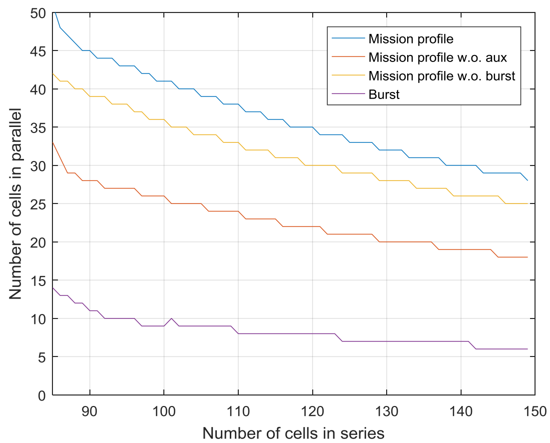

Figure 145 Cells in parallel as function of the cells in series

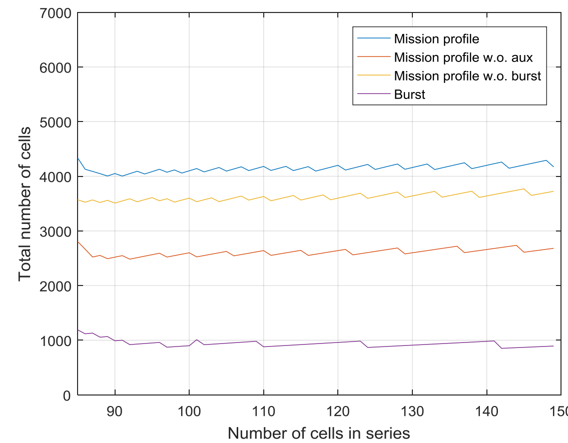

Figure 146 Total number of cells per battery as function of the cells in series

The result of the time simulation is plotted in Figure 147. The battery layout is 105 cells in series and 40 in parallel. It can be concluded that the set MEM power requirements have been met. The same holds for the pseudo discharge state.

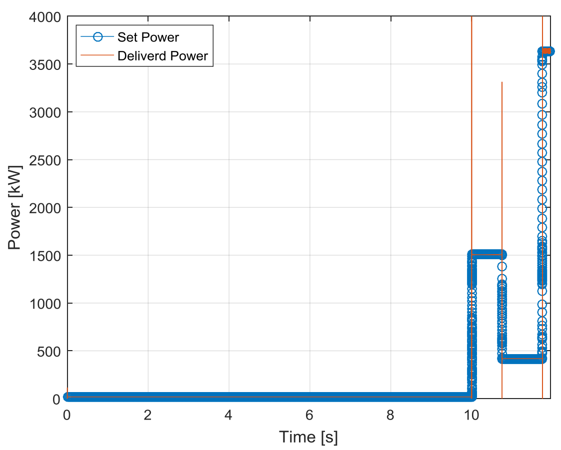

Figure 147 Propulsion motor delivered power

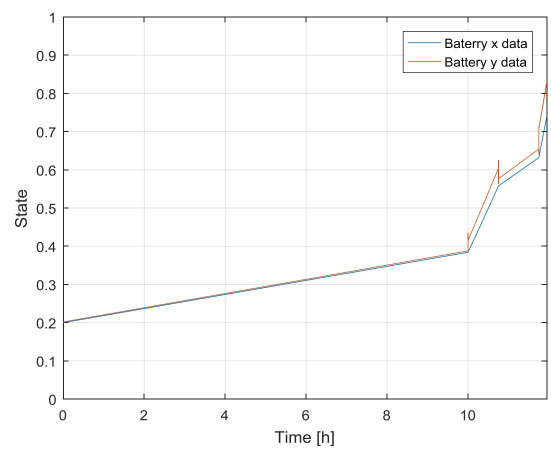

Figure 148 State of discharge(x) and pseudo discharge(y)

Figure 149 illustrates the armature voltage and discharge current acting on the battery. The armature voltage is at the beginning of the mission is 45 [V]. This is the optimum battery voltage with respect to efficiency at 18 kW brake power. This is calculated in chapter 5.7.1.1.

After 10 hours dead-slow speed is the speed increased. The set output power is 1500 [kW]. The switchboard settings are 2 batteries in series and the armatures in parallel. The 2 batteries in series form 210 cells in series. The battery voltage is then 210 times the cell voltage. As the battery voltage decreases, the discharge current increases to maintain constant power.

After the set 1500 [kW] is the set output brake power 400 [kW]. The batteries and the armatures are switched in parallel. The armature voltage is 105 times the battery cell voltage.

The final load is the burst load at the end of the mission. The batteries are switched in series and the armatures in parallel. The armature voltage drops steeply, resulting in a steep increase of the discharge current.

Figure 150 is a plot of the voltage and discharge current of a single battery cell. The steepness in decrease of the cell voltage is caused by the cell discharge current. High cell discharge currents result in steep voltage decreases.

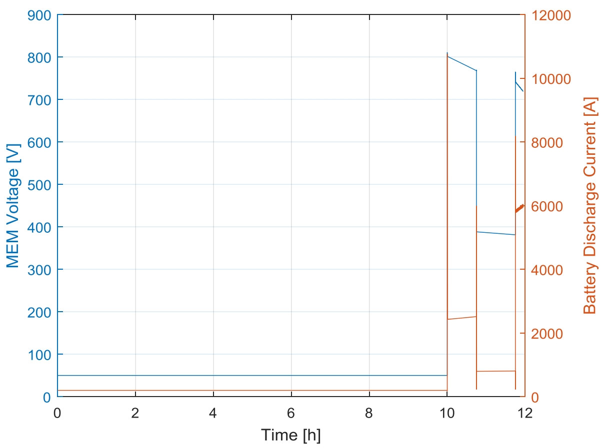

Figure 149 Armature voltage and discharge current

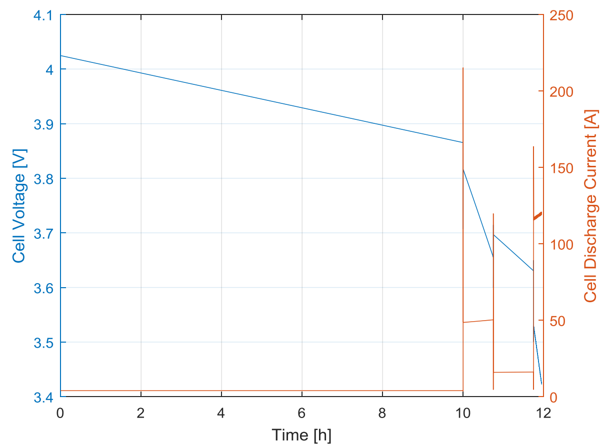

Figure 150 Cell voltage and cell discharge current

The MEM efficiency is plotted in Figure 151. The propulsion motor efficiency is comparable to the propulsion motor efficiency results of concept configuration plant A. The propulsive power delivered by the motor is the same and the battery voltage is comparable.

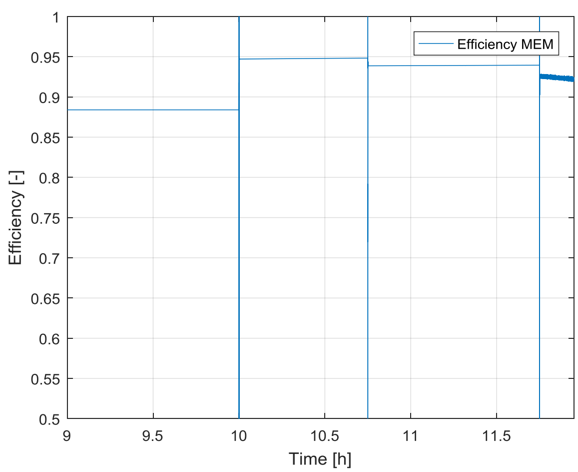

Figure 151 Propulsion motor efficiency

9.4.1 Battery mass and volume prediction

The optimum number of cells is obtained in the previous chapter. The volume and mass of the cells is a good indication of the required mass and volume of the batteries. The packing of the cells into a module is significant as discussed in section 3.4 and illustrated in Figure 70. The packing factor for volume must be multiplied with the volume of the cells. The packing correction factor for the mass must be multiplied with the mass of the cells.

The cell properties are defined in Table 11 Lithium-ion cell dimension properties. The cell volume is 2.12 litres and has a mass of 4.2 kg. The packing factor for the volume is the specific mass of the cell divided by the specific mass of the cell module. This results in a packing correction factor of 1.6. The packing factor for mass is calculated in the same way as volume. The packing correction factor is 1.3. The resulting volume and masses are calculated in equation 9-4 and 9-5.

$$V_{li-ion} = f_{corr\,V} \cdot \left(V_{cell} \cdot n_{bat} \cdot n_{series} \cdot n_{parallel}\right) \tag{9-4}$$

$$V_{li-ion} = 1.6 \cdot (2.12 \cdot 10^{-3} \cdot 2 \cdot 105 \cdot 40) = 29\ [m^3]$$

$$m_{li-ion} = f_{corr\,m} \cdot \left(m_{cell} \cdot n_{bat} \cdot n_{series} \cdot n_{parallel}\right) \tag{9-5}$$

$$m_{li-ion} = 1.3 \cdot (4.2 \cdot 2 \cdot 105 \cdot 40) = 46\ [ton]$$

9.5 Charge power lithium-ion

The required charging power is obtained in similar ways as the lead-acid batteries. The charge current charges the battery up to the point where the battery is filled up to 80%. The results of the charging are combined in Table 27. The calculations are done for different battery settings; 40, 80 and 140 cells in parallel. 40 Cells in parallel is the optimum according to the surveillance and the attack phase of the mission. The 80 cells in parallel have the same submerged endurance time compared to lead-acid batteries, when discharged from 80% to 60% SOC. 140 cells in series is the normalized volume compared to the required lead-acid volume, as calculated in equation 9-6.

$$V_{li-ion} = V_{lead-acid} = f_{corr\,V} \cdot \left(V_{cell} \cdot n_{bat} \cdot n_{series} \cdot n_{parallel}\right) \tag{9-6}$$

$$n_{parallel} = \frac{V_{lead-acid}}{f_{corr\,V} \cdot V_{cell} \cdot n_{bat} \cdot n_{series}} = \frac{99}{1.6 \cdot 2.12 \cdot 10^{-3} \cdot 2 \cdot 105} \approx 140$$

The required generator output power for CT1 is listed in Table 27.

Table 27 Required generator output powers CT1

	Unit	105s-40p	105s-80p	105s-140p
Covert 1 Submerged time	h	10.2	20.4	35.76
Covert 1 Snorting time	h	1.13	2.27	3.97
Indiscretion ratio 1	-	0.10	0.10	0.10
Required Power	kW	1600	1600	1600
Efficiency		93%	93%	93%

It may be clear that an increased number of parallel cells increase the submerged time. An increased submerged time results in an increased snorting time for constant set Indiscretion ratio. The state of charge and the battery voltage are plotted for the three battery settings in Figure 152.

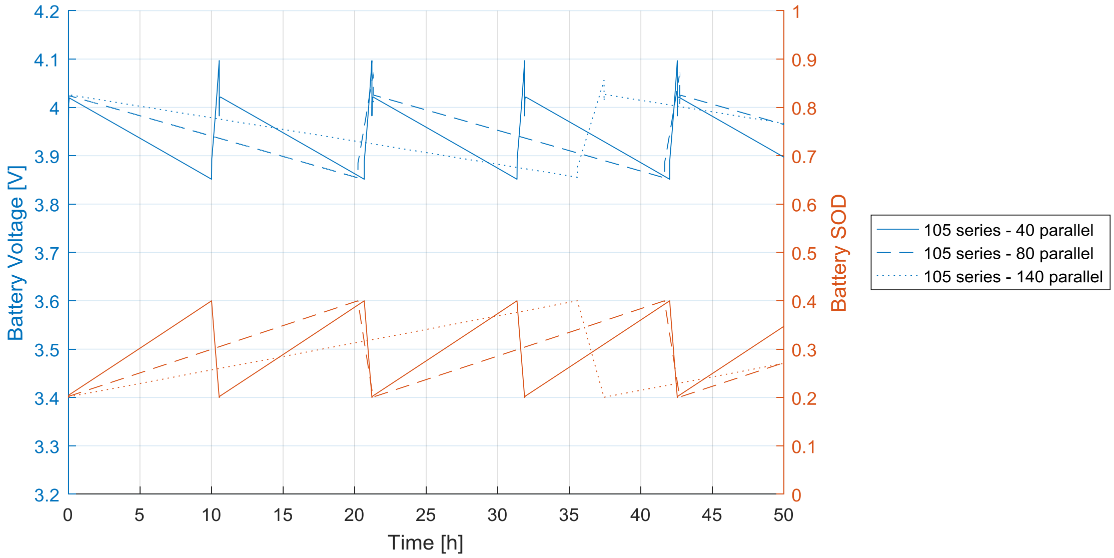

Figure 152 State of charge and battery cell voltage for 3 battery settings

The required generator output power for CT2 is listed in Table 28.

Table 28 Required charging powers CT2

	Unit	105s-40p	105s-80p	105s-140p
Covert 2 Submerged time	h	1.78	3.61	6.35
Covert 2 Snorting time	h	0.69	1.40	2.47
Indiscretion ratio 2	-	0.28	0.28	0.28
Required Power	kW	2800	2800	2800
Efficiency	%	84%	84%	84%

The weight and volume of the different battery layouts are stated in Table 29.

Table 29 Mass and volume

	Unit	105s-40p	105s-80p	105s-140p
Volume batteries	m^3	29	58	99
Mass batteries	ton	46	92	161

9.5.1 Maximum generator power

The maximum charge power is limited by maximum charge current for Lithium-ion battery technology. The maximum charge current is 200 [A]. The charge power is limited to 7.1 [MW] as calculated

$$P_{GEN\ MAX} = n_{bat} \cdot n_{series} \cdot U_{cell\ max} \cdot n_{parallel} \cdot I_{max} \qquad 9\text{-}7$$

$$P_{GEN\ MAX} = 2 \cdot 105 \cdot 4.2\ [V] \cdot 40 \cdot 200\ [A] = 7.1\ [MW]$$

The theoretical IR for the given powers in the mission profile is 0.03 for covert period 1 and 0.11 for covert period 2. The IR as function of the generator power is plotted in Figure 153. The cell charge current during CT1 is 200 [A] as can been seen in Figure 154.

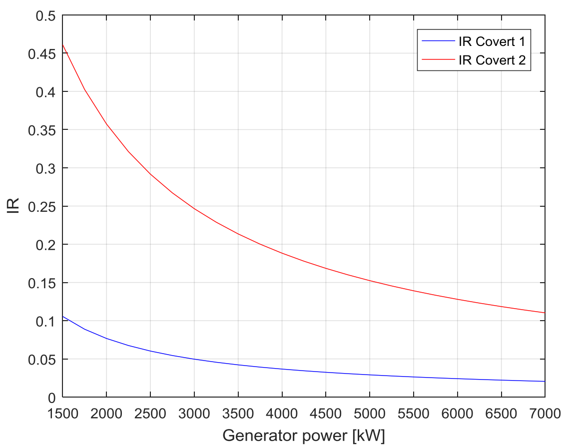

Figure 153 IR as function of the generator power

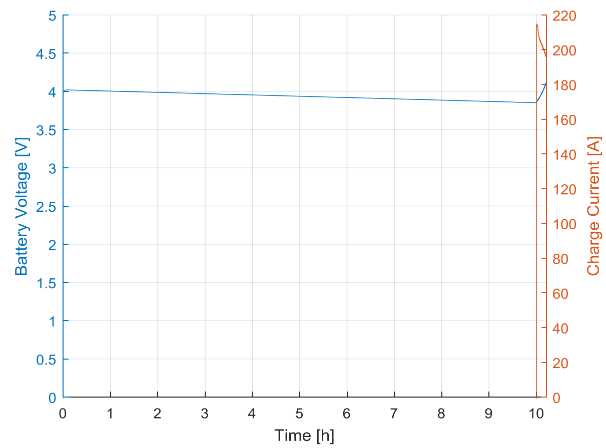

Figure 154 Cell voltage and charging current at 7100 [kW] (105-40 cells – CT1) Resulting IR = 0.02

9.6 Dimensioning diesel generator for concept configuration B

The optimum result for concept configuration B are two V16 propulsion motors, resulting in a volume of 32 m³ and weight of 33 ton.

Table 30 Solutions concept configuration B

Type	Power [EkW]	Brake Power [kW]	n.o. engines [-]	Mass [ton]	Volume [m³]	Max. Power [EkW]	Mass [ton]	Volume [m³]
V6	2800	3200	6	48	45	3400	49	45
V8	2800	3200	4	39	48	3000	39	38
V12	2800	3200	3	40	41	3400	41	41
V16	**2800**	**3200**	**2**	**33**	**32**	**3000**	**33**	**32**

9.7 Propulsion plant efficiency

Table 26 summarizes the efficiency and fuel consumption of the concept configuration A during the assumed mission profile.

Table 31 Efficiency and fuel consumption during the assumed mission profile

	Generator power [kW]	Transit	IR Set	IR Sim.	Time [h]	Efficiency [-]	Efficiency [-]	Fuel Mass [ton]
Concept Conf. B**	810	OT	-	-	490	-	-	95
	3000	CT1	0.10	0.050	470	93%	28%	17
	3000	CT2	0.28	0.244	135	84%	26%	24
Total								**136**

9.8 Conclusion concept propulsion plant configuration B

The concept propulsion plant configuration B is modelled. The model is used to simulate and optimize the behaviour of the plant. The optimum number of cells in series and parallel with respect to the surveillance and attack phases of the mission are found with the algorithm. The optimum number of cells in series is 105 and 40 cells in parallel, a total of 8,400 cells. The active cell mass is 46 ton. The corresponding corrected volume for packing is 29 [m³].

The submerged time during covert transit one is 10.2 hours for the battery layout of 105 cells in series and 40 cells in parallel. This submerged time is shorter compared to the lead-acid batteries (210 – 625 kg). The submerged time for the lead-acid battery is 18.84 hours. From this data it seems that the lead-acid battery is more effective in snorting operation. This is however not true. The optimum battery mass algorithm calculates the minimum cell capacity, during the surveillance and attack part of the mission. The lead-acid battery capacity is highly dependent on the discharge current, and state of charge. The lead-acid cell mass that determines the battery capacity is strongly dependent on the burst at the end of the attack part. This result in a high mass, and a long discharge time at low discharge currents.

The number of cells in parallel is increased to have the same submerged time, and have an equal comparison. By increasing the number of cells in parallel the systems voltage stays unchanged but the capacity increases. The lithium-ion cells that meet the submerged time during covert transit 1 is 105 cells in series and 80 cells in parallel. Resulting in a corrected mass for packing 92 ton and 58 [m³].

The maximum continuous charge current of the lithium-ion cells is 200 [A] up to 0.0 SOD [15]. The required charge power is not limited to the maximum charge current. The requirements set in the mission profile demand a continuous charge current of maximum 50 [A].

The efficiency during covert transit 1 is 93% due to the propulsion motors efficiency and the battery round trip efficiency at 1600 [kW]. The efficiency during covert transit 2 is 84% at 2800 kW. The high efficiency can be explained by the high propulsion motor efficiency, 92% and the high 96.5% round trip efficiency.

10 Life cycle cost

The submarine market is a small market compared to surface ships and land based applications. This will affect the component price. The capital expenditures are based on data of 1992. The prices are converted to 2016 using data of the CBS (Centraal Bureau voor de Statistiek).

10.1 Propulsion motor

The quotations for the MORAY 1400 have been used to make a rough estimation of the price of the propulsion motor in the present. The prices in the quotation are based on DC-propulsion motors. More research has to be done on the operational expenditures.

Table 32 Propulsion MEM - CAPEX

Estimated price per submarine	Price DC €/kW	Propulsion motor 2016
Quotation (1)	2000 €/kW	€ 7.3 million
Quotation (2)	2300 €/kW	€ 8.4 million

10.2 Batteries

10.2.1 Lead-acid

The cycle life of the battery is dependent on the battery treatment. Lead-acid batteries have a typical cycle life of 200 at 100% SOD. In general, batteries have a longer life for lower SOD cycles. Up to 1500 cycles can be attained at 25% SOD. [38] The number of cycles during the given mission profile is 140 cycles. One cycle is a deep discharge cycle of 80% state of discharge and the other cycles are 40Total SOD. Based on the available data the estimated price is € 6,000 per cycle for the total battery layout. This is based on general data and specification of lead-acid batteries, the price is not based on submarine specific batteries.

Table 33 Lead-acid CAPEX

Estimated price per submarine	Lead-acid Moray	Lead-acid €/kg	Mission profile 2016
Quotation (1)	€ 3.5 million	27 €/kg	€ 8.8 million
Quotation (2)	€ 3.7 million	29 €/kg	€ 9.4 million

The cycle life of the battery is dependent on the battery treatment. Lead-acid batteries have a typical cycle life of 200 at 100% SOD. In general, batteries have a longer life for lower SOD cycles. Up to 1500 cycles can be attained at 25% SOD. [38]

	Mission profile 2016 Configuration A 2 x 210 x 625 kg
Estimated price per submarine	€ 10 million
Price per cycle 100% SOD	€ 50.000
Price per cycle 20-40% SOD	€ 6000

Based on the available data the estimated price is € 6,000 per cycle for the total battery layout. This is based on general data and specification of lead-acid batteries, the price is not based on submarine specific batteries.

The operational expenditures are the maintenance of the battery cells. Maintenance of the cells is for instance the check and of the electrolyte level in the cell. Hydrogen gas can be produced as an unwanted by-product resulting in a decrease of electrolyte. The reduced electrolyte level can result in damage to the battery cell [39]. The small space above the cells and the mounting of the cells make the maintenance time consuming.

10.2.2 Lithium-ion

Lithium-ion cells have the longest cycle life. At 100% SOD 4000 cycles are typically. At 20-40% SOD they can last up to 20000 cycles. [15] The estimated price per cell is €1500 [40] [41]. The price is only based on the cells. The packing, battery management system and other auxiliary systems are not included. The price for the total cost is a multiplication of the cell price.

Table 34 Lead-acid CAPEX

	Configuration B 8400 Cells	Configuration B* 16800 Cells	Configuration B** 29400 Cells
Estimated price submarine	€ 15 million	€ 30 million	€ 45 million
Price per cycle 100% SOD	€ 3000	€ 6000	€ 10000
Price per cycle 20-40% SOD	€ 1000	€ 2000	€ 2500

10.2.3 Comparison LCC batteries

The CAPEX of the lithium-ion batteries are estimated to be up to three times higher than the lead-acid batteries. More interesting is the price per cycle. The number of cycles for lithium-ion batteries is especially at low depth of discharge states significantly higher than lead-acid battery cells. Resulting in an estimated price per cycle of €1500 for lithium-ion compared to €6000 per cycle for lead-acid cells.

10.2.4 Aging batteries

More attention needs to be paid to the aging effect of lead-acid and lithium-ion batteries. The performance of the battery cells decrease with increasing aging.

11 Conclusion and recommendations

11.1 Introduction

The conclusion gives a summary and interpretation of results and a review on the research question.

The objective was to evaluate a number of concept propulsion plant configurations that meet the design requirements. The evaluation of the concept propulsion plant results in the concept system that would be most favourable with respect to efficiency, volume, weight and life cycle cost.

The design requirements for the propulsion plant where captured in an assumed mission profile. The mission profile consist all the parts of a possible submarine mission, the overt transit, covert transit, surveillance and attack. The propulsive power varies in time to represent different ship speeds. Slow speed represents the surveillance in an area followed by a burst to simulate a quick getaway. The generic model enables the user to simulate different missions, with varying power demands for varying period of times.

11.1.1 Propulsion motor

The maximum set propulsive power is the input for the first principle dimension prediction of the propulsion motor. The idea behind first principle dimension prediction is that the dimensioning of the propulsion motor, and other electric machines, can be estimated by sizing the core of the machine to the required power output using first principles [21].The first principle modelling is preferred above trend and regression lines because of fidelity. The physical principles in the models make the results not per definition more accurate but make the results a better representation of the real system and a better understanding, where fit functions do not represent physical relations.

The obtained core dimensions are a part of the technical parameters used in the propulsion motor performance model. The performance model is used to simulate the performance of the propulsion motor. The performance is considered to be the efficiency and discharge current as function of the available battery voltage and set propulsive power. The performance model is verified with a realistic propulsion motor. The accuracy is within 5%. It can be concluded that the model is suitable for simulating the current and efficiency.

The propulsion motor efficiency and dimensions is the same for the two concept configurations. The propulsion motor is dimensioned for the maximum defined power output at a defined rate of rotation. The mass, volume, efficiency and CAPEX as function of the assumed mission profile is captured in Table 35.

Table 35 propulsion motor properties for the assumed mission profile

DC-Compound 2 armatures	Mass [ton]	Volume [m³]	Efficiency	CAPEX
3600 [kW] Brake Power	48	19	max. 95%	€ 7.9 million

11.1.2 Batteries

The propulsion motor's load is defined in the assumed mission profile. This load determines the required energy storage capacity. The energy is stored in the batteries. The performance of the batteries is captured in a battery performance model. This model simulates the battery voltage, capacity and resistance as function of the charge and discharge current. The model is verified for lead-acid and lithium-ion battery technology.

The number of batteries and the size of the battery cells are optimized for weight and volume. The optimum is found with a battery optimization algorithm. The algorithm is applicable for lead-acid and lithium-ion battery technology. The algorithm has as input the set propulsive power and time interval corresponding to the set power. Thanks to this approach it is possible to simulate all kinds of mission profiles and the user of the algorithm is not limited to one mission profile. The result of the simulations is the total battery mass and volume.

The battery optimization algorithm has two stop functions; (1) Insufficient delivered power and (2) maximum pseudo state of charge. The lead-acid battery fails mainly on the delivered power. The lithium-ion battery fails mainly on the pseudo state of charge. This is illustrated in Figure 95 and Figure 97 for the lead acid battery cell. For lithium-ion in Figure 147 and Figure 151.

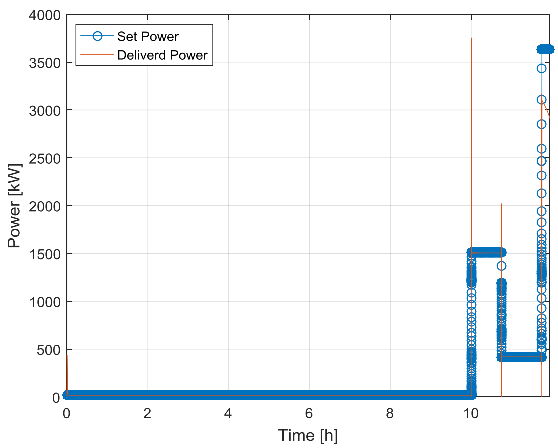

ref. Figure 95 Lead-Acid Battery - Power requirements

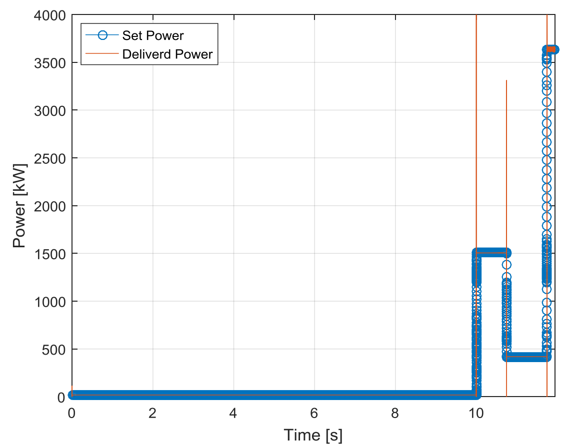

ref. Figure 147 Li-ion Battery - Power requirements

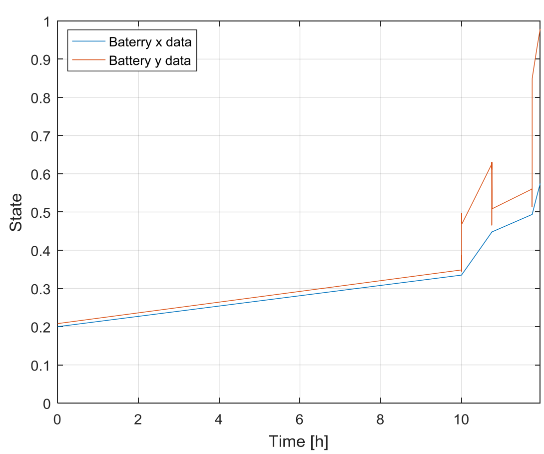

ref. Figure 97 Lead acid Battery – Capacity requirements

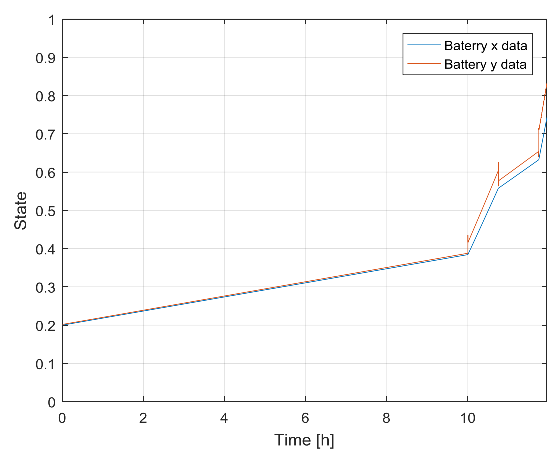

ref. Figure 151 Li-ion Battery - Capacity requirements

The optimum mass and volume of the optimization are combined in Table 36. The battery layout for concept configuration A represents; the number of batteries – the number of cells in series – and the mass per cell. The battery layout for concept configuration B represents the number of batteries – the number of cells in series – the number of cells in parallel.

Table 36 Battery properties for the preassumed mission profile

	Battery Layout	Battery technology	Mass	Volume
Concept Conf. A	2 – 223 – 571	Lead-acid	282 ton	96 m^3
Concept Conf. A*	2 – 210 – 625	Lead-acid	290 ton	99 m^3
Concept Conf. B	2 – 105 – 40	Li-ion	46 ton	29 m^3

The required mass is 6.1 times lower for the lithium-ion battery technology compared to the lead-acid technology for this specific mission. The expected difference in mass is according to Figure 10 between 5.6 and 2.8 times lower for lithium-ion battery cell technology. The difference is higher due to the high burst load at the end of the surveillance and attack part of the mission.

Multiple battery configurations for concept configuration B have been examined. Those are listed in Table 37. Concept Configuration B is the optimized result for the surveillance and attack part of the mission. Conf. B* has the same submerged time during covert transit 1 for 80% to 60% SOC. Concept Conf. B** has the same battery volume compared to concept configuration A*.

Table 37 Concept configurations B

	Battery Layout	Battery technology	Mass	Volume
Concept Conf. B	2 – 105 – 40	Li-ion	46 ton	29 m^3
Concept Conf. B*	2 – 105 – 80	Li-ion	58 ton	92 m^3
Concept Conf. B**	2 – 105 – 140	Li-ion	161 ton	99 m^3

The solutions A, A* and B are a result of the assumed mission profile during the surveillance and attack part of the mission. The found solutions can also be expressed in terms of submerged range as function of the submerged speed. The solutions A* and B are illustrated as continuous lines in Figure 155. The third discontinuous line is the line with the normalized volume compared to lead-acid, this is concept configuration B**. The boundary conditions for the SOC are between 0.8 to 0.2.

It is clearly visible that the submerged range of the lead-acid battery (A*) has a longer range compared to lithium-ion technology (B) for lower submerged speeds. The range of the lead-acid cells is decreasing faster compared to lithium-ion cells. This is due to the higher decrease of capacity as function of the discharge current for lead-acid cells compared to lithium-ion cells. From 18 knots and above the lithium cells have a larger range. The normalized volume configuration, B**, has the same shape as B but a larger range over the total speed range.

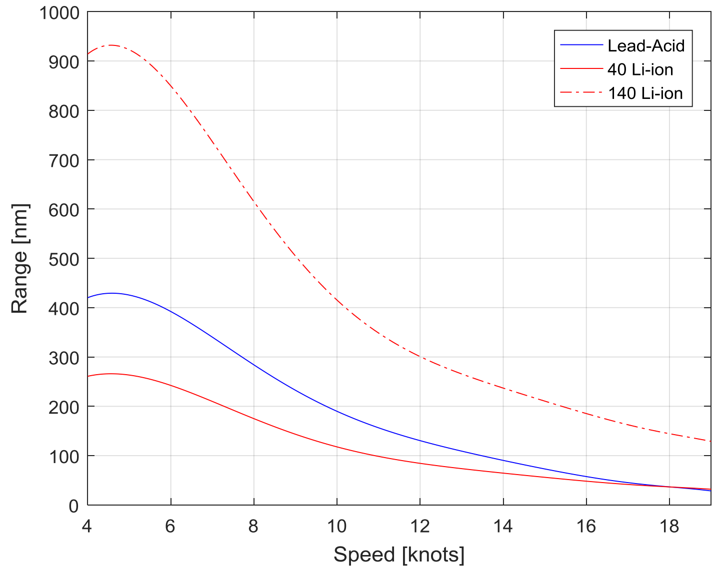

Figure 155 Submerged range as function of speed

The CAPEX cost for the lithium-ion batteries are higher compared to the lead-acid batteries. The cost per cycle is lower for lithium-ion batteries.

Table 38 Lead-acid CAPEX

	Conf. A 2 x 210 x 625 kg	Conf. B 8400 Cells	Conf. B* 16800 Cells	Conf. B** 29400 Cells
Estimated price submarine	€ 10 million	€ 15 million	€ 30 million	€ 45 million
Price per cycle 100% SOD	€ 50.000	€ 3.000	€ 6.000	€ 10.000
Price per cycle 20-40% SOD	€ 6.000	€ 1.000	€ 2.000	€ 2.500

11.1.3 Diesel generator set

The defined indiscretion ratio is the input for the generator output calculations. The required generator output power is the input for dimension prediction of the diesel generator set. The dimensions of the diesel generator set are obtained with first principle dimensions. The technical parameters used are obtained from a submarine diesel engine manufacturer. The core dimensions of the diesel engine are multiplied with a correction factor to come to the weight and volume of the diesel generator set. The time the running time of the diesel engines determines the required fuel for the mission. The required generator output power to meet the design requirements are summarized in Table 39. The required generator output power is higher for the lead-acid batteries. This is due to the higher losses in the lead-acid batteries.

Table 39 Required generator output as function of the assumed mission profile

	Battery Layout	IR 1	IR 2	Volume	Mass
Concept Conf. A	2 – 210 – 625	1900 [EkW]	3000 [EkW]	32 m^3	33 ton
Concept Conf. B	2 – 105 – 40	1600 [EkW]	2800 [EkW]	32 m^3	33 ton
Concept Conf. B*	2 – 105 – 80	1600 [EkW]	2800 [EkW]	32 m^3	33 ton
Concept Conf. B**	2 – 105 – 140	1600 [EkW]	2800 [EkW]	32 m^3	33 ton

The additional advantage of concept configuration B above configuration A is the improved IR. The IR is lower for the assumed mission profile because there are less losses during charging and discharging. Resulting in a higher charge powers. The IR as function of the generator output power for CT1 and CT2 for the configurations A and B are illustrated in Figure 156. The asymptotic shape of the indiscretion ratio as function of the generator power results in significant power differences for the same IR.

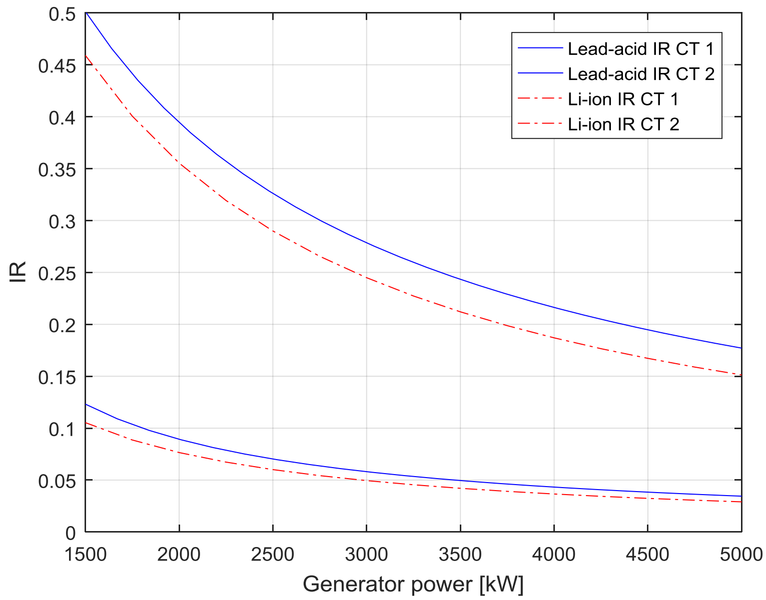

Figure 156 IR as function of generator output power

Another advantage of the lithium-ion technology above lead-acid is the maximum charge power. The cell charge power for lead-acid battery technology is limited to a maximum. During the charging increases the battery voltage, the battery voltage may not exceed the maximum value of 2.45 [V]. This would damage the cells. The cell voltage is dependent on the battery cell state of charge and the charge current. The maximum cell voltage did not occur for the assumed mission profile, but for stricter performance requirements is this expected.

The charging of the batteries during the snorting transit is for tactical reasons limited to 20 minutes snorting. The range associated with 20 minutes snorting at 3000 [EkW] generator power is indicated in Figure 157. After 20 minutes snorting is the lithium-ion battery technology capable of longer submerged ranges. The transmission efficiencies are higher for lithium-ion battery technology.

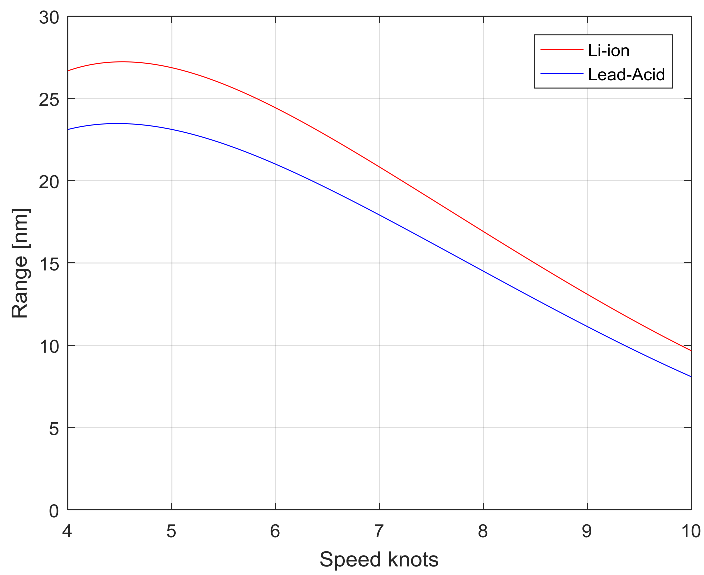

Figure 157 comparison 20 minutes charging

11.1.4 Fuel storage capacity

The required fuel storage capacity for concept configuration A is 145 ton. The fuel storage capacity for conf. B is 6% smaller, due to the efficiency of the propulsion plant during snorting.

11.2 Conclusion research question

The results of the simulation and optimization give answer to the research questions.

Which propulsion plant has the highest efficiency for the assumed mission profile?

The highest efficiency during the covert transit is concept configuration B. The total propulsion plant efficiency is 2% higher for CT1 and CT2 compared to concept configuration A. This is the efficiency from fuel to usable delivered power. The efficiency can also be expressed in the fuel consumption used during the assumed mission profile. The required diesel fuel mass for concept configuration 6% lower.

The efficiency of the batteries in combination with the MEM is more relevant as both system configurations use the same diesel generator set. The difference in efficiency is 9% for CT1 and 7% for CT2 in favour of the lithium-ion battery technology.

A side effect of the higher efficiency is an improved indiscretion ratio that is especially visible for CT, due to the asymptotic shape of the IR as function of the generator power.

Which propulsion plant has the lowest weight for the assumed mission profile?

The propulsion motor's weight is the same for configuration A and B. The diesel generator weight is the same for A and B. The difference in battery weight for the assumed mission profile is a factor 6.1 less for configuration B compared to A. Concept A and concept B* have the same submerged time for CT1. The difference in weight is a factor 5.0.

Which propulsion plant has the lowest volume for the assumed mission profile?

The lowest volume required to meet the requirements is concept configuration B. The required battery volume is 3.3 lower compared to the optimum propulsion plant that meets the requirements of concept A. Concept configuration B** has the same battery volume compared to system A. The range of concept B** is 2.1 times extended for slow speed and 3.5 times for high speeds.

Which propulsion plant has the lowest LCC for the assumed mission profile?

Based on the CAPEX is the lead-acid battery technology the most favourable. If the number of cycles is taken into account, the lithium-ion technology is expected to be more favourable. There is a great uncertainty concerning the obtained numbers.

The performance simulations and the dimension prediction calculations answers the research question: "*What are the optimum propulsion plant configurations for the replacement of the Walrus-class submarine given an assumed mission profile?"* The optimum propulsion plant configuration for the specific assumed mission profile concept configuration B. This is the diesel electric propulsion plant with lithium-ion battery storage technology.

The diesel electric propulsion plant with lithium-ion battery technology requires less weight and less volume compared to the lead-acid variant for the assumed mission profile. Therefore, the submarine design can potentially benefit from the implementation of lithium cells.

Additionally, it may be concluded that the calculated propulsion plant properties as the weight and volume are conventional. No unusual large battery sizes, number of cells or remarkable generator powers required to meet the design requirements. This is not surprising as the design requirements are not very challenging. The requirements are typical conventional diesel electric requirements.

11.3 Recommendations

11.3.1 Approach

The following recommendations are approach related, and can be illustrated in Figure 158. The figure is based on Figure 15.

The optimum propulsion plant configuration is found for a given assumed mission profile. Several mission variations have been executed to illustrate the effect of the burst, auxiliary load and the order of the burst in the mission profile. It is recommended to use the models and define multiple realistic mission profiles and analyse the properties of the optimized propulsion plants.

The concept propulsion configurations are limited to conventional diesel electric propulsion plants. Increasing the library of components by adding atmospheric air independent power generation systems increases the number of possible propulsion configurations and other optimum propulsion plant configurations with respect to the defined criteria. An atmospheric air independent propulsion plant could be the optimum propulsion plant configuration.

The propulsion motor is modelled as a direct current compound machine. The direct current machine has a good efficiency at higher power demands. The efficiency at slow speeds is lower than at higher speeds. A permanent magnet synchronous machine could have higher efficiencies at lower speeds as the rotor of the PM lacks rotor bars conducting the armature current.

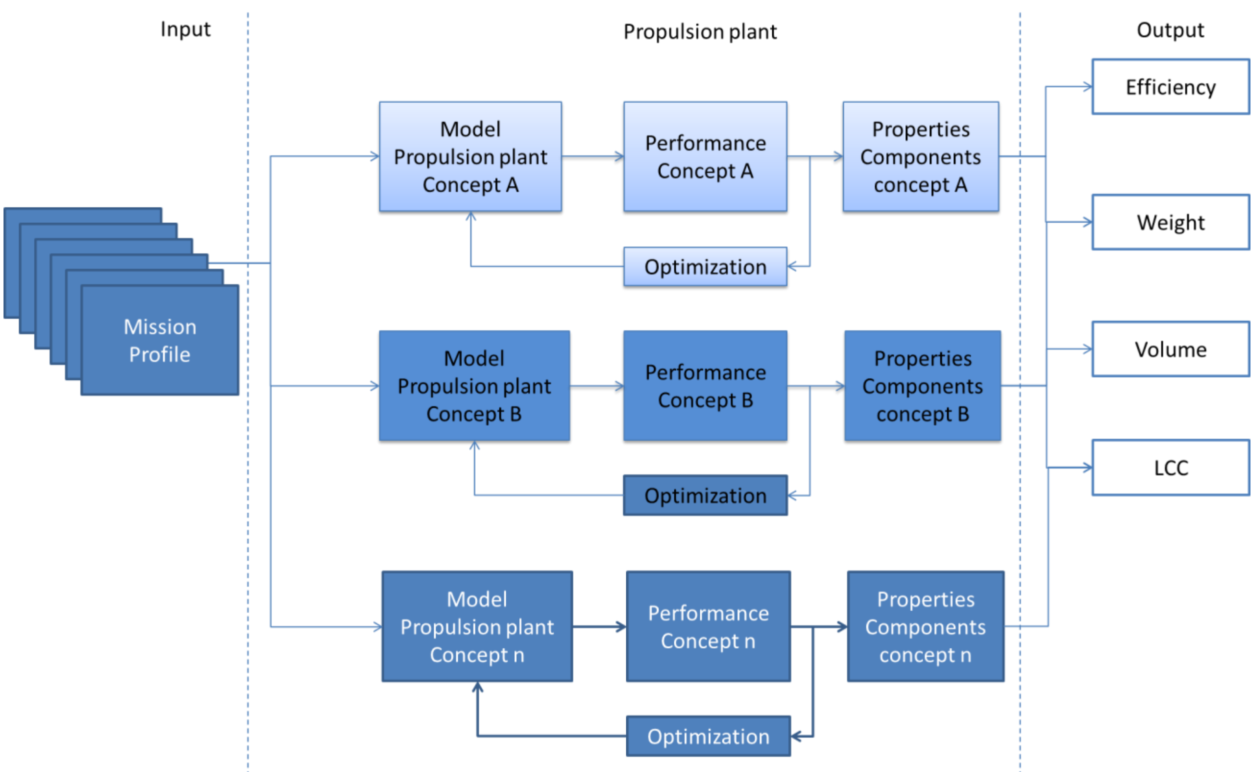

Figure 158 Recommendation Mission profile and plant extensions

11.3.2 Calculation related

The used algorithm will always find a solution for the assumed mission profile. The algorithm will increase the mass that is related to capacity, until the propulsion plant meets the defined mission. This will lead to unrealistic large battery sizes, or switching more cells in parallel. It might be interesting to limit the maximum cell size and investigate at what moment the propulsion plant fails to meet the design requirements.

The computing time is unnecessarily long. The time can be reduced to use a more intelligent way of increasing the battery size. It is plausible finding the solution in minutes instead of hours while using the same methodology.

The propulsion motor uses different battery and armature settings to operate over the total propeller curve. This works fine for the slow, cruise and high speed. The dead-slow speed settings are less robust. The available battery voltage and the set propulsive power have a major influence on the armature current and propulsion motor efficiency. It is recommended to use the defined settings for the dead-slow conditions.

The resistance of the submarine is taken constant. The constant in equation 2-2 changes for submerged, snorting and surfaced sailing.

11.3.3 Lithium-ion technology

Additional research has to be done on safety aspects of lithium-ion battery technology. Thermal runaway is a serious risk that needs to be managed. Extensive testing of the cells and modules in harsh ambient conditions is required to gain confidence in the technology. In addition it is recommended to extend the simulation with an atmospheric air independent power system, that is capable of charging the batteries during submerged operation, and evaluate the influence of that concept configuration.

The auxiliary systems required for the lead-acid batteries and the auxiliary systems required for the lithium-ion technology have similar and different components. Both need a switchboard and cabling, but the cooling might be different. It is recommended to investigate in the required volume and weight of the auxiliary systems associated with the lead-acid and lithium-ion batteries.

Another uncertainty is the applied packing factor. This factor is obtained in a technical meeting with EST-Flowtech. The packing factor has however a significant influence on the total mass and volume.

11.3.4 Life Cycle Cost

The diesel engine dimensions are based on MTU. The diesel engine database for submarine specific diesel engines could be extended.

The CAPEX of the components is based on prices from the past. The prices give an indication, but contain uncertainties. Especially the packing of a single lithium battery cell into multiple cells and the battery management system do influence the costs of the energy storage.

More attention needs to be paid to the aging effect of lead-acid and lithium-ion batteries. The performance of the batteries decreases with increasing aging.

12 ANNEX A Bibliography

[1] M. v. Defensie, “Ministerie van Defensie,” Ministerie van Defensie, [Online]. Available: https://www.defensie.nl/onderwerpen/materieel/inhoud/schepen/onderzeeboten. [Accessed 26 10 2016].

[2] A.-v. d. KM, *Onderzeeboeten van de "Walrus-klass",* Den Haag: Ministerie van Defensie, Marinevoorlichting, Projectgroep Onderzeeboten, RDM., 1989.

[3] Burger&Rydill, Concepts in submarine design, Cambridge: Press Syndicate of the University of Cambridge, 1994.

[4] H. Klein Woud and D. Stapersma, Design of propulsion and electric power generation systems, London: IMarEST, 2002.

[5] HOLEC.

[6] D. Linden, Handbook of Batteries, Michigan: McGraw-Hill, 1995.

[7] EverExceed, “EverExceed,” [Online]. Available: www.everexceed.com.

[8] J. Jaspers, “Tonijn,” [Online]. Available: http://www.heiszwolf.com/subs/tonijn/Tonijn.html.

[9] F.-S. Gady, “The Diplomat,” [Online]. Available: http://thediplomat.com/2015/10/japan-to-offer-australia-its-top-secret-submarine-technology/. [Accessed 19 10 2016].

[10] T. M. Systems, “HDW Class 2016,” [Online]. Available: https://www.thyssenkrupp-marinesystems.com/en/hdw-class-216.html. [Accessed 19 10 2016].

[11] P. Greenfield, “Australian Strategic Policy Instute - The Strategist,” The Strategist, 16 4 2016. [Online]. Available: http://www.aspistrategist.org.au/australias-future-submarine-the-great-battery-debate/. [Accessed 19 11 2016].

[12] F.-S. Gady, “The Diplomat,” The Diplomat, 07 10 2015. [Online]. Available: http://thediplomat.com/2015/10/japan-to-offer-australia-its-top-secret-submarine-technology/. [Accessed 19 11 2016].

[13] “Super-b,” Super-b, 24 11 2016. [Online]. Available: http://www.super-b.com/en/marine-2. [Accessed 24 11 216].

[14] Valence, “Valence Marine Solutions,” Valence, 24 11 2016. [Online]. Available: https://www.valence.com/solutions/marine/. [Accessed 24 11 2016].

[15] Kokam, “Kokam Li-ion/Polymer Cell,” Kokam, 2015. [Online]. Available: kokam.com/cell/. [Accessed 07 11 2016].

[16] C. Davies, “The Guardian,” The Guardian, 19 8 2015. [Online]. Available: https://www.theguardian.com/business/2015/aug/19/lithium-battery-review-boeing-dreamliner-fire-heathrow. [Accessed 23 10 2016].

[17] O. Solon, “The Gardian,” The Gardian, 19 10 2016. [Online]. Available: https://www.theguardian.com/technology/2016/oct/19/samsung-galaxy-note-7-fire-damage-owners-angry. [Accessed 23 10 2016].

[18] A. P. i. N. York, “The Gardian,” The Gardian, 15 2 2013. [Online]. Available: https://www.theguardian.com/business/2013/feb/15/airbus-lithium-ion-batteries-dreamliner. [Accessed 23 10 2016].

[19] T. Telegrapgh, “The Telegraph,” The Telegraph, 11 10 2016. [Online]. Available: http://www.telegraph.co.uk/technology/2016/10/11/why-is-the-samsung-galaxy-note-7-catching-fire-the-lithium-ion-b/. [Accessed 23 10 2016].

[20] Meuldijk, “Compoundmotor theorie,” Delft, 2014.

[21] D. Stapersma and P. d. Vos, *Dimension prediction models of ship system components,* Delft: TU-Delft, 2015.

[22] D. Stapersma, “Theory and model for battery charging and discharging,” Royal Netherlands Naval Collage, Den Helder, 1998.

[23] VARTA. [Online].

[24] K. Deleroi, Bepaling van de grootte en massa van een hoofdelektromotor van een onderzeeboot, Den Haag: Vakgroep OEMO, 1993.

[25] P. Sen, Principles of Electric Machines and Power Electronics, Kingston: Wiley, 2013.

[26] Boogaart, *Information about DC motor speed schematics,* Alblasserdam, 2016.

[27] R. Houwens, *Elektrische voedingsinstallatie voortstuwing,* Rotterdam, 1986.

[28] P. Schulten, D. Stapersma and M. D.M, *Parameterfile MEM,* Delft, 2011.

[29] V. B. AG, “MO-P2231-300,” VARTA, 1994.

[30] T. Wildi, Electric Machines, Drives, and Power Systems, Essex: Pearson, 2014.

[31] D. Stapersma, “Diesel Engines Volume 2 Turbocharging,” in *Diesel Engines*, Delft, TU-Delft, 2010, pp. 231-449.

[32] P. Hield, “The Effect of Back Pressure on the Operation of a Diesel Engine,” Defence Science and Technology Organisation, 2011.

[33] D. v. A, “Charge air systems for submarine engines,” MTU, 2014.

[34] B. Kraemer, *Understanding load factor,* Mankato: MTU , 2011.

[35] A. v. Drathen, “Charge Air Systems for Submarine Engines,” MTU, Friedrichshaven, 2014.

[36] *Operating Instructions V4000 Productgroup.*

[37] Submariner, *Conversation,* 2017.

[38] C.-Y. R. Wang and D. Christophe, Battery Systems Engineering, Wiley, 2013.

[39] K. Posthumus, *De hoofdbatterij van conventionele onderzeeboten,* ROERING, 1993.

[40] F. Jacobs, “Zero emission concept of a future Amsterdam canal boat,” TU-Delft, Delft, 2015.

[41] P. EV, “Pro EV,” [Online]. Available: www.proev.vom/P1Batt. [Accessed 11 12 2016].

[42] W. Deleroi, Elektrische Machines III, Delft: TU-Delft, 1993.

[43] C. G. Nat, A knowledge-bades Concept Exploration Model for Submarine Design, Delft: Delft University Press, 1999.

[44] Hommes and Paap, Elektrische Machines IA, Delft: TU-Delft, 1981.

[45] F. Fockens and A. v. Heeswijk, Constructie-elementen, Delft : TU-Delft, 1986.

[46] Siemens, “Permasyn,” [Online]. Available: http://www.industry.siemens.com/verticals/global/en/marine/submarines/propulsion/permasyn/Pages/Default.aspx#Low_20signatures_20making_20the_20boat_20harder_20to_20detect.

[47] SAAB, “Kockums Gotland Class,” [Online]. Available: http://saab.com/naval/Submarines-and-Warships/submarines/Kockums-Gotland-Class/.

[48] E. Pel, “SUB-PROP,” TU-Delft, Delft, 1995.

[49] El-Hawary, Principles of Electric Machines with Power Electronic Applications, Wiley-IEEE Press, 2002.

[50] R. Dingemanse, “SMART B1.7 Charging Batteries,” RH Marine, Rotterdam, 2016.

[51] R. v. Kuilenburg, “Dimensions of a submarine diesel as funcrion of engine power and speed,” TU Delft, Delft, 1994.

[52] S. Tak, “First Principle Based Mass and Volume Determination method for diesel engines in submarine application,” Nevesbu, Alblasserdam, 2016.

[53] J. Buckingham, “Submarine power and propulsion: balancing the energy elements,” in *Pacific 2012*,

Sydney, 2012.

[54] A. Mills, *Basic Heat and Mass Transfer,* Upper Saddle River: Prentice Hall, 1999.

[55] H. Bosman, “Future urban ferry,” TU-Delft, Delft, 2015.

[56] G. d. Vries, “Feasibility study advanced MEM,” Nevesbu, Den Haag, 92.

[57] “Defensie.nl,” Ministerie van Defensie, 11 6 2015. [Online]. Available: https://www.defensie.nl/actueel/nieuws/2015/06/11/minister-hennis-wil-onderzeeboten-vervangen. [Accessed 22 9 2016].

[58] B. Scrosati, K. Abram, W. v. Schalkwijk and J. Hassoun, Lithium Batteries, New Jersey: Wiley, 2013.

[59] C. Mikolajczak, M. Kahn, K. White and R. T. Long, Lithium-Ion Batteries Hazard and Use Assessment, Menlo Park: Springer, 2011.

[60] R. v. d. Mheen, “Submarine Power System Design Tool,” University College London, London, 2013.

[61] K. Jong de, *Beproevingsverslag van de HEM.*

[62] A. Mellegers and K. Jong de, “Beproevingsverslag van de hoofdelectromotor,” Holec - Machines & systemengroep, Ridderkerk, 1985.

[63] KOKAM, Writer, *KOKAM Lithium cell datasheet.* [Performance]. KOKAM, 2016.

13 ANNEX B Table of Figures

14 ANNEX C Glossary

AC	Alternating current
AIP	Air independent power generation
BMS	Battery management system
DC	Direct current
DMO	Defensie materieel organisatie
EFD	Energy Flow Diagram
HVAC	Heating Ventilation and Air Conditioning
IPW	Instandhoudingsprogramma Walrusklasse
IR	Indiscretion Ratio
LCC	Life Cycle Cost
MARIN	Maritime Research institute Netherlands
MEM	Main Electric Motor
MP	Mission Profile
MOSES-CD	Model-based Ship Energy System Conceptual Design
MSI	Mechanical Systems and Integration
Nevesbu	Nederlandse verenigde scheepsbouw bureaus
NMC	Nickel Manganese Cobalt Lithium Cell
PID-Controller	Proportional-integral-derivative
PM	Permanent Magnet Machine
RNLN	Royal Netherlands Navy
SEWACO	Sensoren, wapensystemen en commandosystemen
SOC	State of Charge
SOD	State of Discharge
SWB	Switch board
SWBS	Ship Work Breakdown Structure
TNO	Nederlandse organisatie voor toegepast-natuurwetenschappelijk onderzoek
TU Delft	Technical University Delft

15 ANNEX D Nomenclature

A_d	area cross section d-axis	m^2
A_q	area cross section q-axis	m^2
B_{gap}	air gap flux density	T
B_{sat}	flux density saturation value	T
B_δ	air gap magnetic flux density	T
C_t	battery capacity	Ah
D_r	diameter rotor	m
H_n	The depth of the slot	m
I_a	armature current	A
I_a	armature current	A
I_{char}	characteristic current	A
I_{charge}	charge current	A
I_f	shunt current	A
I_{prop}	propulsion current	A
J_a	Current density in the armature	A/m^2
K_a	motor constant	-
K_v	Loss coefficient related to Eddy current	-
L_{rotor}	length rotor	m
N_a	number of armature windings	-
N_c	number of compensating windings	-
N_f	number of shunt windings	-
N_s	number of series windings	-
P_{aux}	auxiliary power	kW
$P_{b\ max}$	maximum brake power	kW
$P_{b\ mem}$	brake power main electro motor	kW
$P_{b\ set}$	set brake power	kW
P_b	brake power	kW
P_d	delivered power	kW
P_g	generator power	kW
R_a	armature resistance	Ohm
R_f	field winding resistance	Ohm
R_i	Internal resistance battery model	Ohm
R_s	series winding resistance	Ohm
T_{snort}	snorting time	h
T_{subm}	submerged time	h
U_a	armature voltage	V
U_{bat}	battery voltage	V
U_{cell}	cell voltage	V
U_f	shunt voltage	V
V_R	rotor volume	m^3
V_{bat}	battery volume	m^3
V_{cell}	battery cell voltage	V
V_{de}	diesel engine volume	m^3
V_{dg}	diesel generator volume	m^3
V_g	generator volume	m^3
V_{mem}	propulsion motor volume	m^3
Z_a	number of armatures	-
c_0	capacity at 1.2 h discharge time	Ah/kg
c_5	capacity at 5 h discharge time	Ah/kg
c_∞	capacity at 100 h discharge time	Ah/kg
c_{cell}	cell capacity	Ah/kg

f_d	correction factor diameter	-
f_l	correction factor length	-
$k_{cu,a}$	Filling factor slots	-
l_d	magnetic length d-axis	m
l_{yq}	magnetic length q-axis	m
l_{yrd}	Stator length d-axis	m
m_{batt}	mass batteries	ton
m_{cell}	battery cell mass	kg
m_{de}	diesel engine mass	ton
m_{dg}	diesel generator mass	ton
m_g	generator mass	ton
m_{mem}	mass propulsion motor	ton
$n_{p\,max}$	maximum rate of rotation propeller	s^{-1}
n_p	rate of rotation propeller	s^{-1}
t_5	characteristic time constant	h
v_t	transversal velocity	m/s
Φ_{sat}	flux saturation value	Vs
η_{de}	diesel engine efficiency	-
η_{dg}	diesel generator efficiency	-
η_g	generator efficiency	-
η_{mem}	propulsion motor efficiency	-
η_{scaled}	Scaled efficiency	-
η_{trm}	transmission efficiency	-
μ_0	permeability in a vacuum	H/m
μ_r	relative permeability of iron	H/m
ρ_{cell}	battery cell density	kg/m^3
τ_R	shear stress	Nm/m^2
τ_{char}	characteristic	
ω_e	electrical frequency	Hz
ω_m	mechanical frequency	Hz
Δ	plate thickness Eddy current	m
B	flux density	T
H	Magnetic field intensity	A/m
IR	indiscretion ratio	-
Q	charge	C
T	Torque	Nm
U	voltage	V
a	constant in open voltage function	-
b	constant in open voltage function	-
c	Increase of resistance battery model	-
c	constant in internal resistance function	-
d	constant in internal resistance function	-
e	fit function tail battery model	-
n	rate of rotation	s^{-1}
n	number of	-
p	number of pole pairs	-
x	absolute discharge state	-
y	pseudo discharge state	-
α	constant in capacity function	-
α	pole cover factor	-
β	constant in capacity function	-
δ	air gap length	m
τ	time constant	h
ω	frequency	Hz

16 ANNEX E Propulsion motor dimensions

Selection table (Examples of calculated sets of data)

Rating	Operating values at rated output							
Type	Rated output [kW]	Rated speed [rpm]	Net weight approx. [t]	Operating voltage ranges [V]	Rated current approx. [A]	R approx. [mm]	G approx. [mm]	K approx. [mm]
1FR6134-...	1700	120	28	300 - 560	< 6000	2080	2240	1590
1FR6439-...	3300	150	50	520 - 830	< 6700	2500	3340	2310
1FR6439-...	3900	150	54	520 - 830	< 8000	2500	3340	2310
1FR6839-...	5000	150	71	550 - 830	< 9600	2700	4000	2800

Details to be set in context with an offer/order. All data are without obligation.

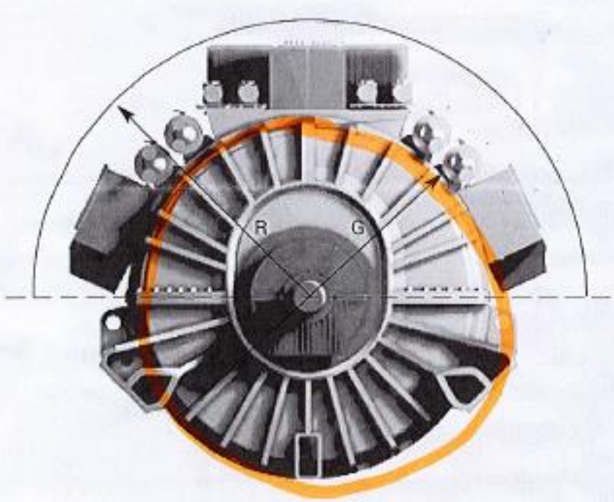

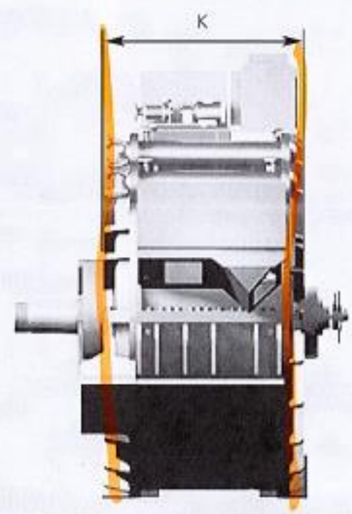

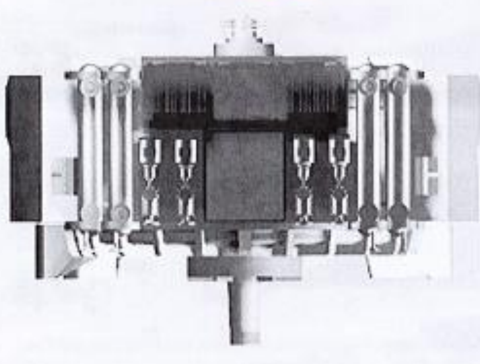

13

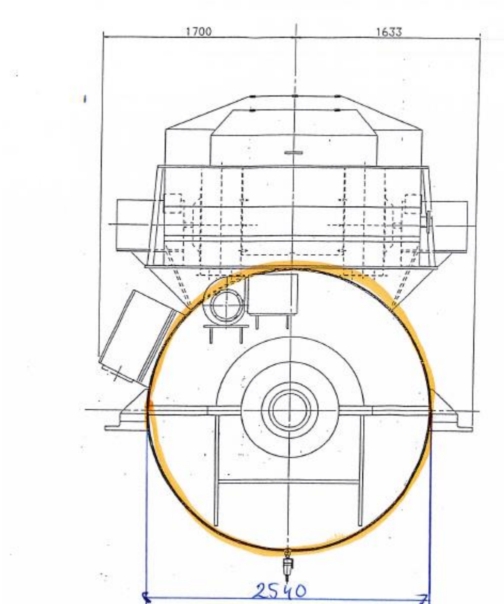

Fig. 1.2: DC MEM wit closed cooling air system (Holec type)

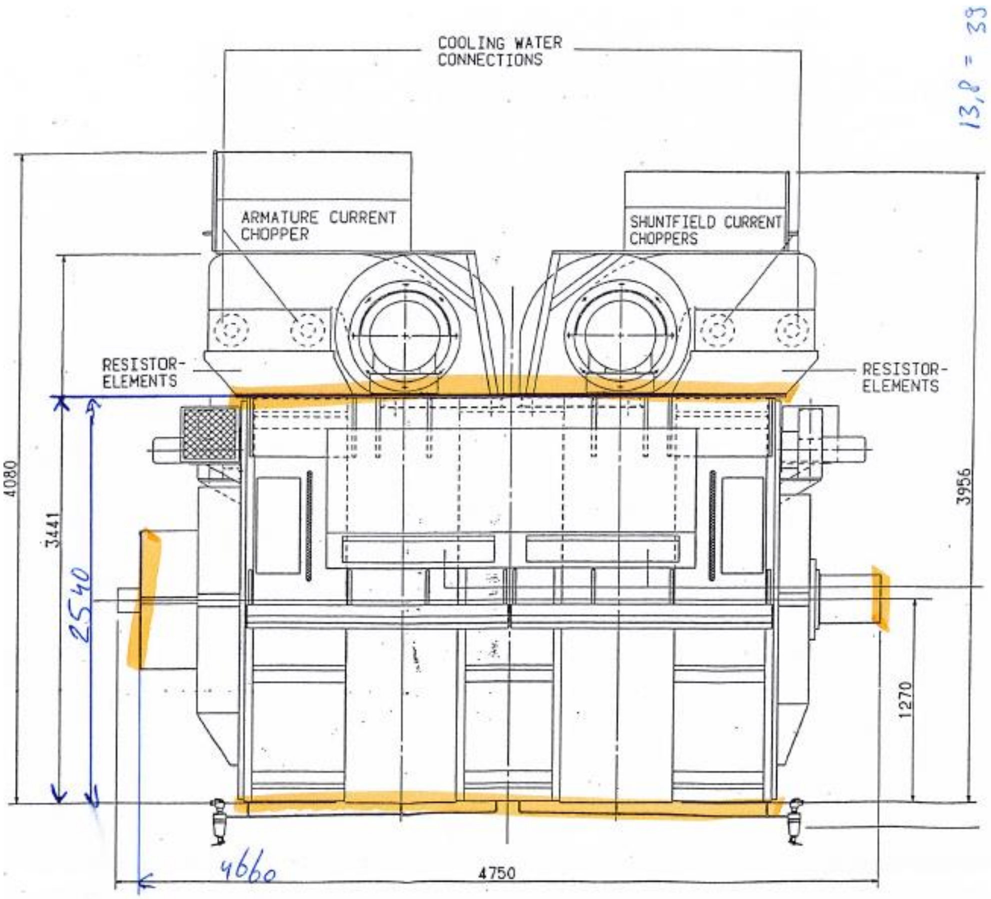

Fig. 1.1: DC MEM wit closed cooling air system (Holec type)

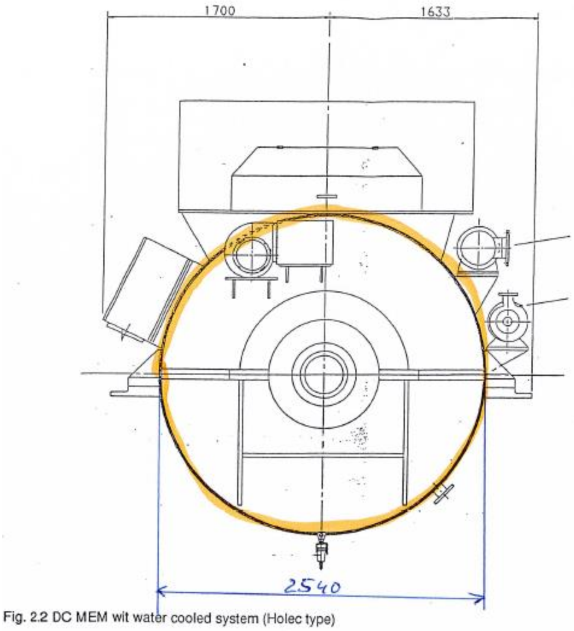

Fig. 2.2 DC MEM wit water cooled system (Holec type)

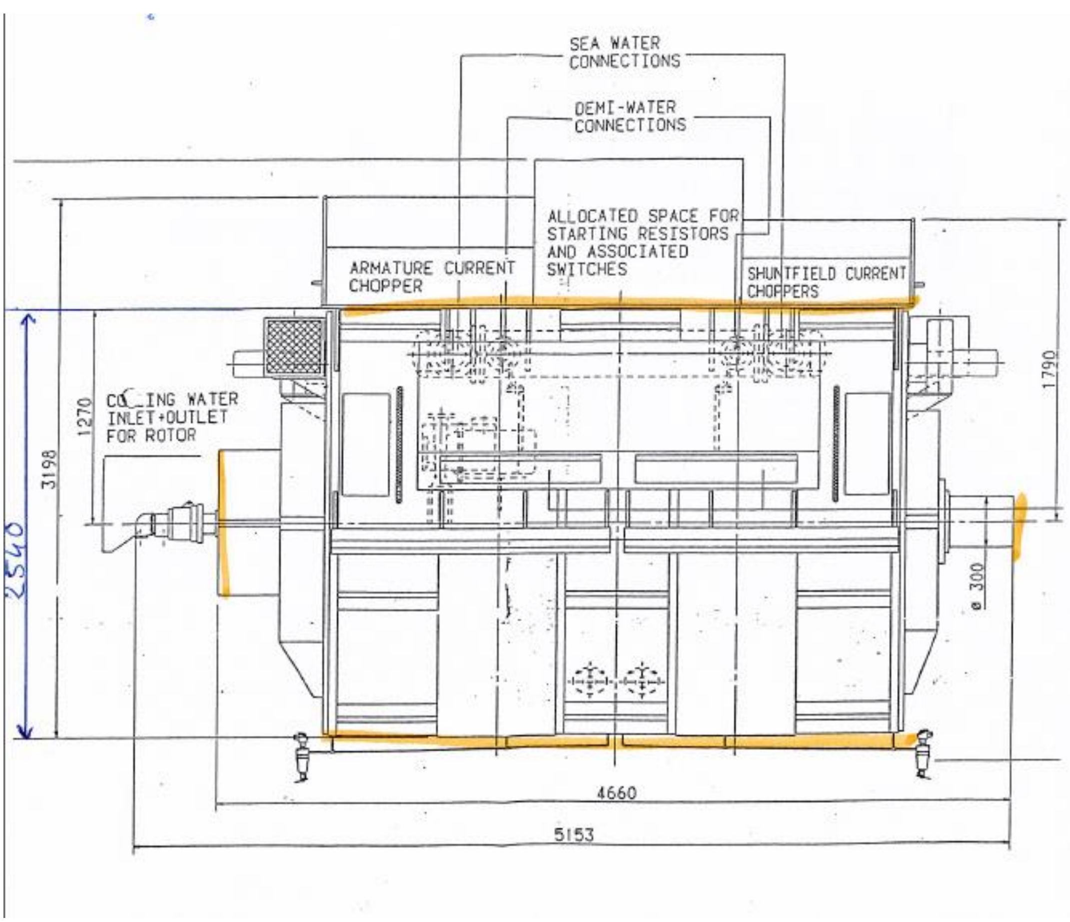

17 ANNEX F Schematic propulsion motor model